MYOFILAMENT DYNAMICS MODULATE CELLULAR DRIVERS OF ARRHYTHMOGENESIS IN HUMAN CARDIAC DISEASE

by
Melanie Anne Zile

A dissertation submitted to Johns Hopkins University in conformity with the requirements for the degree of Doctor of Philosophy

Baltimore, Maryland
October, 2017

© Melanie Anne Zile 2017
All rights reserved

Abstract

Cardiac arrhythmia is common in cardiac disease, but our understanding of the cellular mechanisms underlying arrhythmia is incomplete. Alternans, the beat-to-beat alteration in cardiac electrical or mechanical signals, has been linked to susceptibility to lethal arrhythmias in human heart failure (HF) as well as in human chronic atrial fibrillation (cAF). In addition, early afterdepolarizations (EADs), a type of aberrant cellular behavior that causes spontaneous slowing or reversal of normal repolarization, have been implicated as an arrhythmogenic trigger in human hypertrophic cardiomyopathy (HCM). Abnormal myofilament dynamics has been observed in human HF, HCM, and cAF, but whether this aberrant behavior alters the formation of alternans or EADs remains unknown.

To address this gap in understanding, a computational modeling approach was taken. Three mechanistically-based bidirectionally coupled human electromechanical myocyte models were constructed, under the conditions of HF, HCM, or cAF. Our goal was to elucidate whether aberrant myofilament dynamics modulate the cellular drivers of arrhythmogenesis in human cardiac disease. In simulations with our human HF ventricular myocyte model, we found that the magnitudes of force, calcium, and action potential voltage alternans were modulated by heart failure induced-remodeling of mechanical parameters and sarcomere length due to the presence of myofilament feedback (MEF) at clinically-relevant pacing rates. In simulations with our human HCM ventricular myocyte model, we found that incorporating MEF diminished the degree of repolarization reserve reduction necessary for EADs to emerge and increased the frequency of EAD occurrence, especially at faster pacing rates. Longer sarcomere lengths and HCM-induced enhanced

thin filament activation diminished the effects of MEF on EADs. Finally, in simulations with our human cAF atrial myocyte model, we found that MEF, via cooperativity in Troponin C buffering of cytoplasmic Ca^{2+}, diminished the magnitude of action potential duration alternans. Also, enhanced thin filament activation, via either cAF-induced myofilament remodeling or longer sarcomere lengths, enhanced action potential duration alternans.

Together, this thesis provides evidence that myofilament protein dynamics mechanisms play an important role in EAD and alternans formation, suggesting that targeting MEF or reversing disease induced myofilament remodeling may be alternative treatment approaches for prevention of arrhythmia in cAF patients.

Advisor: Natalia A. Trayanova, Ph.D.

Readers: Natalia A. Trayanova, Ph.D., Raimond L. Winslow, Ph.D.

Thesis Committee: Feilim Mac Gabhann, Ph.D., Natalia A. Trayanova, Ph.D., Raimond L. Winslow, Ph.D.

Acknowledgements

The work presented here in my thesis would not have been possible with the support and mentorship of my advisor, Dr. Natalia Trayanova. I thank her for her guidance and for teaching me how to become a better scientist and writer. I would also like to thank the other members of my thesis committee, Dr. Raimond Winslow and Dr. Feilim Mac Gabhann, who have provided invaluable insight and guidance on my thesis work. I thank the Computational Cardiology Lab (Trayanova Lab) for their help over the years and for being a fantastically fun group of friends. I will miss the lab pushups, the "Crying Tom Brady" birthday cards, and the happy hours at Rocket to Venus. In particular, I would like to thank Dr. Patrick Boyle for his helpful critique of my papers, posters, and presentations, Robert Blake for creating and editing the "mech_bench" code, and Dr. Yasser Aboelkassem for his help brainstorming ideas and discussing the minutia of myofilament processes.

Most importantly, I would like to thank my fantastic family, without whom I would have never had the confidence, support, nor opportunity to achieve all of the many successes in my life. Billy, Mom and Steve, Dad and Jill, Gram and Gramps, and GBob, to you I owe a lifetime of thanks. Thank you for your unconditional love and encouragement during the best and the worst of times, as well as all of the times in between. I am truly blessed to have such an amazing family. And finally, I would like to thank my wonderful friends who have turned Baltimore into my home.

Contents

List of Tables

List of Figures

Chapter 1 Introduction

1.1 Organization and Summary of the Thesis

The organization of this thesis, which investigates the myofilament dynamics mechanisms that modulate cellular drivers of arrhythmogenesis in human cardiac disease, is as follows:

Chapter 2 presents a brief background of cardiac electrophysiology and electromechanics, which are crucial for understanding the research presented in this thesis. In addition, general information regarding arrhythmogenesis in cardiac disease and its cellular drivers is also included. Information regarding arrhythmogenesis and its cellular mechanisms in human heart failure (HF), hypertrophic cardiomyopathy (HCM), and atrial fibrillation (AF) are discussed in Section 1 of *Chapters 4, 5, and 6* respectively.

In *Chapter 3*, we explain our rationale for using computational modeling approaches to understand the mechanisms underlying the cellular drivers of arrhythmogenesis. Additionally, general approaches for modeling the human cardiomyocyte are discussed.

Chapter 4 describes our methodology to build a mechanistically-based electromechanical model of the human ventricular myocyte and to incorporate HF-induced ionic and myofilament remodeling. We used this model to study the mechanisms linking force alternans to action potential voltage alternans (a known cellular driver of arrhythmogenesis) in the human failing myocyte, with emphasis on those acting at the clinically-relevant pacing rates of <110 bpm.

In *Chapter 5*, we explored whether myofilament protein dynamics mechanisms modulate EAD formation (another type of cellular driver of arrhythmogenesis) in human HCM for varying degrees of reduced repolarization reserve, and to uncover how these

mechanisms are affected by pacing rate, sarcomere length, and the degree of HCM-induced myofilament remodeling. This investigation utilized our previously developed model of the human ventricular myocyte (described in *Chapter 4*), which we modified to incorporate HCM-induced ionic and myofilament remodeling.

In *Chapter 6*, we developed a biophysically-accurate electromechanical model of the human atrial myocyte and incorporated AF-induced ionic and myofilament remodeling. Using this model, we investigated whether remodeling of myofilament protein dynamics mechanisms modulate action potential duration alternans (also a cellular driver of arrhythmogenesis) in cAF. We also aimed to uncover how these mechanisms are affected by sarcomere length and the degree of AF-induced myofilament remodeling.

Finally, *Chapter 7* concludes this thesis by discussing the significance of the results and findings in *Chapters 4-6* and by expounding on the future directions of this research.

Chapter 2 Background:

Basic Cardiac Electrophysiology and Electromechanics

2.1 Blood Flow and the Healthy Human Heart

The purpose of the heart is to pump blood throughout the body to bring oxygen and essential nutrients to cells and to remove carbon dioxide and waste products from them. The human heart consists of 4 chambers: the right atrium, the left atrium, the right ventricle, and the left ventricle as shown in Figure 2.1. In healthy hearts, deoxygenated blood is carried to the right atrium from the inferior and superior vena cavae, which receive blood from the other veins in the systemic circulatory system. This deoxygenated blood passes through the tricuspid (right atrioventricular) valve into the right ventricle, where it is propelled past the pulmonary valve into the pulmonary arteries due to the coordinated contraction of the cardiac cells (cardiomyocytes) in the right ventricle. From the pulmonary arteries, the blood moves via the arterioles into the pulmonary capillary bed where carbon dioxide in the blood is exchanged for oxygen contained in the alveoli of the lungs. The newly oxygenated blood returns to the heart via the pulmonary venules and veins. After entering the left atrium, it passes through the mitral valve into the left ventricle where is it propelled past the aortic valve and into the aorta due to contraction of the left ventricle. The oxygenated blood then moves through the arteries and arterioles of the systemic circulatory system until it reaches the systemic capillary bed. Oxygen is delivered to the cells and carbon dioxide moves from

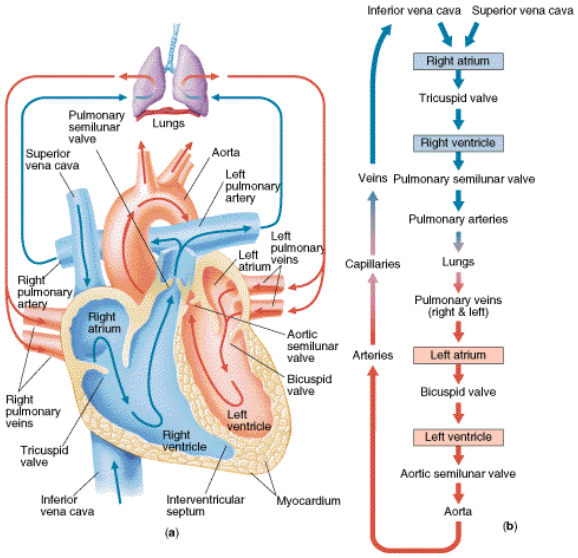

Figure 2.1 Cardiac Blood Flow

This figure was provided by https://biologyresearch2013.wordpress.com/activity-4/

the cells into the blood. The now deoxygenated blood returns via the venules to the veins and ultimately the right atrium.

2.2 Electrophysiology and Electromechanics of the Healthy Human Heart

2.2.1 Normal Cardiac Rhythm

Proper blood flow in the human body relies on ability of the heart's four chambers to work as a synchronized unit, thus contracting and pumping blood in a coordinated manner. To facilitate this coordinated contraction, timed electrical signals propagate in a regularly timed manner along a specialized conduction pathway as shown in Figure 2.2.1. In the healthy human heart, the signals are initiated by specialized pacemaker cells in the sinoatrial node, located at the roof of the right atrium. These electrical signals propagate through the cardiomyocytes in right and left atrium via intracellular gap junctions until they arrive at the atrioventricular node, located at the floor of the right atrium between the atria and ventricles. The conduction of the signals slows in

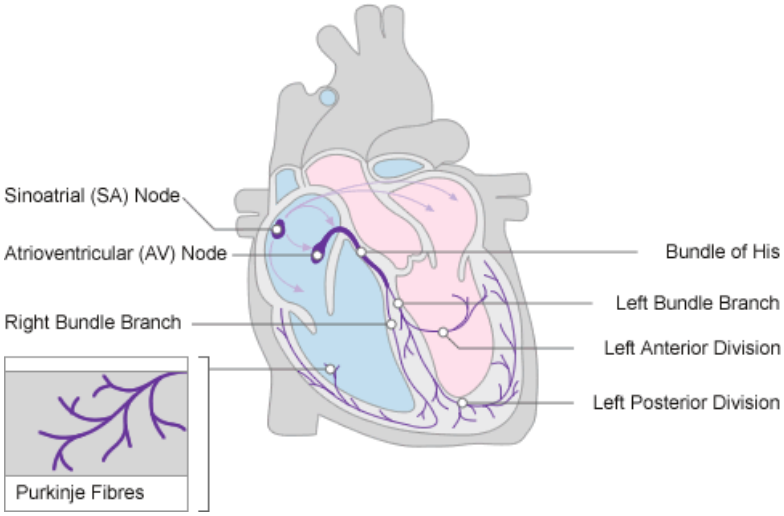

Figure 2.2.1 Cardiac Conduction System

This figure was provided by http://www.nottingham.ac.uk/nursing/practice/resources/cardiology/function/conduction.php/

the atrioventricular node to ensure completion of contraction in the atria and to provide sufficient time for the ventricles to fill with blood. The electrical impulses then propagate to the bundle of His, which allows them to cross the fibrous tissue separating the atria and ventricles and arrive at the Purkinje fibers. From there, the electrical signals travel down the fast conducting Purkinje fibers until they reach and activate the working ventricular cardiomyocytes. This precisely orchestrated electrical signaling system allows the mechanical contraction of the chambers to occur synchronously, allowing the heart to efficiently pump blood throughout the body.

2.2.2 Cardiac Action Potential

The electrical signals produced and propagated throughout the cells of the heart are called action potentials (APs). An AP is characterized by the depolarization and repolarization of the excitable, semipermeable cell membrane (called the sarcolemma). The voltage across the sarcolemma is called the transmembrane potential (V_m) and is changed over time as ions flow into and out of the cardiomyocyte due to ion channels, transporters, and exchangers. When V_m is negative (positive), there is a net negative (positive) charge inside the cell relative to the extracellular space which is located outside the cell beyond the sarcolemma boundary. Although the AP is unique for each type of cardiomyocyte, there are two main types of APs, that experienced by the pacemaker cells in the sinoatrial node, and that experienced by the working cardiomyocytes such as ventricular and atrial cells. Since the work in this thesis pertains to atrial and ventricular cells, this background will focus on the APs of those cells.

There are five distinct phases in the AP of working cardiomyocytes as shown in Figure 2.2.2. In the first phase, called phase 4 or the resting phase, the cardiomyocyte has a resting V_m of approximately -80 mV, which occurs due to the electrochemical balance of ions, predominantly sodium, calcium, and potassium. In this phase, the sodium-calcium exchanger (I_{NaCa}), the sodium-potassium pump (I_{NaK}), and the inward rectifying potassium current (I_{K1}) are active, although I_{K1} is dominant. As a result, the V_m during phase 4 is close to the reversal potential for potassium (-90 mV). When the second phase (called phase 0) occurs, the sodium channel (I_{Na}) opens, allowing positively charged sodium ions (Na^+) to enter the cell, resulting in a positive inward current that raises V_m toward the Nerst potential for sodium (55 mV). When I_{Na} inactivates, transiently activated potassium channels open (I_{to}) briefly allowing positively charged potassium ions (K^+) to exit the cell, causing a short period of repolarization (phase 1). In phase 2, L-type calcium channels (I_{CaL}) open, allowing positively charged calcium ions (Ca^{2+}) to enter the cell. In addition, I_{NaCa} and I_{NaK} operate in the inward direction (produce positive inward current), and the slow delayed outward potassium current (I_{Ks}) begins to activate, allowing potassium ions to leave the cell. Together the balance of these ion currents, cause the "plateau" of V_m in the AP. In the final phase (phase 3), the outward rapid rectifier

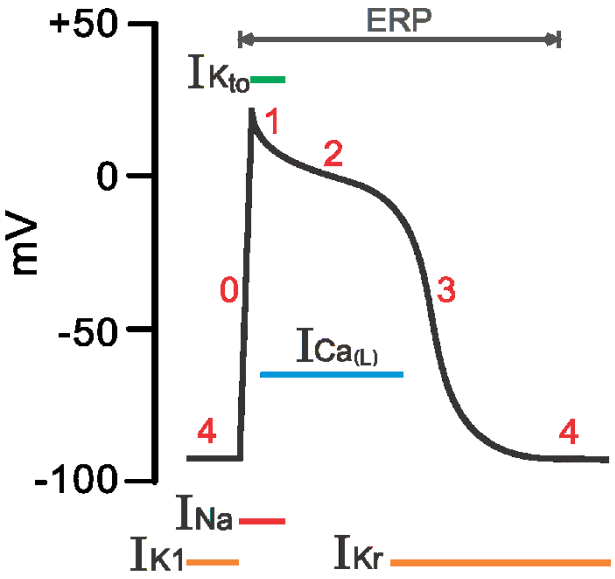

Figure 2.2.2 Cardiac Action Potential

This figure was provided by
http://www.cvphysiology.com/Arrhythmias/A006/

potassium current (I_{Kr}) and I_{K1} open, while I_{Ks} continues to be open, and I_{CaL} inactivates. This causes a swift depolarization of V_m. Once V_m depolarizes back to its resting value (-80 mV), the cardiomyocyte has returned back to phase 4. Although atrial and ventricular cells both go through the five distinct AP phases described above, there are slight differences. However, the primary difference is that the plateau in V_m in phase 2 is shorter in atrial cells than in ventricular cells.

2.2.3 Excitation-Contraction Coupling

The process by which electrical APs generate contractile force in cardiomyocytes is called excitation-contraction coupling (shown in Figure 2.2.3.1) and occurs due to the interaction of free intracellular Ca^{2+} ions with myofilament protein complexes. As described in the preceding section, during phase 2 of the AP, Ca^{2+} ions pass through the sarcolemma via I_{CaL} and enter a region of the cell next to the sarcolemma that is also adjacent to the sarcoplasmic reticulum (SR) and contains

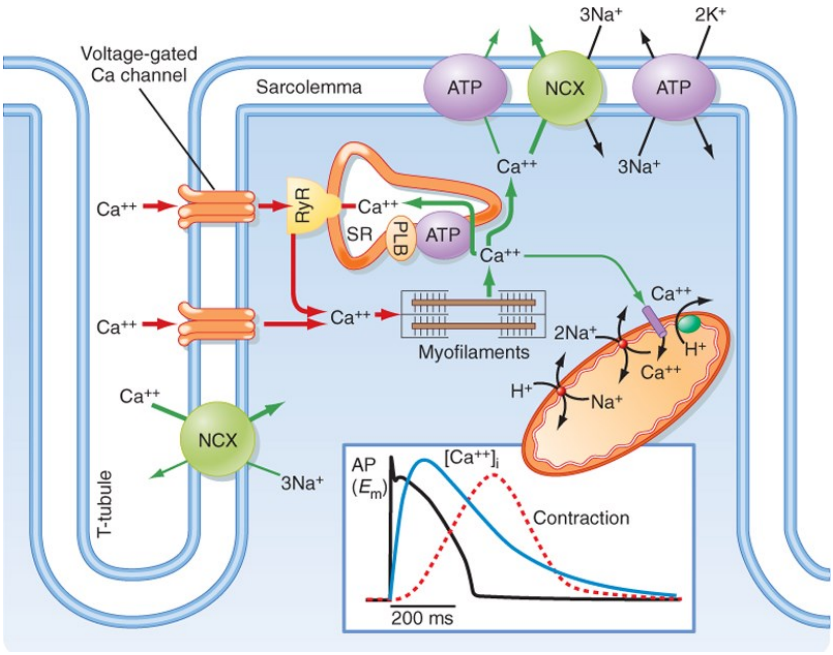

Figure 2.2.3.1 Excitation Contraction Coupling

Reprinted with permission from Nature Publishing Group: Bers *et al (Bers, 2002)*

ryanodine receptors. There are a variety of names given to this region, including dyadic space, subspace, junctional space, and cleft. The Ca^{2+} ions bind to the ryanodine receptors in this region, causing a conformational change that allows a rapid release of large amounts of Ca^{2+} ions stored in the SR (I_{rel}). This positive feedback process is termed 'calcium induced calcium release'. When the Ca^{2+} ions are release from the SR and enter the cleft, they diffuse into the intracellular space, where the concentration of Ca^{2+} ions is termed $[Ca]_i$. These free Ca^{2+} ions in the intracellular space can bind to Troponin C or to other Ca^{2+} buffers like calmodulin. When Ca^{2+} binds to Troponin C, a conformation change occurs in Troponin I, causing tropomyosin to leaves its groove on the actin filament. This removes the inhibitory effect of Troponin I, making it possible for myosin heads to bind to actin, and thus making crossbridge (XB) formation and cycling permissible.

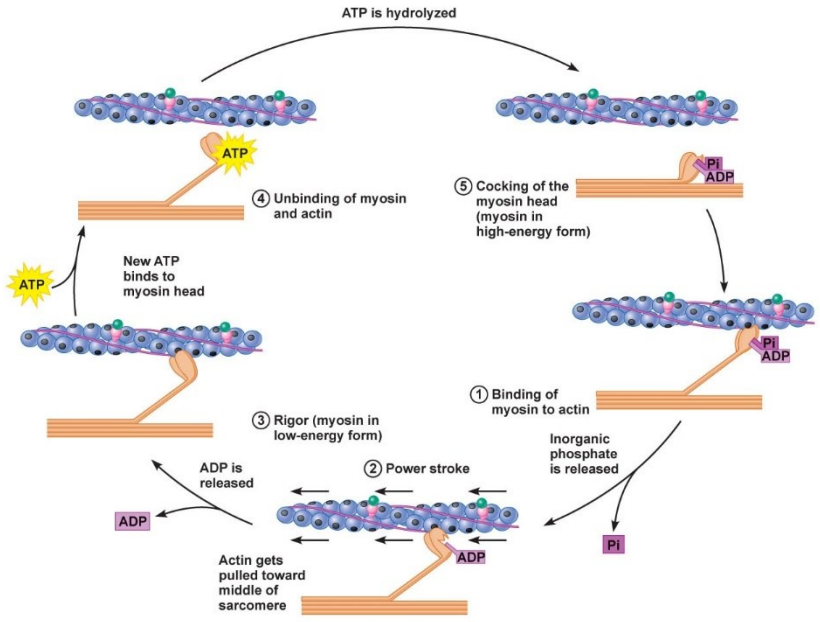

Figure 2.3.2.2 Crossbridge Cycling

This figure was provided by http://droualb.faculty.mjc.edu

In the first step of XB cycling, the myosin head, which is already attached to an ADP-P_i, weakly binds to the now available actin binding site as shown in Figure 2.3.2.2. This is considered a weakly bound crossbridge, since the myosin head forms a bridge between the thin myofilament (actin) and the thick myofilament (myosin) that is weak in strength. Then P_i is released from the complex, causing the myosin head to be strongly bound to the actin site. Next, the myosin head undergoes a conformational rotation, resulting in active force generation. This step is often called the "power stroke." ADP is then released from the myosin head, allowing it to dissociate from the actin filament and bind preferentially to ATP. The ATP is then hydrolyzed by the myosin ATPase, resulting again in a myosin-ADP-P_i configuration. This cycle of crossbridge formation can occur at all of the other sites along the actin filament where myosin heads are nearby, provided that the actin site has been made available by Ca^{2+} binding to Troponin C. The cumulative active force generation produced by crossbridge cycling allows the sarcomere, the smallest structural unit of a cardiac muscle fiber, to shorten. Shortening of the thousands of sarcomeres that make up a single cardiomyocyte, leads to contraction of the myocyte.

Once phase 3 of the AP begins, I_{CaL} closes and Ca^{2+} ions are no longer being released from the SR. The free Ca^{2+} ions in the intracellular space are pumped back into the SR by an ATPase calcium pump (SERCA2a; current is referred to as I_{up}), or moved from the intracellular to extracellular space by I_{NaCa} or the sarcolemmal calcium pump ($I_{Ca,P}$). The Ca^{2+} ions that enter the SR are then bound to the calcium binding protein calsequestrin, to keep the calcium concentration gradient low, allowing more Ca^{2+} ions to enter the SR. Since the calcium influx into the intracellular space has abated, the above-mentioned processes become dominant and $[Ca]_i$ begins to diminish. Since Ca^{2+} unbinds

from Troponin C once the myosin head dissociates from the actin head and since $[Ca]_i$ is becoming progressively smaller during phase 3, fewer and fewer Ca^{2+} ions bind to Troponin C, causing more and more actin sites to become unavailable to myosin heads. Thus, as $[Ca]_i$ decreases, active force generation diminishes and sarcomeres begin to relax and return to their resting length. Once the next AP begins, the calcium cycle repeats and the cycle of muscle contraction and relation occurs again.

2.2.4 Mechanoelectric Feedback

While excitation-contraction coupling refers to the process by which electrical activation leads to mechanical contraction, mechanoelectric feedback (MEF) is the process by which mechanical activity alters electrical activity. MEF occurs at both the organ scale and the cellular scale. Details on MEF occurring at the organ scale can be found in this review by Pfeiffer *et al* (Pfeiffer et al., 2014). However, since the work in this thesis focuses on the mechanisms underlying the cellular drivers of arrhythmogenesis, this background will focus on MEF that occurs at the cellular scale. One mechanism of MEF at the cellular scale is stretch-activated currents. These ionic currents are mechanosensitive, meaning that the opening of the channels is modulated by cell stretch. A second mechanism of MEF is cell to cell coupling via gap junctions at intercalated disks, which occur at the intersection of two cells. Mechanical loading can increase the expression of gap junction proteins, which can lead to increased conduction velocity, thus altering electrical activity (Gopalan et al., 2003; Zhuang et al., 2000). A final mechanism of MEF is myofilament calcium sensitivity and cooperativity. It is well known that there is a steeply nonlinear relationship between force and calcium in cardiomyocytes and that the amount of force generated is

highly dependent on the amount of calcium present and on sarcomere length. The nonlinear relationship between calcium and active force generation is believed to occur because strongly bound crossbridges can shift tropomyosin into a more favorable location on the thin filament, dramatically enhancing the binding affinity of nearby myosin heads to actin sites. This enhanced Ca^{2+}-Troponin C binding affinity is also modulated by sarcomere length. Thus, if sarcomere length is altered due to a mechanical perturbation, myofilament calcium sensitivity and cooperativity are both modulated. This would change the availability of calcium in the intracellular space, thus altering calcium handling in the cardiomyocyte and the progression of the AP. It is this final mechanism of MEF, myofilament calcium sensitivity and cooperativity, that will be investigated in this thesis.

2.3 Electrophysiology and Electromechanics of the Diseased Human Heart

Cardiac disease is a common problem in Americans and others worldwide. While cardiac disease can take many forms, the work in this thesis will focus on the following three: HF (*Chapter 4*), HCM (*Chapter 5*), and AF (*Chapter 6*). Although details of each are described in the first section of their respective chapters, these cardiac diseases share several important features. First, the cardiomyocytes in the hearts of patients with these diseases have been shown to have electrical and mechanical remodeling (also referred to as ionic and myofilament remodeling). Additionally, patients with HF and HCM have an increased susceptibility to lethal ventricular arrhythmia, while AF is a type of chaotic cardiac arrhythmia that occurs in the atria.

2.3.1 Arrhythmias

A cardiac arrhythmia is defined as a condition in which the regular pattern of electrical propagation is deranged. Arrhythmias can occur when the heart is beating too quickly (tachyarrhythmias) or too slowly (bradyarrhythmias). They can be caused by altered electrical impulse formation or conduction.

Abnormal electrical impulse formation can occur due to a disruption in parasympathetic or sympathetic activity, abnormal automaticity (such as ectopic foci), or triggered activity. Triggered activity can be caused by early afterdepolarizations (EADs) or delayed afterdepolarizations (DADs). EADs, which are a focus of *Chapter 5*, are discussed in more detail in *Section 2.3.3* below.

Irregular electrical impulse conduction includes slow conduction, conduction block, and reentry. Reentry occurs when an electrical wave encounters an area of conduction block, is able to propagate around the area of block, and always encounters excitable tissue in the direction of propagation, including when it reaches previously refractory tissue. Therefore, the distance traveled by the electrical wave during one refractory period (wavelength) must always be shorter than the length of the reentrant circuit. Reduced electrical conduction and shortened APD can both diminish the wavelength and thus promote reentry. Reentry can be either anatomical or functional. Anatomical reentry occurs when there is a physical, non-conducting area of block, such as scar, that the electrical wave must propagate around. Functional reentry occurs when the electrical wave propagates around a small unexcited (though excitable) region of tissue. This can occur due to spatial heterogeneity in excitability or refractoriness. Action potential

duration (APD) alternans and action potential voltage (APV) alternans have both been shown to increase spatial dispersion of repolarization across the myocardium, leading to unidirectional conduction block and reentry. APD alternans, which are the focus of *Chapter 6*, and APV alternans, the focus of *Chapter 4*, are both described in more detail in *Section 2.3.2* below.

2.3.2 Cardiac Alternans

Alternans is defined as the beat-to-beat alteration in cardiac electrical or mechanical signals and can occur at the tissue level or at the cellular level. Types of tissue level alternans that have been observed in humans and that have been linked to susceptibility to lethal arrhythmias include T-wave alternans and pressure alternans. T-wave alternans occurs when there is beat-to-beat variation in the amplitude of the T-wave of an electrocardiogram (ECG). Studies have shown that small amplitude T-wave alternans (microvolt T-wave alternans; MTWA) is driven by APV alternans in human heart failure (Bayer et al., 2010; Narayan et al., 2008), which occurs on the cellular level when the V_m amplitude during phases 2 and 3 of the AP oscillates from beat to beat. APV alternans is driven by alternans in intracellular calcium transient amplitude, which in turn occurs due to altered SR calcium uptake or release (Bayer et al., 2010). Pressure alternans are defined as the beat-to-beat oscillation of the amplitude of systolic pressure and can be measured noninvasively with an infrared finger photoplethysmograph. At the cellular level, pressure alternans are thought to arise from force alternans, defined as the beat-to-beat oscillations in the strength of active force production in cardiomyocytes. The molecular mechanisms

underlying APV alternans and whether it is linked to force alternans is further investigated in *Chapter 4*.

Another type of cellular level alternans is APD alternans, defined as the beat-to-beat oscillation in APD, which has been shown to be an important clinical marker for AF risk (Narayan et al., 2002). APD alternans have been shown to be driven by calcium transient alternans due to altered ryanodine receptor (RyR) kinetics and down regulation of the I_{CaL}. Although the ionic mechanisms of APD alternans have been investigated, little is known about the effects of myofilament protein dynamics on APD-ALT in human AF, which we investigate in *Chapter 6*.

2.3.3 Afterdepolarizations

EADs are a type of aberrant cellular behavior that cause spontaneous (yet triggered) slowing or reversal of normal repolarization. EADs occur during late phase 2 or phase 3 of a cardiac AP and can lead to several rapid APs or a prolonged series of APs. In contrast, DADs occur in late phase 3 or early phases 4 of an AP. Since we investigate the mechanistic basis of EADs in human HCM in *Chapter 5*, we will focus on EADs in this background section. EADs occur more commonly when APD is increased and require reduced repolarization reserve to be present. Reduced repolarization reserve can result from a decreased outward current, an increased inward current, or a combination of both. Due to these compromised circumstances, a current that progressively increases as V_m depolarizes can potentially overcome and reverse repolarization. I_{CaL} and I_{NaCa} both fit this positive feedback criterion and are the major currents normally implicated in EAD formation. If

activity of any of the potassium rectifying channels is diminished, APD lengthens and EAD likelihood increases due to a reduction in the repolarizing current.

Chapter 3 Background:

Computational Modeling

3.1 Rationale for Computational Modeling of Cardiac Myocytes

Computational modeling of cardiac myocytes is the use of computer algorithms and tools to unveil mechanisms underlying sub-cellular cardiac phenomena to enhance our understanding of cardiac disease and potentially aid in the development of improved therapeutic approaches. Computational modeling was used for all aspects of the work in this thesis.

Computational modeling was used in this thesis because it has several advantages over traditional ("wet lab") experimental approaches. First, using computer simulations allows the scientist to make predictions regarding complex phenomena that are too difficult or significantly more difficult to study experimentally. Second, computational modeling can illuminate the significance of individual parameters in a particular system, which may difficult or impossible to isolate using traditional approaches. Third, computational modeling allows the scientist to study a system hypothetically, which is often cheaper and faster than studying the system experimentally. This can help aid in the design of traditional experiments that can then be used to confirm the computational findings.

3.2 Modeling Cell Membrane Kinetics

The first mathematical model of an excitable cell membrane was published in 1952 by Hodgkin and Huxley in a seminal paper titled "A quantitative description of membrane current and its application to conduction and excitation in nerve" (Hodgkin and Huxley, 1952). Their model of the squid giant axon membrane was able to accurately reproduce the

experimentally measured AP for the first time. In 1962, Denis Noble built upon the work of Hodgkin and Huxley and published the first model of a cardiac AP (Noble, 1962). The basic tenets are as follows. The total membrane current is divided into capacitive and ionic components as shown in Equation 3.2 below:

$$I_m = C_m \frac{dV_m}{dt} + I_{ion} + I_{trans}$$

(Equation 3.2)

where I_m is the total membrane current density, C_m is the membrane capacitance per unit area, V_m is the transmembrane potential, I_{ion} is the ionic current density, and I_{trans} is the current density of a transmembrane stimulus. In the Hodgkin and Huxley formulation, I_{ion} is comprised of the summation of I_{Na}, I_{Kr}, and a background leak current (I_l). The ionic conductances of I_{Na} and I_{Kr} depend on gating variables that have opening and closing rates dependent on V_m. These current equations were derived by fitting mathematical equations to the experimental measurements Hodgkin and Huxley obtained from voltage clamp experiments. Today, we know there are many more currents involved in the cardiac AP, as described in *Section 2.2.2* above. Modern ionic models incorporate these currents in their formulation of I_{ion}. In addition, modern ionic models incorporate key features that enable them to model different animal species (including humans), as well as different cell types (such as atrial and ventricular cells). The ionic models used in the three studies in this thesis are described in their respective methods sections.

3.3 Modeling Calcium Handling

Modern ionic models differ slightly in how they represent the flow of Ca^{2+} ions in and out of the cell. Generally, Ca^{2+} ions enter the cell's diadic space via I_{CaL} and then diffuse into the intracellular space, where they are eventually pumped back into the SR via I_{up} or back out of the cell via I_{NaCa} and $I_{Ca,P}$. Cardiac ionic models generally represent these regions (diadic, intracellular, SR) as separate lumped compartments within the cell, each with its own distinct Ca^{2+} concentration and its own distribution of ionic currents. Some older models do not include the representation of the diadic space. Some newer models also include a space called the sub-sarcolemma that lies adjacent to the sarcolemma on the interior of the cell but is distinct from the diadic cleft. The ionic models in *Chapters 4 and 5* does not contain a sub-sarcolemmal space, while the model in *Chapter 6* does. In addition, some models sub-divide the SR into junctional and network components. Simple diffusion of Ca^{2+} ions occurs between the compartments that are not separated by membranes, such as the SR.

3.4 Modeling Cardiac Myofilament Dynamics

Cardiac myofilament models are designed to quantitatively capture the interaction between the active and myosin filaments, and calcium based activation of them. The earliest known crossbridge cycling model was developed by Huxley (Huxley, 1957) in 1957. It consisted of only two states for the XB, attached and detached, and the rate constants were only dependent on the relative positions of the actin binding site and the equilibrium position of the closest XB. Models range from the 2 XB states found in the

Huxley model to 7 XB states in a model developed by Pate and Cooke (Pate and Cooke, 1986). Although models with more states are able to more accurately represent experimentally observed biochemical XB states, they are computationally expensive. Therefore, modern myofilament models aim to balance biophysical accuracy with computational efficiency. The Rice *et al* model (Rice et al., 2008) was chosen for the work in this thesis since it optimized the balance of accuracy and efficiency. In addition, the Rice *et al* model incorporates important calcium-based activation and sarcomere length-based sensitivity mechanisms. An extensive review of this topic can be found in Trayanova and Rice (Trayanova and Rice, 2011b).

Chapter 4 Study 1:

Rate-dependent force, intracellular calcium, and action potential voltage alternans are modulated by sarcomere length and heart failure induced-remodeling of thin filament regulation in human heart failure: A myocyte modeling study

This study has been published in Progress in Biophysics and Molecular Biology (Zile and Trayanova, 2016) and reprinted with permission from Elsevier publishing.

4.1 Introduction

Ventricular arrhythmias are the most common cause of sudden cardiac death, resulting in > 300,000 US deaths annually (Lloyd-Jones et al., 2009). The standard procedure for preventing sudden cardiac death is to implant a cardioverter defibrillator (ICD), which delivers a strong electric shock to terminate arrhythmias. Since current methods for identifying patients who require ICDs have only been partially successful (Bardy et al., 2005), there is a need for noninvasive predictors with high sensitivity and specificity. Indeed, robust methods for stratifying the risk of lethal cardiac arrhythmias would decrease morbidity and mortality in patients with cardiovascular disease and reduce health care costs (Goldberger et al., 2011). Approaches for stratifying risk of cardiac arrhythmias involve testing for abnormalities in the ECG, then using the results to identify patients who would benefit from ICD therapy. ECG-based risk stratification methods scan for abnormalities in ventricular depolarization (late potentials (Kuchar et al., 1987), fractionated QRS complexes (Das et al., 2006)) and repolarization (T-wave alternans (Rosenbaum et al., 1994), and QT variability, dispersion, and instability (Berger et al., 1997; Chen et al., 2011; Chen et al., 2013; Chen and Trayanova, 2012; Couderc et al., 2007)). However, the mechanisms underlying these ECG indices, and their relationship to lethal cardiac arrhythmias, are not fully understood. This lack of knowledge likely explains why results of clinical trials to correlate surface EGG indices to lethal cardiac arrhythmias are often contradictory (Goldberger et al., 2011).

Of the above ECG indices, T-wave alternans have received possibly the most attention. Research has reported a strong correlation between increased arrhythmia risk and the presence of T-wave alternans (Narayan, 2006; Qu et al., 2010), defined as the beat-to-beat alternation of the timing or shape of the repolarization wave of the ECG. In the clinical setting, testing for Microvolt T-wave Alternans (MTWA) has been found to be a risk marker for lethal ventricular arrhythmias and sudden cardiac death (Cutler and Rosenbaum, 2009), to have high negative predictive power (Narayan, 2006) and to be particularly promising in dichotomizing patients that would and would not benefit from ICD therapy (Bloomfield et al., 2006; Hohnloser et al., 2009). However, the mechanistic basis of MTWA preceding lethal ventricular arrhythmias has long been under debate. Until the last decade, it was believed that a steep action potential duration (APD) restitution (>1) at rapid heart rates (Weiss et al., 2006) produces alternans in APD that underlie T-wave alternans and the genesis of fibrillation (Pastore et al., 1999). However, MTWA is most successful in stratifying risk in patients at near-resting heart rates <110 bpm, where APD restitution is flat (Narayan et al., 2007). Computational models of the LV wall in combination with clinical data revealed that abnormal handing of intracellular calcium underlies alternans in action potential voltage (APV-ALT), defined as the oscillation of the plateau voltage of the action potential, which results in MTWA at moderate heart rates, i.e. <110 bpm (Bayer et al., 2010; Narayan et al., 2008). Thus APV-ALT is the cell-level driver of MTWA at these rates under the conditions of heart failure.

Alternatively, noninvasively measured pressure alternans, defined as the beat-to-beat oscillation of the amplitude of systolic pressure, has been found to be a predictor of worsening heart failure and increased cardiac mortality (Hirashiki et al., 2010; Hirashiki et

al., 2006; Ito et al., 2012; Kashimura et al., 2014; Kim et al., 2014; Selvaraj et al., 2011). Pressure alternans also occurs simultaneously with MTWA in patients at near resting heart rates, thus indicating that pressure alternans, which have higher signal-to-noise ratio (Selvaraj et al., 2011), may be a better predictor of the propensity for ventricular arrhythmias and sudden cardiac death, however the mechanisms remain unknown.

At the cellular level, pressure alternans arise from force alternans (FORCE-ALT), defined as the beat-to-beat oscillations in the strength of active force production in cardiac muscle. APV-ALT at heart rates <110 bpm has been found to be driven by beat-to-beat fluctuations in the amplitude of the intracellular calcium concentration (CA-ALT) (Bayer et al., 2010; Narayan et al., 2008). CA-ALT has also been shown to underlie force alternans (FORCE-ALT), in animal experiments with cardiac muscle preparations (Kihara and Morgan, 1991; Kotsanas et al., 1996; Lab and Lee, 1990; Orchard et al., 1991) and perfused hearts (Brooks et al., 1994; Lee et al., 1988), but only at fast pacing rates. Clearly, to date, no studies have investigated FORCE-ALT in human myocytes at rates <110 bpm, and although calcium dysregulation is a likely candidate, the exact mechanistic link between APV-ALT and FORCE-ALT in the failing human myocyte at the clinically important near-resting heart rates remains unknown. Therefore, our goal was to investigate the mechanisms linking FORCE-ALT to APV-ALT in the human failing myocyte, with emphasis on those acting at the clinically-relevant pacing rates of <110 bpm, and to uncover how the link between FORCE-ALT and APV-ALT is affected by various physiological conditions such as sarcomere length and heart failure induced-remodeling of mechanical parameters.

4.2 Methods

4.2.1 Human Electromechanical Myocyte Model

To uncover the mechanism linking FORCE-ALT to APV-ALT, a mechanistically-based human electromechanical myocyte model was used. The electromechanical model combined the human endocardial ventricular membrane kinetics model by ten Tusscher *et al* (ten Tusscher and Panfilov, 2006) and the myofilament dynamics model by Rice *et al* (Rice et al., 2008). The 2006 ten Tusscher *et al* formulation was used because it incorporated an extensive description of intracellular calcium handling, which was found to be critical in the development of APV-ALT in previous studies of human heart failure (Bayer et al., 2010; Narayan et al., 2008). The Rice *et al* model, which describes the activation of the thin filament by intracellular calcium binding to Troponin C as well as thin filament binding to thick filament crossbridges (XBs) using a 5 state Markov model, was chosen because it was computationally efficient while incorporating important biophysical detail and cooperativity mechanisms. Since the Rice *et al* myofilament model was developed based on rabbit data we adjusted it to match human force data. This was done by modifying XB cycling and calcium-based thin filament activation parameters following the approach in de Oliveira *et al* (de Oliveira et al., 2013). To account for the differences between the ionic model used by de Oliveira *et al* (the 2004 formulation of the ten Tusscher *et al* model (ten Tusscher et al., 2004)) and by us (ten Tusscher and Panfilov, 2006), additional modifications to calcium-based thin filament activation were made. Specifically, we decreased thin filament activation by reducing k_{on}, a parameter regulating the binding affinity of Ca to high and low regulatory sites on Troponin C, to 95% of the

baseline value used in Rice *et al*, in order to increase the time to peak force value so that it fell in the physiological range of human values (Mulieri et al., 1992; Pieske et al., 1996).

The ionic and myofilament models were strongly coupled by incorporating myofilament feedback on calcium dynamics (Figure 4.1); this was done by incorporating a dynamic term for troponin buffering of intracellular calcium ($[Ca]_{Troponin}$) using the approach in Rice *et al*. Strongly coupling the models with a dynamic representation of $[Ca]_{Troponin}$ was important and necessary, because it has been shown to be crucial for accurately reproducing contractile experiment data in myocyte simulations (Ji et al., 2015). This $[Ca]_{Troponin}$ term represents the amount of calcium bound to troponin and incorporates the cooperativity of calcium-troponin binding due to strongly bound nearby XBs. However, in the 2006 ten Tusscher and Panfilov model, troponin buffering of calcium is combined with calmodulin buffering of calcium and is represented using a steady state approximation. Therefore, to incorporate feedback from the myofilament model to the ionic model, we separated the combined buffering term in ten Tusscher and Panfilov into two terms. The $[Ca]_{Troponin}$ term from Rice *et al*, calculated using ordinary differential equations, was used for troponin buffering of calcium, and a steady state approximation was used for calmodulin buffering of calcium ($[Ca]_{Calmodulin}$) using the same approach as de Oliveira *et al*. The following equation from de Oliveira *et al* was used to update the intracellular calcium concentration in the ionic model, using the $[Ca]_{Troponin}$ term calculated by the myofilament model, at each time step:

$$[Ca]_{Total} = [Ca]_i + [Ca]_{Calmodulin} + [Ca]_{Troponin}$$

(Equation 4.1)

where $[Ca]_{Total}$ is the total calcium in the cytoplasm, $[Ca]_i$ is the free calcium in the cytoplasm, $[Ca]_{Calmodulin}$ is the total calcium buffered by calmodulin in the cytoplasm, and $[Ca]_{Troponin}$ is the total calcium bound to Troponin C.

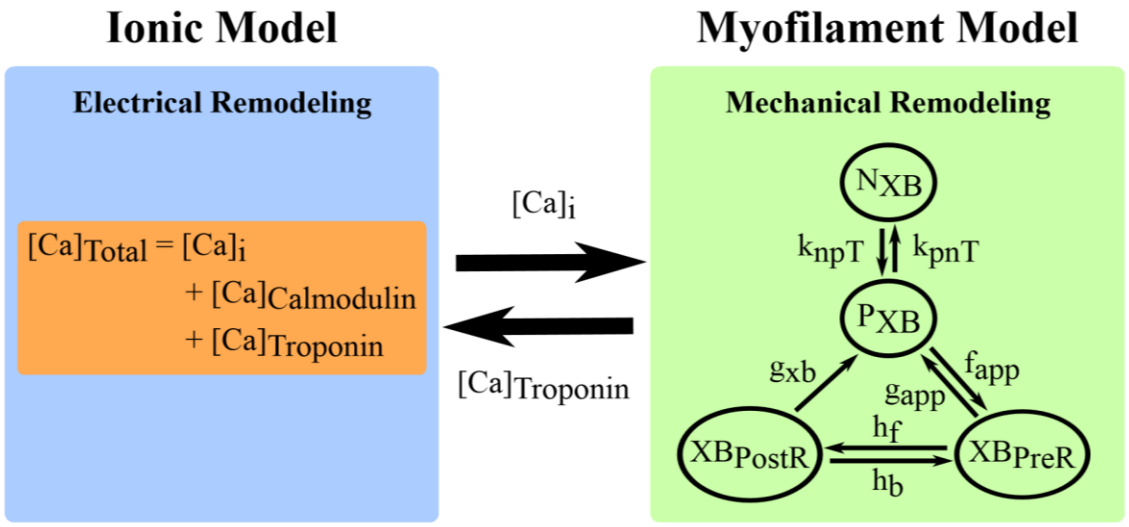

Figure 4.1 Strongly Coupled Human Electromechanical Myocyte Model with myofilament feedback via $[Ca]_{Troponin}$. A modified version of the Markov state diagram of the myofilament model from Rice *et al*, which describes the activation of the thin filament by intracellular calcium binding to Troponin C as well as thin filament binding to thick filament crossbridges (XBs), is shown. The transition rates (k_{npT} and k_{pnT}) between the thin filament states where XB formation is inhibited (N_{XB}) and where weakly bound XB formation is possible (P_{XB}) are both functions of $perm_{50}$, k_{on}, k_{offH}, and k_{offL}. The rate k_{npT} is also dependent on k_{n_p}, and k_{pnT} is additionally dependent on k_{p_n}. The XB_{PreR} and XB_{PostR} states represent a thin filament with a strongly bound XB that do not and do, respectively, have rotated myosin heads which induced strain (Rice et al., 2008).

A weakly coupled version of the model (with no feedback) was created by removing the $[Ca]_{Troponin}$ term from Equation 4.1. Its sole purpose was to aid in examining how myofilament feedback affected the development of alternans.

The model did not incorporate stretch-activated channels since there is no experimental evidence that heart-failure induced APV-ALT at low heart rates would be affected by a potential opening of the channel.

4.2.2 Incorporating Heart Failure Remodeling

We simulated human heart failure in our electromechanical model by incorporating electrical and mechanical remodeling. Electrical remodeling was represented by abnormal calcium handing. Specifically, we reduced the sarcoplasmic reticulum calcium uptake current (I_{up}) to 27% of its baseline value in the ten Tusscher *et al* model (Table 4.1), similar to Narayan *et al* (Narayan et al., 2008) and Bayer *et al* (Bayer et al., 2010), to represent reduced SERCA2a expression (Hasenfuss et al., 1994) and increased dephosphorylated phospholamban (Schmidt et al., 1999) observed in human heart failure. This specific feature of heart failure remodeling was incorporated because it has been shown to be crucial to the development of APV-ALT in previous studies of human heart failure (Bayer et al., 2010; Narayan et al., 2008).

Mechanical remodeling was incorporated to simulate altered thin filament activation and XB cycling rates found in human heart failure. Changes in thin filament activation have been linked to altered phosphorylation of cardiac Troponin I (cTnI) (Messer et al., 2007), which has been shown to be decreased by up to 87% (Messer et al., 2007; Zaremba et al., 2007). Alterations in XB cycling rates have been linked to changes in phosphorylation of myosin light chain 2 (MLC-2) (Levine et al., 1996; Moss and Fitzsimons, 2006; Olsson et al., 2004; Patel et al., 1998) and cardiac myosin-binding protein C (cMyBP-C) (Coulton and Stelzer, 2012; Flashman et al., 2004). Studies have found that phosphorylation of the two isoforms of MLC-2 is unchanged (van der Velden

et al., 2003a) or reduced by 34%-69% (van Der Velden et al., 2001; van der Velden et al., 2003a; van der Velden et al., 2003b; Zaremba et al., 2007). Additionally, cMyBP-C has been shown to be decreased by at least 50% (El-Armouche et al., 2007; Zaremba et al., 2007). Furthermore, myocardial Ca^{2+} sensitivity, which incorporates the combination of the effects of thin filament activation and XB cycling rates on force production, has been shown to be altered in human heart failure. In studies, myocardial Ca^{2+} sensitivity has been found to increase by 2-6% in human heart failure (van der Velden et al., 2000; van der Velden et al., 2006; Wolff et al., 1996) and by 1-2% in animal models of heart failure (de Waard et al., 2007; Lamberts et al., 2007; Wolff et al., 1995), not change in human heart failure (Ambardekar et al., 2011), and decrease by 2-3% in animal models of heart failure (Belin et al., 2007; Belin et al., 2006).

Despite the uncertainty regarding the exact amount by which the mechanical properties outlined above are altered in heart failure, these studies indicate that mechanical parameters involved in thin filament activation and XB cycling are important components of the disease manifestation and therefore might contribute to the development of FORCE-ALT. To elucidate if and how changes to mechanical parameters in human heart failure promote or modulate FORCE-ALT, we incorporated mechanical remodeling into the Rice *et al* myofilament model. Specifically, we altered thin filament activation, embodied in the Rice *et al* model by these 6 parameters: $perm_{50}$, k_{offL}, k_{offH}, k_{on}, k_{n_p}, and k_{p_n}. k_{npT} and k_{pnT} are nonlinear transition rates that are functions of these 6 parameters and represent calcium based activation of the thin filament, which is shown in Figure 4.1 as the transition of the thin filament from the N_{XB} state (XB formation is inhibited) to the P_{XB} state (weakly bound XB formation is possible). Specifically, $perm_{50}$ is the half activation constant for shift of a

thin filament regulatory unit (RU) from N_{XB} to P_{XB}, k_{offH} (k_{offL}) is the rate constant for Ca^{2+} unbinding from the high (low) affinity binding site of Troponin C, and k_{on} is rate constant for Ca^{2+} binding to Troponin C. k_{n_p} and k_{p_n} are constant scaling factors of the k_{npT} and k_{pnT} transition rates. We also altered XB cycling rates, expressed by these Rice *et al* parameters: f_{app}, g_{app}, h_f, h_b, and g_{xb}. The rates fapp and gapp regulate the transition of the thin filament from the P_{XB} state to the strongly bound XB state where the myosin head has not yet rotated and induced strain in the neck region (XB_{PreR}). h_f and h_b are transition rates between the XB_{PreR} and XB_{PostR} state (thin filament is strongly bound to a XB which has a rotated myosin head and has induced distortion). g_{xb} represents the ATP consuming transition rate from XB_{PostR} to P_{XB}. Due to the uncertainty in the literature regarding the exact amount that these parameters change in heart failure, as described above, we explored heart failure –induced remodeling of these 11 myofilament parameters within the range of 80% to 120% of their baseline values (Table 4.1).

Parameter	Control Value (CV)	Heart Failure Value	Effect of HF Remodeling on Alternans
I_{up}	0.006375 mM/ms	**CV*27%**	**Required for alternans to occur**
$perm_{50}$	0.5 (unitless)	Range of Values (Increments of 1%): **CV*80% to CV*120%**	**Largest** effect on alternans magnitude
k_{on}	47.5 1/μMs		**Large** effect on alternans magnitude
k_{offH}	25 1/s		**Large** effect on alternans magnitude
k_{offL}	250 1/s		Negligible effects on alternans magnitude
k_{n_p}	0.61 1/ms		
k_{p_n}	0.016 1/ms		
f_{app}	4.8 1/ms		
g_{app}	0.093 1/ms		
h_f	0.010 1/ms		
h_b	0.035 1/ms		
g_{xb}	0.030 1/ms		

Table 4.1 Control and Heart Failure Values for Important Model Parameters. Iup is from the ten Tusscher et al ionic model (ten Tusscher and Panfilov, 2006). All other parameters are from the Rice et al myofilament model (Rice et al., 2008).

4.2.3 Alternans Protocol

Clinical studies in patients with human heart failure have shown that APV-ALT arises at moderate pacing rates (Narayan et al., 2008); APV-ALT has also been induced, at these rates, in computational electrophysiological models of human myocytes and LV wedges with abnormal calcium handing by pacing the models with a dynamic pacing protocol (Bayer et al., 2010). To induce APV-ALT in our electromechanical model of the myocyte, we used a pacing protocol similar to that in Bayer *et al*. (Bayer et al., 2010). We first paced the myocyte at near resting pacing rates (850 ms; 71 bpm) until steady state was reached. Then, a dynamic pacing protocol was executed with pacing beginning at a cycle

length (CL) of 650 ms (92 bpm) and decreasing by 50 ms every 100 beats, until loss of 1:1 capture occurred.

Since our myocyte model is a strongly coupled electromechanical model, the procedure used to induce APV-ALT was also expected to result in the generation of FORCE-ALT. We aimed to test this hypothesis and to uncover the mechanism linking FORCE-ALT to APV-ALT. The pacing protocol also allowed us to probe the sensitivity of FORCE-ALT to CL.

To elucidate if altered thin filament activation and XB cycling rates found in human heart failure exacerbated or alleviated FORCE-ALT, we examined how each remodeled parameter described above individually affected FORCE-ALT; 11 sets of simulations were thus run using the dynamic pacing protocol, each including the electrical remodeling and the remodeling of one of the myofilament parameters. To uncover the effect of disease severity for each remodeled myofilament parameter, each set of simulations consisted of 41 unique simulations in which the chosen mechanical parameter was assigned a value in the range of 80% to 120% of its baseline value in Rice *et al* (incremented by 1%). To discover if FORCE-ALT can be induced by mechanical remodeling and dynamic pacing alone, the 451 simulations just described were executed again but without the inclusion of electrical remodeling.

Finally, since active force generation is known to be modulated by sarcomere length (SL) (Gordon et al., 1966), we wanted to uncover if FORCE-ALT was also sensitive to SL. To do this, the aforementioned 451 simulations (with the electrical remodeling) were each run 16 times, during which we held SL constant at a different value for each simulation. SL values ranged from 1.65 μm to 2.4 μm, in increments of 0.05 μm. This range of SL

values was chosen because it is in the operating range for cardiac myocytes (Trayanova and Rice, 2011a).

4.2.4 Alternans Analysis

The magnitudes of alternans in active force, intracellular calcium concentration ($[Ca]_i$), and transmembrane voltage (V_m) were each calculated using the following formula commonly used in the quantification of alternans (Kockskamper and Blatter, 2002; Shkryl et al., 2012; Xie et al., 2013):

$$ALTM = 1 - \frac{Small\ Amplitude}{Large\ Amplitude}$$

(Equation 4.2)

where *Small Amplitude* is the peak value minus the minimum value during the small beat and *Large Amplitude* is the peak value minus the minimum value during the large beat. Alternans magnitude was calculated for each pair of beats during the final 64 beats of each CL, following the approach in Bayer *et al* (Bayer et al., 2010) and the largest alternans magnitude per CL for each simulation was recorded. APV-ALT was calculated, as described above, during the period from the start of Phase II until the end of Phase III of the action potential. Alternans occurred if ALT > 0.

4.3 Results

4.3.1 Abnormal Intracellular Calcium Handling Results in Force Alternans

Incorporating heart failure electrical remodeling in our strongly coupled cellular electromechanical model (as described in Methods) resulted, as expected, in intracellular

calcium alternans (CA-ALT) that caused action potential voltage alternans (APV-ALT), similar to those shown previously (Bayer et al., 2010; Narayan et al., 2008). An example of CA-ALT as a function of time and as superimposed beats is shown in Figure 4.2, panels A and E respectively, for pacing at a CL of 650 ms (92 bpm) and for a SL of 2.1 µm (a typical length during the normal cardiac cycle). The superimposed beats emphasize the presence of CA-ALT and the difference in the Ca^{2+} transient between the odd (small $[Ca]_i$ transient) and even (large $[Ca]_i$ transient) beats. The corresponding APV-ALT is shown in Figure 4.2, panels B and F. CA-ALT also induced alternans in active force (FORCE-ALT), shown as a function of time (Figure 4.2C) and as overlaid beats (Figure 4.2H).

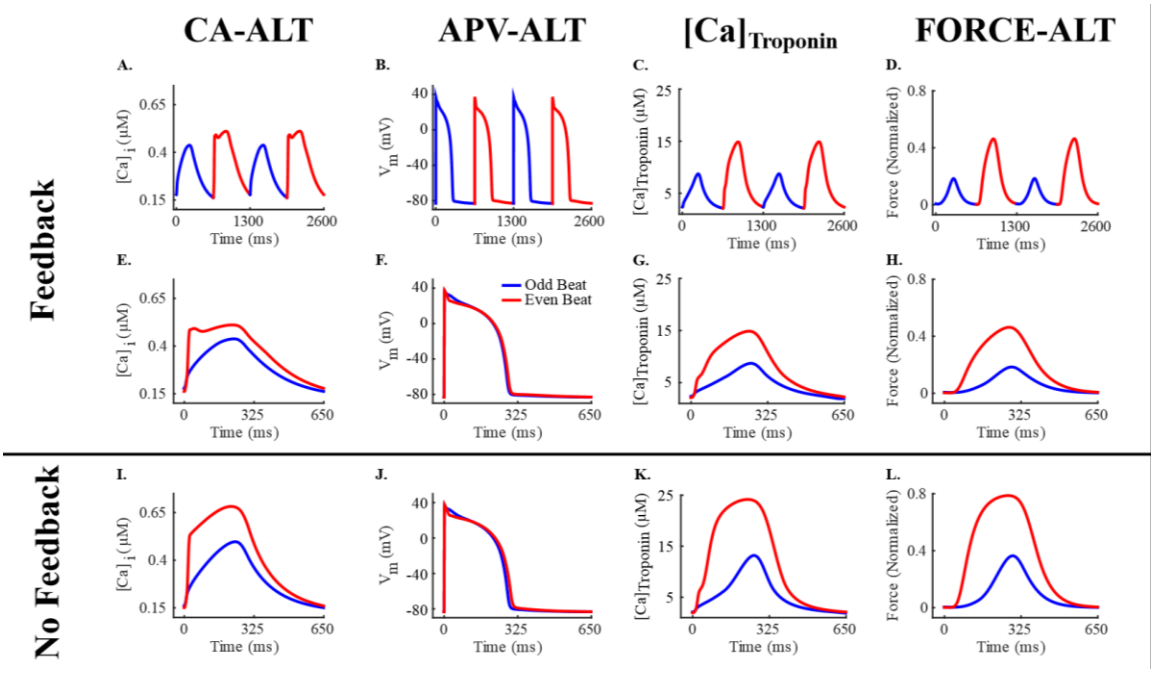

Figure 4.2 CA-ALT (column 1), APV-ALT (column 2), $[Ca]_{Troponin}$ (column 3), and FORCE-ALT (column 4) for simulations incorporating electrical remodeling in the absence of mechanical remodeling for a pacing CL of 650 ms and for SL=2.1 µm. Alternans are plotted over time in row 1 showing that CA-ALT was sufficient to produce APV-ALT, $[Ca]_{Troponin}$ alternans, and FORCE-ALT. Odd (blue) and even (red) beats from row 1 are superimposed to illustrate that the magnitude of alternans in rows 2 (strongly coupled simulations) and 3 (weakly coupled simulations) were different with and without myofilament feedback.

Due to myofilament feedback in our strongly coupled model (Figure 4.2, panels C and G), CA-ALT and APV-ALT differed from those obtained by Bayer et al and Narayan et al (Bayer et al., 2010; Narayan et al., 2008). We used the weakly coupled version of the model to explore the effects of myofilament feedback on CA-ALT, APV-ALT, and FORCE-ALT (compare rows 2 and 3 of Figure 4.2). The magnitudes of $[Ca]_i$ and CA-ALT (CA-ALTM) were both smaller in the strongly coupled model as compared to those in the weakly coupled ($[Ca]_i$: 0.44 μM vs 0.50 μM for odd beat, 0.51 μM vs 0.68 μM for even beat; CA-ALTM: 21% vs 35%). Since Troponin C binds free intracellular calcium and thus removes those calcium ions from the pool of free calcium available in the cytoplasm ($[Ca]_i$), the feedback via the $[Ca]_{Troponin}$ term (Equation 4.1) in the strongly coupled model resulted in a smaller magnitude of $[Ca]_i$. Smaller CA-ALTM was due to the fact that Troponin C buffers more $[Ca]_i$ when $[Ca]_i$ transient is large (even beat) than when it is small (odd beat), thus reducing the peak magnitude of $[Ca]_i$ during the even beat relative to that of the odd and consequently decreasing CA-ALTM, as calculated according to Equation 4.2. The magnitude of APV-ALT (APV-ALTM) was also smaller in the strongly coupled model (46% vs. 68% with no feedback) due to diminished CA-ALTM. The magnitude of $[Ca]_{Troponin}$ was smaller in the strongly vs weakly coupled model ($[Ca]_{Troponin}$: 8.73 μM vs 13.19 μM for odd beat, 14.86 μM vs 24.17 μM for even beat) due to diminished $[Ca]_i$. The strong coupling also resulted in a smaller magnitude of the active force due to the decreased $[Ca]_i$ transient (0.18 vs 0.36 normalized force for odd beat, 0.46 vs 0.79 for even beat). However, the magnitude of FORCE-ALT (FORCE-ALTM) was 5% greater in the case of myofilament feedback than without (60% vs. 55%), despite the smaller CA-ALTM in the former case. This was due to a smaller amount of calcium bound to Troponin

C during both the odd and even beats, resulting from the reduced $[Ca]_i$ in this case. Since calcium binding to Troponin C activates the thin filament, less thin filament regulatory units (RUs) transitioned from the non-permissive (N_{XB}; XB formation is inhibited) to the permissive (P_{XB}; weakly-bound XBs formation possible) state, (Figure 4.1) resulting in less RUs transitioning from P_{XB} to the states with strongly-bound XBs (XB_{PreR} and XB_{PostR}). Since active force is generated by the rotation of the thick filament, fewer RUs in the pre-rotated (XB_{PreR}) state caused less RUs to transition from it to the post-rotated (XB_{PostR}) state, producing less active force. However, since the presence of strongly bound XBs is known to enhance the binding affinity of Troponin C to calcium on nearby thin filament RUs and since Rice et al (Rice et al., 2008) incorporated this nonlinear cooperativity mechanism, the relatively smaller amount of strongly bound XBs during the odd (smaller $[Ca]_i$) beat resulted in greater reduction of active force generation relative to the even (larger $[Ca]_i$) beat. This resulted in enhanced FORCE-ALTM in the strongly coupled model as calculated according to Equation 4.2.

4.3.2 Sensitivity of Alternans to Pacing Rate

Simulations with our strongly coupled electromechanical myocyte model revealed that FORCE-ALTM has a non-monotonic dependence on CL (Figure 4.3A, solid line), with a local minimum at CL=400 ms. CA-ALTM monotonically increased with increased pacing rate, while APV-ALTM remained relatively small at slower pacing rates and increased at faster pacing rates (Figure 4.3B-C, solid line). No alternans occurred for pacing CLs>650 ms. An important observation here is that for all clinically relevant pacing rates (as discussed in the Introduction, <110 bpm; CL>=550 ms), CA-ALTM, ranging 21%-31%, induced smaller APV-ALTM (ranging 46-48%) but larger FORCE-ALTM

(ranging 51-61%), consistent with the results presented in Figure 4.2. However, at faster pacing rates (CL<500 ms), larger CA-ALTM induced smaller FORCE-ALTM. This was due to elevated $[Ca]_i$, which occurred due to a buildup of diastolic intracellular calcium as a result of insufficient time between beats for the SERCA pump and the Na/Ca^{2+} exchanger to restore $[Ca]_i$ to normal. During the large (even) beat, this abnormally large $[Ca]_i$ transient saturated Troponin C prior to reaching its peak magnitude, preventing additional free calcium from binding to Troponin C and thus preventing an increase in thin filament activation. This prevented further thin filament RUs from transitioning to the P_{XB}, XB_{PreR} and XB_{PostR} states from the N_{XB} state (Figure 4.1). Since no additional rotation of the thick filament occurred, no added active force was generated during the even beat, despite additional free calcium becoming available as the $[Ca]_i$ transient increased from the value at which Troponin C saturated to its peak magnitude. This resulted in diminished FORCE-ALTM at faster pacing rates, according to Equation 4.2.

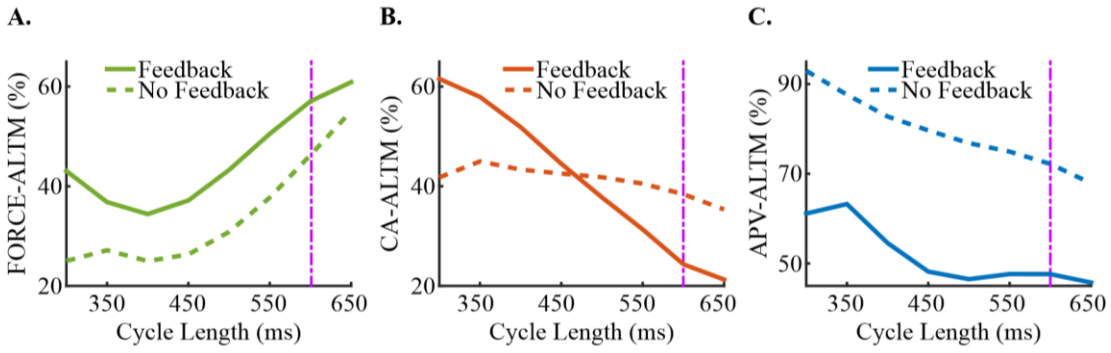

Figure 4.3 Dependence of FORCE-ALTM (A), CA-ALTM (B), and APV-ALTM (C) to CL in simulations with electrical remodeling in the absence of mechanical remodeling at SL=2.1 μm for both the strongly (solid lines) and weakly coupled (dashed lines) models. The purple dashpot line indicates where the data in Figure 4.4 are taken from (CL=600 ms). No alternans occurred for pacing CLs>650 ms for either the strongly or weakly coupled model.

Eliminating myofilament feedback reduced FORCE-ALTM at all CLs on average by 11%, flattened the CA-ALTM dependence, and increased APV-ALTM (Figure 4.3A-C, dashed line), rendering the latter similar to the dependence documented by Bayer *et al* and Narayan *et al* (Bayer et al., 2010; Narayan et al., 2008). CA-ALTM was smaller for the strongly verses the weakly coupled model at slower pacing rates (CL>450 ms), consistent with the results presented in Section 3.1 for CL=650 ms (Figure 4.2). However, CA-ALTM became larger than that for the weakly coupled model at faster pacing rates (CL<400 ms) due to diminished myofilament feedback during the even but not the odd beat. As CL decreased, $[Ca]_i$, was elevated and saturated Troponin C during the even beat, preventing both additional free calcium from binding to Troponin C, and additional thin filament RUs from transitioning from the N_{XB} to the P_{XB} and strongly-bound XB states, as discussed in the preceding paragraph. Since $[Ca]_{Troponin}$ is a function of the amount of calcium bound to Troponin C and of the number of RUs in the strongly-bound XB states, myofilament feedback was diminished during the even beat more than the odd, thus reducing the magnitude of $[Ca]_i$ more during the odd beat. This resulted in larger CA-ALTM for the strongly coupled model at faster rates.

4.3.3 Dependence of Force, Calcium and Voltage Alternans on Sarcomere Length

Simulations with our strongly coupled electromechanical myocyte model showed that, alternans magnitude changed as SL decreased from 2.4 to 1.65 μm. An example of the dependence of the three types of alternans magnitude on SL functions for pacing at a CL of 600 ms (100 bpm) is shown in Figure 4.4A-C, solid line. CA-ALTM increased for SL>2.05 μm (in Figure 4.4B) due to diminished myofilament feedback during the even

beat only, which occurred as a result of a progressive increase in the fraction of single-overlap thin filament apposing the thick filament as SL increased. Since this portion of the thin filament has a higher binding affinity to calcium, a larger fraction of it caused greater calcium-Troponin C binding for a given $[Ca]_i$. This progressively lowered the $[Ca]_i$ threshold at which Troponin C became saturated, preventing additional free calcium from binding to Troponin C, despite the peak magnitude of the $[Ca]_i$ transient being greater than the $[Ca]_i$ threshold for saturation. This saturation only occurred during the even beat due to its larger $[Ca]_i$ magnitude. Since $[Ca]_{Troponin}$ is a function of the amount of calcium bound to Troponin C, myofilament feedback was increasingly diminished at progressively larger SLs during the even beat relative to the odd, thus steadily reducing the magnitude of $[Ca]_i$ during the even beat (according to Equation 4.1). This resulted in progressively larger CA-ALTM, according to Equation 4.2, at increasingly greater SLs for SL>2.05 μm. The saturation of Troponin C during the even beat also prevented enhanced thin filament activation, which, as described in Section 3.2., resulted in progressively diminished FORCE-ALTM, as shown for SL increasing above 2.05 μm in Figure 4.4A. APV-ALTM decreased for SL>2.05 μm, despite increased CA-ALTM, due to increasingly diminished $[Ca]_{Troponin}$ during the even beat (as described above), which caused the $[Ca]_i$ transient during the even beat to have a notched appearance similar to Figure 4.2A (red lines). As SL increased, the $[Ca]_i$ magnitude prior to the $[Ca]_i$ notch became increasingly large (due to reduced $[Ca]_{Troponin}$), causing CA-ALTM to increase in accordance with Equation 4.1. However, the $[Ca]_i$ transient quickly decreased from the peak value preceding the notch in $[Ca]_i$ to an increasingly smaller value as SL increased, thus shortening Phase II of the action potential and reducing its magnitude during the even beat and inducing smaller APV-

ALTM. CA-ALTM also increased for SL<2.05 μm. As SL became progressively smaller, the fraction of single-overlap thin filament that was apposed to thick filament decreased, causing reduced calcium-Troponin C binding for a given $[Ca]_i$. This diminished thin filament activation and decreased the number of RUs that transitioned from N_{XB} to P_{XB}, thus reducing the number of RUs that transitioned to strongly-bound XB states. Since $[Ca]_{Troponin}$ is a function of the amount of calcium bound to Troponin C and of the number of RUs in the strongly-bound XB states, myofilament feedback was progressively diminished during the even relative to the odd beat as SL decreased, thus increasing the magnitude of $[Ca]_i$ more during the even beat. This resulted in progressively larger CA-ALTM as SL decreased for SL<2.05 μm. FORCE-ALTM and APV-ALTM were large at SL<2.05 μm due to large CA-ALM. The trends for CA-ALTM and APV-ALT as functions of SL were different at slow and fast pacing rates (Figure 4.4E-F), while the dependence of FORCE-ALTM held true at all CLs (Figure 4.4D).

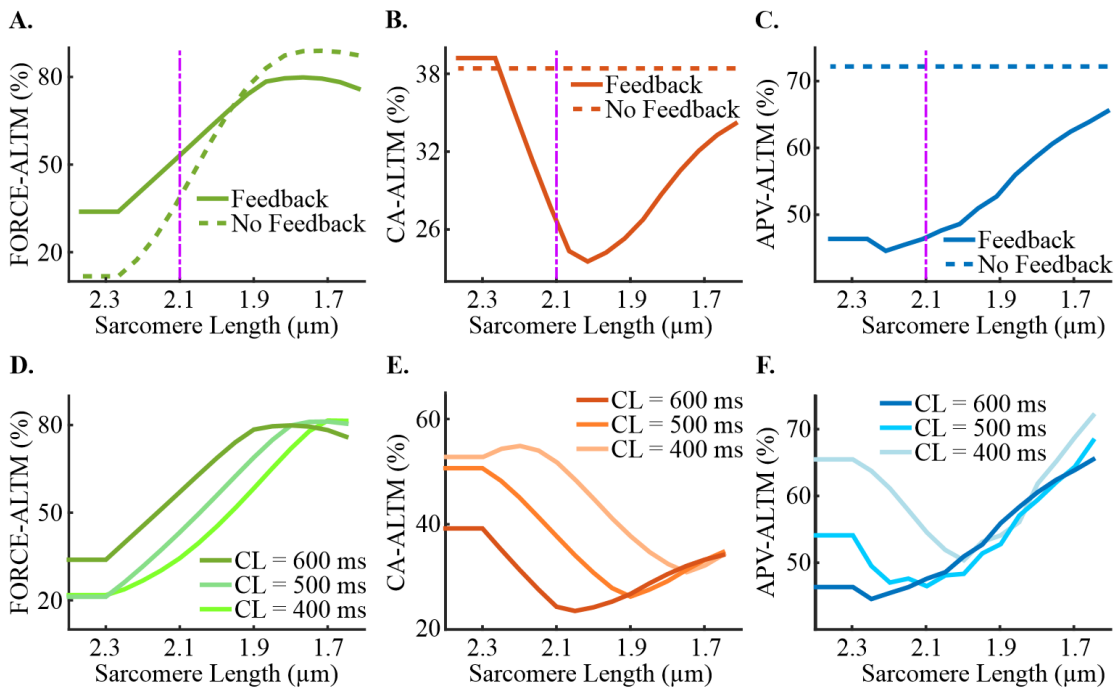

Figure 4.4 Sensitivity of FORCE-ALTM (A), CA-ALTM (B), and APV-ALTM (C) to SL in simulations with electrical remodeling in the absence of mechanical remodeling at CL=600 ms for both the strongly (solid lines) and weakly (dashed lines) coupled models. Plots of the dependence of FORCE-ALTM (D), CA-ALTM (E), and APV-ALTM (F) on SL are shown for slow and fast pacing rates for the strongly coupled model. The purple dashpot line indicates where the data displayed in Figure 4.3 are from (SL=2.1 μm).

Eliminating myofilament feedback expanded the range of FORCE-ALTM (Figure 4.4A, dashed line) without altering the shape of its dependence on SL. As expected, the removal of myofilament feedback rendered CA-ALTM and APV-ALTM insensitive to SL changes (Figure 4.4B-C, dashed line). FORCE-ALTM was larger in the weakly coupled model at SL<2.0 μm due to larger CA-ALTM; it was smaller at SL>2.0 μm due to enhanced saturation of Troponin C caused by the larger $[Ca]_i$ magnitudes shown to occur in the weakly coupled model (Figure 4.2I). This resulted in smaller peak active force generation during the even beat and thus diminished FORCE-ALTM (via Equation 4.2) in the weakly coupled model.

4.3.4 Effect of Heart Failure Induced- Remodeling of Mechanical Parameters on Force, Calcium and Voltage Alternans

Incorporating heart failure induced-remodeling of both electrical and mechanical parameters in simulations with our strongly coupled electromechanical myocyte model demonstrated that of the mechanical parameters involved in thin filament activation and XB cycling, only remodeling in $perm_{50}$ (half activation constant for shift of a thin filament RU from N_{XB} to P_{XB}), k_{offH} (rate constant for Ca^{2+} unbinding from the high affinity binding site of Troponin C), and k_{on} (rate constant for Ca^{2+} binding to Troponin C) caused appreciable alterations in FORCE-ALTM, CA-ALTM, and APV-ALTM. Of these three, $perm_{50}$ was the most important because changes to it had the most profound effects on FORCE-ALTM, CA-ALTM, and APV-ALTM. Examples of these functions are shown in Figure 4.5 for $perm_{50}$ (row 1), k_{offH} (row 2), and k_{on} (row 3) for pacing at a CL of 600 ms and SL of 2.1 μm, where each remodeled parameter is displayed as a percent of its normal value. By definition, increasing $perm_{50}$ diminishes thin filament activation. As $perm_{50}$ was progressively increased above 102%, thin filament activation was increasingly reduced, which steadily increased CA-ALTM, FORCE-ALTM and APV-ALTM, via the mechanisms described in Section 3.3 for SL<2.05 μm. As $perm_{50}$ was decreased below 102%, thin filament activation was increasingly enhanced, which increased the transition rate of N_{XB} to P_{XB} and decreased the reverse rate, causing more RUs to transition to P_{XB}. A greater number of RUs in the P_{XB} state induced additional RUs to transition to the strongly-bound XB states, increasing the fraction of total RUs with strongly-bound XBs. Therefore, achieving the maximum fraction of RUs in the XB_{PreR} and XB_{PostR} states could be attained with increasingly less activating calcium as $perm_{50}$ decreased. Since $[Ca]_{Troponin}$

is a function of the fraction of total RUs in strongly-bound XB states and since during the even beat $[Ca]_i$ was large enough to attain that maximum fraction, myofilament feedback was progressively diminished during the even relative to the odd beat as $perm_{50}$ decreased, thus increasing the magnitude of $[Ca]_i$ more during the even beat. This caused progressively larger CA-ALTM. Active force, which is also a function of the fraction of total RUs in strongly-bound XB states, was progressively diminished during the even verses the odd beat (similar to $[Ca]_{Troponin}$), which resulted in progressively smaller FORCE-ALTM, despite enhanced CA-ALTM, as $perm_{50}$ decreased. APV-ALTM was enhanced due to larger CA-ALTM. By definition, a decrease in k_{offH} or an increase in k_{on} increases the binding affinity of Troponin C to calcium. As k_{offH} was progressively decreased below 103% and k_{on} increased above 92%, binding affinity was increased (thus enhancing calcium-Troponin C binding for a given $[Ca]_i$), which progressively enhanced CA-ALTM and diminished FORCE-ALTM and APV-ALTM, in the same manner as described in Section 3.3. for SL>2.05 μm. k_{offH}>103% and k_{on}<92% decreased the binding affinity of Troponin (thus diminishing thin filament activation), which progressively increased CA-ALTM, FORCE-ALTM and APV-ALTM as described in Section 3.3 for SL<2.05 μm. Removing myofilament feedback decreased FORCE-ALTM for nearly all values of $perm_{50}$, k_{offH}, and k_{on} (Figure 4.5, column 1, dashed line), and as expected, rendered CA-ALTM and APV-ALTM insensitive to remodeling of those mechanical parameters. FORCE-ALTM was diminished due to enhanced saturation of Troponin C caused by the larger $[Ca]_i$ magnitudes occurring in the weakly coupled model (Figure 4.2I) in the same manner as described for SL>2.0 μm in Section 3.3.

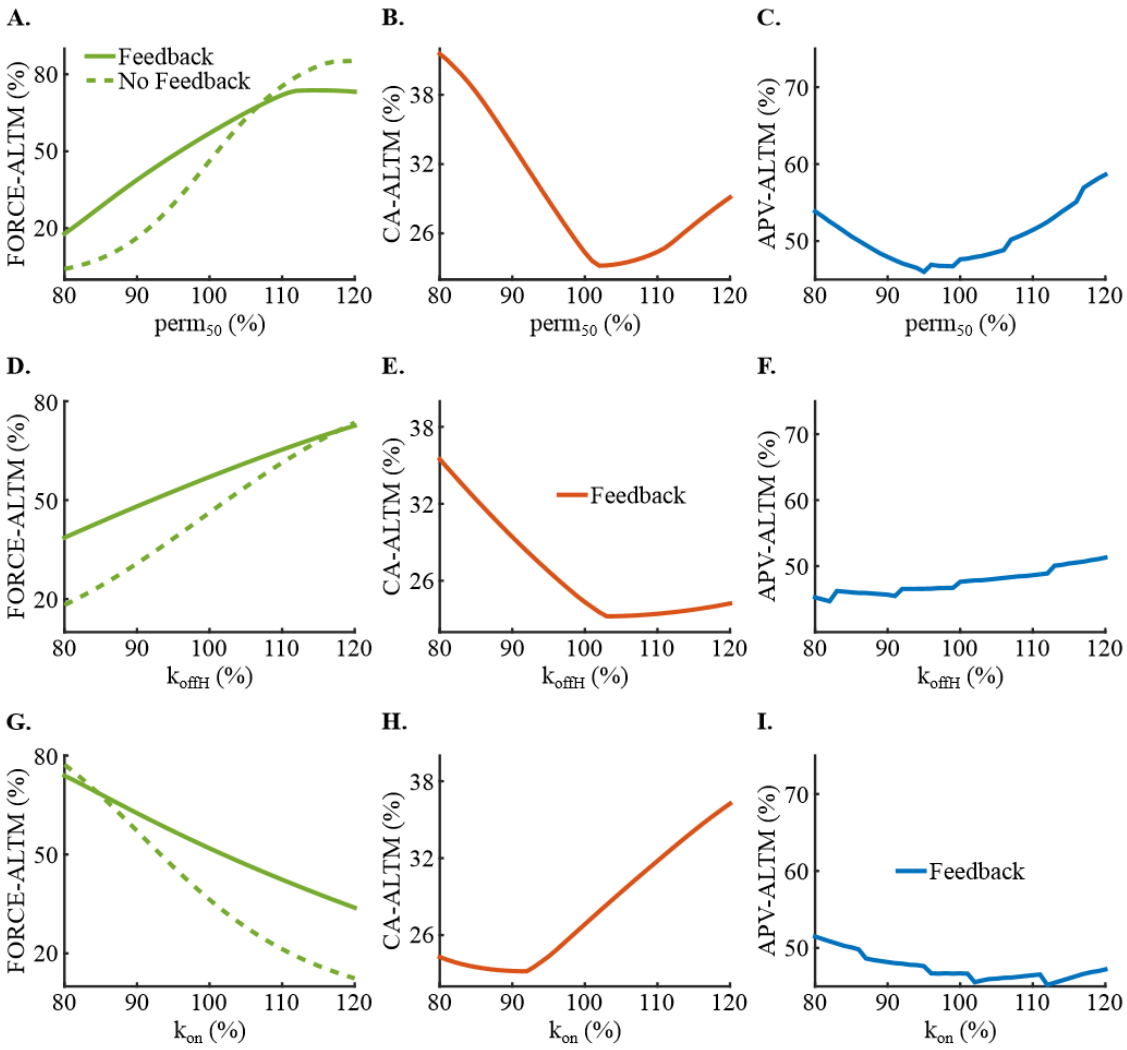

Figure 4.5 Dependence of FORCE-ALTM (column 1), CA-ALTM (column 2), and APV-ALTM (column 3) on the level of mechanical remodeling for pacing CL=600 ms and SL=2.1 μm for the strongly coupled model (solid lines). Dashed line in the FORCE-ALTM refers to the weakly coupled model. Heart-failure remodeling mechanical parameters $perm_{50}$ (row 1), k_{offH} (row 2), and k_{on} (row 3), are displayed as a percent of their normal values.

Finally, simulations were run incorporating only mechanical remodeling (no electrical remodeling). For all CLs and SLs studied, there was no FORCE-ALT, demonstrating that abnormal intracellular calcium handling and thus CA-ALT was necessary for the generation of FORCE-ALT.

4.4 Discussion

The present study examines the cellular mechanisms underlying the formation of pressure alternans (FORCE-ALT) in the presence of MTWA (APV-ALT), which have been shown to be predictors of worsening heart failure and lethal ventricular arrhythmias, respectively. The goals of this study were to uncover the mechanisms linking APV-ALT and FORCE-ALT in failing human myocytes and to investigate how the link between those alternans was affected by pacing rate and various physiological conditions. Using a strongly coupled human electromechanical myocyte model, we showed that CA-ALT, induced by decreased I_{up}, was the link between APV-ALT and FORCE-ALT and that FORCE-ALTM was largest at clinically-relevant slow to moderate pacing rates (<110 bpm), where APV-ALT was smallest. We found that FORCE-ALTM, CA-ALTM and APV-ALTM were altered by heart failure induced-remodeling of mechanical parameters and by sarcomere length; this was due to the presence of myofilament feedback. Together these findings link FORCE-ALT to APV-ALT and suggest that pressure alternans is directly linked to MTWA via calcium dysregulation and may be a better predictor of the propensity for ventricular arrhythmias at clinically relevant pacing rates (<110 bpm).

4.4.1 Calcium Alternans Link Action Potential Voltage Alternans to Force Alternans

MTWA is caused by CA-ALT predominantly as a result of decreased sarcoplasmic reticulum calcium uptake current (I_{up}) in heart failure patients at near resting heart rates (Bayer et al., 2010; Narayan et al., 2008). In addition, MTWA and pressure alternans have

been shown to occur simultaneously in patients at such pacing rates (Selvaraj et al., 2011). Furthermore, patients with pressure alternans have significantly lower amounts of sarcoplasmic reticulum Ca^{2+}-ATPase (SERCA) mRNA than patients without (Hirashiki et al., 2010; Hirashiki et al., 2006). Finally, FORCE-ALT, the cellular manifestation of pressure alternans, has been found to be regulated by calcium dysregulation in animal experiments with cardiac muscle preparations (Kihara and Morgan, 1991; Kotsanas et al., 1996; Lab and Lee, 1990; Orchard et al., 1991) and perfused hearts (Brooks et al., 1994; Lee et al., 1988), paced at fast rates. Taken together, the results from these previous studies have suggested that CA-ALT, due to reduced I_{up}, is a likely candidate to underlie FORCE-ALT in human heart failure. Our results presented here provide the proof that CA-ALT, via reduced I_{up}, drove the formation of FORCE-ALT at clinically relevant pacing rates.

4.4.2 Force Alternans Are Large at Slow Pacing Rates and May Be Undetectable at Faster Pacing Rates

Studies have shown that the mean heart rate onset at which pressure alternans were first detected in pacing studies was 606 ms (99 bpm) (Hirashiki et al., 2006), and 517 to 571 ms (116 bpm – 105 bpm) (Selvaraj et al., 2011). In addition, a study conducted during normal sinus rhythm found that patients with pressure alternans had significantly slower heart rates than those without (81.0 bpm vs 93.1 bpm) (Kim et al., 2014). That same study also showed that patients with both MTWA and pressure alternans had slower heart rates than those with only MTWA (81.0 bpm vs 92 bpm, not statistically significant), suggesting that patients with only MTWA may have had small yet undetectable pressure alternans due to the alternans magnitude being markedly reduced at faster heart rates. One study further

supported this hypothesis by showing that the amplitude of pressure alternans declined at increasingly faster pacing rates for four patients, three of whom lost pressure alternans when pacing rates exceeded 120, 130 and 140 bpm (500, 462, 400 ms) respectively (Kashimura et al., 2013). The present study provided support of this finding, since we demonstrated that FORCE-ALTM was greatest at slower pacing rates (>109 bpm) and declined significantly at faster pacing rates (<109 bpm). However, the outcome of one study contradicted these findings and reported that the magnitude of pressure alternans increased from 600 ms to 500 ms (Selvaraj et al., 2011). This conflicting evidence might have arisen from the method of calculating pressure alternans magnitude in that study, which differed from ours (spectral analysis versus measuring the amplitude change between the odd and even beats). To date, few patient studies have investigated the effects of pacing rate on the detection and magnitude of pressure alternans. However, as we have shown, pacing rate affects FORCE-ALTM and could explain why some patients with MTWA do not have detectable pressure alternans despite having underlying abnormal calcium handling. Additional studies of pressure alternans in heart failure patients are needed to investigate this phenomenon in greater detail.

4.4.3 Implications of Heart Failure-Induced Mechanical Remodeling for Alternans Severity

Studies have shown that thin filament activation can be altered in human heart failure. Specifically, decreased phosphorylation of cardiac Troponin I has been shown to be significantly decreased in human heart failure (Messer et al., 2007; Zaremba et al., 2007), resulting in reduced sliding speed and an increased Ca2+-sensitivity. Although this

change in thin filament activation has been observed in human heart failure, to date no studies have investigated whether it is reduced in patients with pressure alternans or MTWA. Here we demonstrated that heart failure-induced mechanical remodeling of parameters that modify thin filament activation can both exacerbate and diminish FORCE-ALT, CA-ALT, and APV-ALT. These results could explain the results of some studies which have revealed two different populations of patients with alternans: those with both MTWA and pressure alternans and those with only MTWA (Kim et al., 2014; Kodama et al., 2001; Selvaraj et al., 2011). The patient population with both types of alternans could have calcium handling abnormalities and reduced thin filament activation, which would (as our results suggest) result in larger and thus more easily detectable pressure alternans. The patients in which only MTWA were detectable may either have less severe reductions in thin filament activation or no abnormalities at all, and thus have smaller and undetectable pressure alternans. Furthermore, one study has shown that the magnitude of MTWA in patients with both MTWA and pressure alternans is larger than in patients with only MTWA (Kim et al., 2014), suggesting that if those patients had reduced thin filament activation as we speculated, then that would enhance the magnitude of MTWA, in agreement with our results (Figure 4.5).

4.5 Conclusions

APV-ALT and FORCE-ALT are linked via CA-ALT, resulting from reductions in sarcoplasmic reticulum calcium uptake current, in a strongly coupled electromechanical model of the failing human myocyte. Our results demonstrate that the magnitude of FORCE-ALT is largest at clinically relevant pacing rates (<110 bpm), where APV-ALT

was smallest. The magnitudes of FORCE-ALTM, CA-ALTM and APV-ALTM were dependent on pacing rate. Due to myofilament feedback, the magnitude of the alternans was also dependent on sarcomere length, and on the level of heart failure induced-remodeling of mechanical parameters involved in thin filament regulation. These findings provide important insight into the cellular mechanisms underlying pressure alternans at clinically relevant pacing rates (<110 bpm) and may aid in investigating whether pressure alternans is an improved and reliable predictor of propensity for ventricular arrhythmias in human heart failure.

Chapter 5 Study 2:

Myofilament Protein Dynamics Modulate EAD Formation in Human Hypertrophic Cardiomyopathy

This study has been published in Progress in Biophysics and Molecular Biology (Zile and Trayanova, 2017) and reprinted with permission from Elsevier publishing.

5.1 Introduction

Hypertrophic cardiomyopathy (HCM), defined by unexplained ventricular hypertrophy, is the most commonly inherited cardiac disease, with a reported prevalence of 1 in 500 worldwide (Maron et al., 1995; Maron and Maron, 2013). Although the annual mortality from HCM is low (0.5 – 2%) (Elliott et al., 2014; Maron et al., 2014), certain patient subsets, such as young athletes, have enhanced risk of sudden cardiac death (SCD) (Maron et al., 2014; Maron et al., 2007). Thus far, the only treatment proven to prolong life and prevent SCD in HCM patients is implantation of a cardioverter defibrillator (ICD) (Gersh et al., 2011; Maron and Maron, 2013; Maron et al., 2003; Maron et al., 2000; Maron et al., 2013; Maron et al., 2007; Schinkel et al., 2012; Vriesendorp et al., 2013). The main risk markers used to identify those patients who will benefit most from an ICD include family history of HCM SCD, unexplained syncope, multiple-repetitive non-sustained ventricular tachycardia (NSVT) episodes, abnormal exercise blood pressure response, late gadolinium enhancement ≥15% of left ventricular mass, and massive left ventricular hypertrophy ≥ 30 mm (Gersh et al., 2011; Maron, 2002; Maron, 2010; Maron and Maron, 2013; Maron et al., 2003; Spirito et al., 2014; Spirito et al., 2009; Spirito et al., 2000). However, HCM patients who lack all risk factors are still not immune to SCD (Pastore et al., 1999; Spirito et al., 2014). In addition, the risk stratification models used to identify high risk adult patients are not as effective at identifying children with high risk (Maron et al., 2013). Furthermore, since SCD risk in HCM patients is highest in younger patients

(<30 years old) (Maron et al., 2014), ICDs must be implanted early in life, increasing the likelihood that those individuals will experience device-related complications (Maron et al., 2013). Despite the challenges of SCD risk stratification in young HCM patients and their increased probability of device complications, other treatment options are limited. In fact despite wide prevalence, many consider HCM an orphan condition because it lacks disease-specific pharmacological treatment (Spoladore et al., 2012), which may be a consequence of the wide genetic and phenotypic heterogeneity among HCM patients. In particular, more than 1500 mutations identified on at least 11 genes, encoding thick and thin myofilament protein components, have been found to underlie HCM (Bos et al., 2009; Ingles et al., 2013; Maron et al., 2012; Niimura et al., 1998; Seidman and Seidman, 2011), though the causality and contribution to disease progression for each is not fully understood (Bezzina et al., 2015). To complicate matters, a new HCM subgroup, described as 'genotype positive-phenotype negative,' has been discovered in which patients have one or more pathogenic mutations but no disease phenotype (Gersh et al., 2011; Gray et al., 2011; Maron and Semsarian, 2010; Maron et al., 2011). The lack of disease-specific pharmacological treatment, the challenges of accurately stratifying HCM SCD patients, and the incomplete understanding of the relationship between HCM genotype, phenotype and outcome (Charron et al., 2010) underscore the need to improve SCD prevention strategies for HCM patients by improving our understanding of how sarcomeric mutations in HCM patients contribute to the enhanced arrhythmogenesis underlying SCD (Coppini et al., 2013; Maron et al., 2000).

Patients with HCM often have cardiac arrhythmias, including atrial fibrillation, NSVT, and sustained ventricular tachycardia, as well as prolonged QTc (Coppini et al.,

2013; Coppini et al., 2014; Maron et al., 2000). Early afterdepolarizations (EADs), defined as a slowing or reversal of normal repolarization during the plateau or rapid depolarization phases, have been implicated as the primary mechanism underlying many arrhythmias associated with HCM (Weiss et al., 2010; Yan et al., 2001) and have also been found in patients with HCM (Coppini et al., 2013). Many studies have investigated the ionic mechanisms of EADs in lethal ventricular arrhythmias and have found that EADs occur when repolarization reserve is reduced due to enhanced inward current, diminished outward current, or both. In addition, there must also be a regenerative increase in net inward current that has the ability to overcome and reverse repolarization. The ion channels typically implicated in this positive feedback are the L-type Ca^{2+} current (I_{CaL}) and the Na^{+}-Ca^{2+} exchange current (I_{NaCa}) (Weiss et al., 2010). New studies have also begun to explore the ionic mechanisms of EADs in human HCM tissue, finding that I_{CaL} and I_{NaCa} play an important role along with the rapid delayed rectifier current (I_{Kr}), the late Na^{+} current (I_{NaL}), and Ca^{2+}/calmodulin-dependent protein kinase II (CaMKII) (Coppini et al., 2013).

Although the ionic mechanisms of EADs have been studied, whether there are also myofilament protein dynamics mechanisms at play is poorly understood. Since mechanoelectric feedback (MEF) is known to be essential for normal function of the heart and is believed to be important in disease (Quinn, 2014; Taggart and Sutton, 1999; Tardiff et al., 2015; Zile and Trayanova, 2016) and since HCM is a disease caused by sarcomeric mutations, it is important to explore whether myofilament protein dynamics mechanisms could also contribute to EADs in human HCM. Thus, our goal was to utilize the capability of mechanistic computer simulations to investigate whether myofilament protein dynamics mechanisms modulate EAD formation in HCM for varying degrees of reduced

repolarization reserve, and to uncover how these mechanisms are affected by pacing rate, sarcomere length, and the degree of HCM-induced myofilament remodeling.

5.2 Methods

5.2.1 Human Electrophysiology-Force Myocyte Model

To investigate whether myofilament protein dynamics mechanisms modulate EAD formation under the conditions of human HCM, a mechanistically-based human electrophysiology-force myocyte model was used. The electrophysiology-force model combined the human endocardial ventricular membrane kinetics model by Vandersickel *et al* (Vandersickel et al., 2014) and the myofilament protein dynamics model by Rice *et al* (Rice et al., 2008). The Vandersickel *et al* model, an extension of the ten Tusscher *et al* model (ten Tusscher and Panfilov, 2006), which incorporates updated L-type Ca^{2+} channel kinetics, was used because it is capable of generating EADs during reduced repolarization reserve. The Rice *et al* model, which describes the activation of the thin filament by intracellular calcium binding to Troponin C as well as thin filament binding to thick filament crossbridges (XBs) using a 6 state Markov model, was chosen for its computational efficiency and incorporation of important biophysical detail and cooperativity mechanisms. Since the Rice *et al* myofilament model was developed based on rabbit data, we adjusted it to match human force data as described elsewhere (Zile and Trayanova, 2016).

The ionic and myofilament models were bidirectionally coupled by incorporating MEF on calcium dynamics (Figure 5.1); this was done by incorporating a dynamic term for troponin buffering of intracellular calcium ($[Ca]_{Troponin}$) using our previously developed

approach (Zile and Trayanova, 2016) where we refer to this as "strong coupling." In summary, the following equation was used to update the intracellular calcium concentration in the ionic model, using the $[Ca]_{Troponin}$ term calculated by the myofilament model, at each time step:

$$[Ca]_{Total} = [Ca]_i + [Ca]_{Calmodulin} + [Ca]_{Troponin} \quad \text{(Equation 5.1)}$$

where $[Ca]_{Total}$ is the total calcium in the cytoplasm, $[Ca]_i$ is the free calcium in the cytoplasm, $[Ca]_{Calmodulin}$ is the total calcium buffered by calmodulin in the cytoplasm, and $[Ca]_{Troponin}$ is the total calcium bound to Troponin C and incorporates the cooperativity of calcium-troponin binding due to strongly bound nearby XBs. Bidirectionally coupling the models with a dynamic representation of $[Ca]_{Troponin}$ was important and necessary, because it has been shown to be crucial for accurately reproducing contractile experiment data in myocyte simulations (Ji et al., 2015).

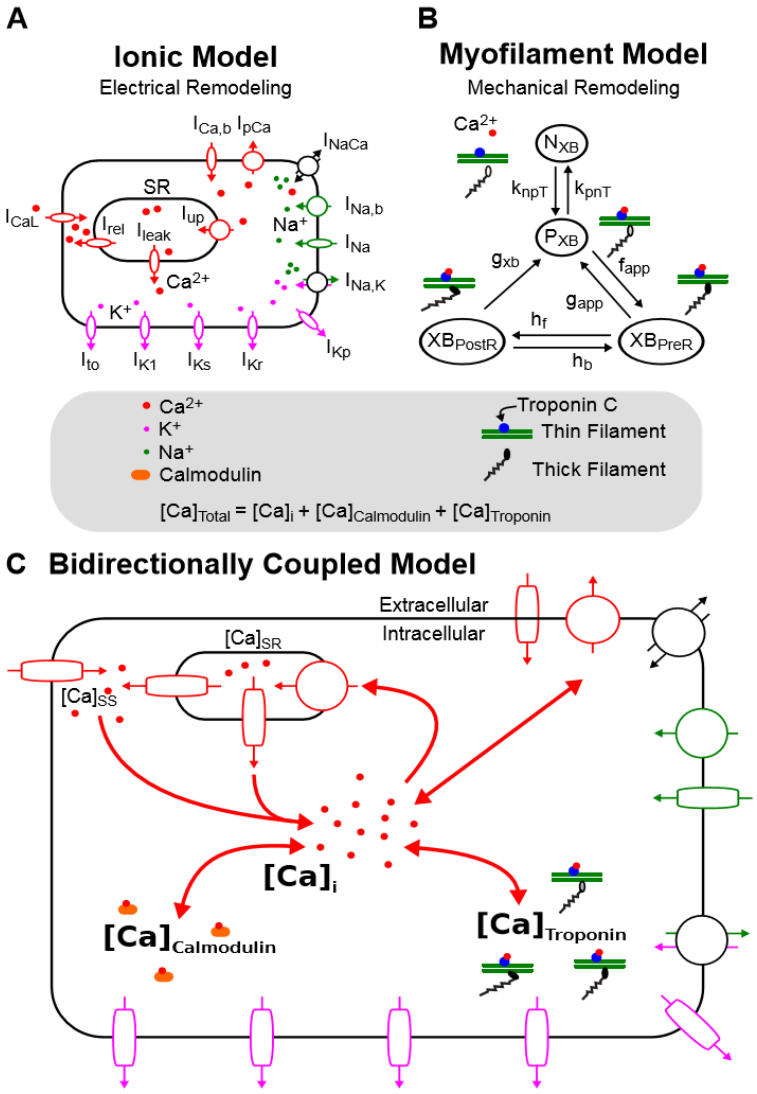

Figure 5.1 Ionic (A) and Myofilament (B) models combined to form the Bidirectionally Coupled Human Electrophysiology-Force Myocyte Model (C). A modified version of the ten Tusscher ionic model from Vandersickel *et al* (Vandersickel et al., 2014) was used for the ionic model. A modified version of the Markov state diagram of the myofilament model from Rice *et al*, which describes thin filament activation via free intracellular calcium ($[Ca]_i$) binding to Troponin C as well as thin filament binding to thick filaments to form crossbridges (XBs), was used for the myofilament model. The transition rates (k_{npT} and k_{pnT}) between the thin filament states where XB formation is inhibited (N_{XB}) and where weakly bound XB formation is possible (P_{XB}) are both functions of $perm_{50}$, k_{on}, k_{offH}, and k_{offL}. The rate k_{npT} is also dependent on k_{n_p}, and k_{pnT} is additionally dependent on k_{p_n}. The XB_{PreR} and XB_{PostR} states represent a thin filament with a strongly bound XB that do not and do, respectively, have rotated myosin heads which induced strain (Rice et al., 2008). Bidirectional coupling was obtained by incorporating MEF on calcium dynamics via Equation 5.1, where the total cytoplasmic calcium ($[Ca]_{Total}$) is equal to the sum of $[Ca]_i$, the total calcium bound to calmodulin ($[Ca]_{Calmodulin}$), and the total calcium bound to troponin C ($[Ca]_{Troponin}$).

A unidirectionally coupled version of the model (with no MEF and referred to as "weakly coupled" in our previously developed approach (Zile and Trayanova, 2016)) was created by removing the $[Ca]_{Troponin}$ term from Equation 5.1. The sole purpose of this model was to aid in examining how MEF altered EAD emergence and the frequency of EAD occurrence, by comparing its simulations to those of the bidirectionally coupled model.

5.2.2 Incorporating HCM-Induced Remodeling

We simulated human HCM in our single cell electrophysiology-force models by incorporating ionic and myofilament remodeling. Ionic remodeling was represented by reducing repolarization reserve. Specifically, we increased the maximal conductance of the L-type Ca^{2+} current (G_{CaL}) 2.5-5 fold (0.05 increments) and decreased the maximal conductance of the rapid delayed rectifier current (G_{Kr}) to 10-100% of its baseline value (in increments of 0.1%) in the ten Tusscher *et al* model, similar to Vandersickel *et al* (Vandersickel et al., 2014) and Zimik *et al* (Zimik et al., 2015) to represent increased I_{CaL} density, CaV1.2 protein and CaCNA1.2, and decreased I_{Kr} density and HERG1b observed in human HCM (Coppini et al., 2013). These specific features of HCM remodeling were incorporated because they have been shown to be important to the development of EADs in previous studies of human HCM (Coppini et al., 2013). A range of values was used because HCM remodeling has been shown to be progressive over time (Gersh et al., 2011; Semsarian et al., 1997).

Myofilament remodeling was incorporated to simulate altered thin filament activation and myofilament Ca^{2+} sensitivity found in human HCM. Changes in thin filament activation have been linked to altered phosphorylation of cardiac Troponin I

(cTnI) (Messer et al., 2007), mutations in cardiac troponin T (cTnT) (Miller et al., 2001) and mutations in cardiac myosin binding protein C (cMyBP-C) (Carrier et al., 2015; Kampourakis et al., 2014; Mun et al., 2014; Previs et al., 2015; Sequeira et al., 2015; Witayavanitkul et al., 2014), which occur in HCM in humans (Carrier et al., 2015; Sequeira et al., 2015) and animals (Miller et al., 2001; Warren et al., 2015). Although there are more sarcomeric mutations that cause HCM, such as in cardiac actin (ACTC), cardiac troponin C (TNNC1), and α-tropomyosin (TPM1) (Olivotto et al., 2015), less is known about how these affect thin filament activation, if at all. Furthermore, myocardial Ca^{2+} sensitivity, defined as the amount of Ca^{2+} necessary to produce half maximal force, is a function of thin filament activation and XB cycling rates and has been shown to be altered in HCM. Myocardial Ca^{2+} sensitivity has been found to increase by 1-7% in human HCM (Coppini et al., 2013; Robinson et al., 2007; Warren et al., 2015) and by 3-10% in animal models of HCM (Miller et al., 2001).

Despite the lingering uncertainty in the mechanisms by which these sarcomeric mutations lead to the altered myofilament properties outlined above and the uncertainty of the exact amount by which the myofilament properties are altered in HCM, these studies indicate that myofilament parameters involved in thin filament activation and Ca^{2+} sensitivity are important components of the disease manifestation and therefore may contribute to the emergence of EADs. To elucidate if and how changes to myofilament parameters in human HCM promote the emergence of EADs or modulate the frequency of EAD occurrence, we incorporated HCM remodeling into the Rice *et al* myofilament model. Specifically, we altered thin filament activation, embodied in the Rice *et al* model by these 3 parameters: $perm_{50}$, k_{offH}, and k_{on}. The parameters k_{npT} and k_{pnT} are nonlinear transition

rates that are functions of these 3 parameters and represent nearby regulatory unit (RU)-based and calcium-based activation of the thin filament, which is shown in Figure 5.1 as the transition of the thin filament from the N_{XB} state (XB formation is inhibited) to the P_{XB} state (weakly bound XB formation is possible). The parameter $perm_{50}$ is the half activation constant for the shift of a thin filament RU from N_{XB} to P_{XB}, k_{offH} is the rate constant for Ca^{2+} unbinding from the high affinity binding site of Troponin C, and k_{on} is rate constant for Ca^{2+} binding to Troponin C. Due to the uncertainty in the literature regarding the exact amount that these parameters change in HCM, as described above, we explored HCM – induced remodeling of these 3 myofilament parameters within the range of 85% to 115% of their baseline values (increments of 5%) (Table 5.1).

<table>
<tr><th>Parameter</th><th>Baseline Value (BV)</th><th>HCM Value</th><th colspan="2">Effect of HCM Remodeling on EADs</th></tr>
<tr><td>G_{CaL}</td><td>$7.96*10^{-5}$ cm/(ms*μF)</td><td>Range of Values (Increments of 0.1):

BV*2.5 to BV*5.0</td><td colspan="2">Increase necessary for EAD Emergence</td></tr>
<tr><td>G_{Kr}</td><td>0.153 nS/pF</td><td>Range of Values (Increments of 0.1%):

BV*10% to BV*100%</td><td colspan="2">Decrease necessary for EAD Emergence</td></tr>
<tr><td>$perm_{50}$</td><td>0.5 (unitless)</td><td rowspan="3">Range of Values (Increments of 5%):

BV*85% to BV*115%</td><td>Increase</td><td rowspan="3">Enhances MEF effects on EAD emergence & frequency of occurrence</td></tr>
<tr><td>k_{offH}</td><td>25 1/s</td><td>Increase</td></tr>
<tr><td>k_{on}</td><td>47.5 1/μMs</td><td>Decrease</td></tr>
</table>

Table 5.1 Baseline and HCM Values for Important Model Parameters.
G_{CaL} and G_{Kr} are from the ten Vandersickel *et al* ionic model (Vandersickel et al., 2014). $perm_{50}$, k_{on}, and k_{offH} are from the Rice *et al* myofilament model (Rice et al., 2008).

5.2.3 EAD Protocol

Studies of cardiomyocytes from HCM patients have shown that EADs arise at pacing frequencies ranging from 0.25-1 Hz (Coppini et al., 2013), consistent with clinical studies in which arrhythmias arose in HCM patients who were sedentary, asleep, or performing normal daily activities (Maron et al., 1994; Maron et al., 2009); EADs have also been induced, at these rates, in computational electrophysiological models of human ventricular arrhythmias associated with HCM (Vandersickel et al., 2014; Zimik et al., 2015). To induce EADs in the bidirectionally and unidirectionally coupled HCM

electrophysiology-force myocyte models, we used a pacing protocol similar to those in Zimik *et al* (Zimik et al., 2015) and Vandersickel *et al* (Vandersickel et al., 2014). We isometrically paced the myocyte models at one of three pacing cycle lengths (CLs) (1000 ms; 1Hz, 2000 ms; 0.5 Hz, or 4000 ms; 0.25 Hz) for 100 beats. After the first 50 beats, all of our simulations had reached steady state, similar to previous studies (Zile and Trayanova, 2016). The final 50 beats were used to analyze the emergence of EADs and the frequency of their occurrence. Since sarcomere length (SL) changes during the cardiac cycle (ranging from 1.70 – 2.40 μm) (Trayanova and Rice, 2011a) and since it is known to modulate MEF (Zile and Trayanova, 2016), isometric simulations for each pacing rate were run three times, once at a constant SL of 1.70, 1.90 or 2.40 μm.

To determine if MEF modifies EAD formation for varying degrees of HCM-induced reduced repolarization reserve in HCM myocytes, we compared EAD formation in simulations with the bidirectionally vs unidirectionally coupled HCM myocyte models using the protocol above. Since there is a wide spectrum of HCM-induced myofilament remodeling (including no myofilament remodeling at all) (Gersh et al., 2011; Gray et al., 2011; Maron and Semsarian, 2010; Maron et al., 2011), we first compared simulations with and without feedback that incorporated only HCM-induced ionic remodeling.

Then, to elucidate how the severity of HCM-induced myofilament remodeling alters the effects of MEF on EAD formation, we compared bidirectionally coupled simulations with only HCM-induced ionic remodeling (described above) to those with HCM-induced ionic remodeling and different amounts of HCM-induced myofilament remodeling (described below) using the aforementioned protocol. To incorporate different amounts of HCM-induced myofilament remodeling in the simulations, one of the 3

myofilament parameters ($perm_{50}$, k_{offH}, k_{on}) was assigned a value 5-15% below or above its baseline value (as described in the previous section) for a given simulation.

5.2.4 Analysis of EADs

An EAD was defined as a slowing or reversal of normal repolarization during the plateau or rapid depolarization phases (phases 2 or 3) of an action potential (AP) (Vandersickel et al., 2014; Weiss et al., 2010). We narrowed this definition by requiring that the spontaneous depolarization(s) in phase 2 or 3 be larger than 1 mV. Therefore, an EAD was said to be elicited in a simulation if at least 1 of the final 50 APs had at least one spontaneous depolarization(s) in phase 2 or 3 that was larger than 1 mV.

The frequency of EAD occurrence was calculated as the number of beats that elicited an EAD. Specifically,

$$\text{frequency of EAD occurrence} = \frac{\text{\# of action potentials with 1 or more EADs}}{\text{total number of beats}} \quad \text{(Equation 5.2)}$$

where the total number of beats were defined as the final 50 beats of each simulation.

5.3 Results

5.3.1 MEF Alters EAD Emergence and Frequency of Occurrence

Incorporating HCM-induced repolarization reserve reduction in the bidirectionally and unidirectionally coupled cellular electrophysiology-force models without HCM-induced myofilament remodeling elicited EADs similar to those shown previously

(Vandersickel et al., 2014; Zimik et al., 2015), which resulted in an elongated active force transient, as expected (Coppini et al., 2013). However, there needed to be a sufficient reduction in repolarization reserve for EADs to emerge (Vandersickel et al., 2014; Zimik et al., 2015). An example of unaffected APs (without EADs) when repolarization reserve reduction is insufficient (G_{Kr} 50% of baseline, G_{CaL} 3.8 fold above baseline) in the bidirectionally (light blue) and unidirectionally (red) coupled models is shown in Figure 5.2A, where transmembrane voltage (V_m) is plotted as a function of time for pacing at a CL of 2000 ms (0.5 Hz) and a SL of 1.90 μm. The corresponding active force traces, as a function of time (Figure 5.2C), were also unchanged. There were no differences in the APs or normalized active force traces between the bidirectionally and unidirectionally coupled models, despite a slight difference (32 μM vs 40 μM) in peak $[Ca]_{Troponin}$ (Figure 5.2B), the term that represents the feedback from the myofilament model to the ionic model.

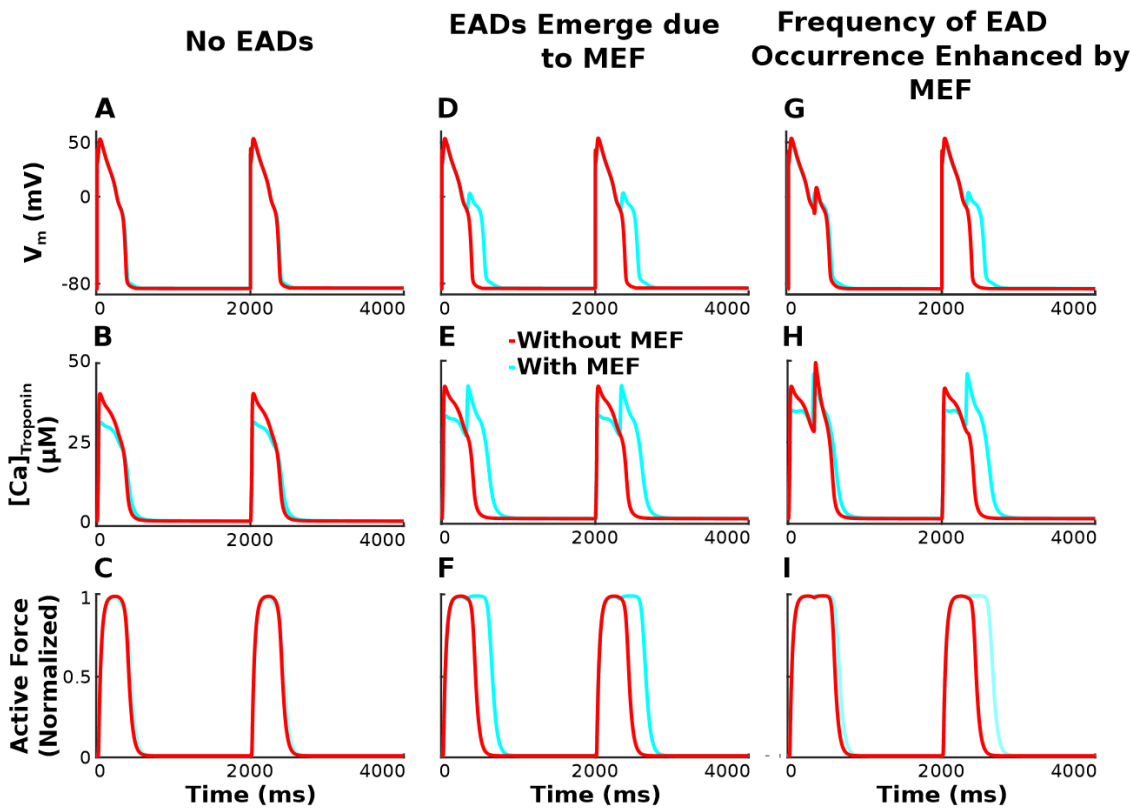

Figure 5.2 V_m (row 1), $[Ca]_{Troponin}$ (row 2), and active force (row 3) are plotted over time for simulations incorporating HCM-induced ionic remodeling in the absence of myofilament remodeling for a pacing CL of 2000 ms, SL=1.90 μm, and G_{Kr} 50% of baseline. Columns 1-3 have progressively enhanced G_{CaL} (3.8, 4.0, 4.2 fold above baseline), illustrating that the degree of repolarization reserve reduction affects the emergence of EADs and the frequency of their occurrence differently for simulations with the bidirectionally coupled model (with MEF; light blue) vs the unidirectionally coupled model (without feedback; red).

An example of APs with EADs (sufficient reduction in repolarization reserve ensured by G_{CaL} 4.0 fold vs 3.8 fold above baseline, other parameters identical to those in Figure 5.2A-C) in the bidirectionally coupled model (light blue) is shown in Figures 5.2D and 5.3A, and the corresponding prolonged active force trace in Figures 5.2F and 5.3B. If MEF is removed, the resulting unidirectionally coupled model does not exhibit EADs or prolongation of the active force trace, despite the significant reduction in repolarization reserve. In the bidirectionally coupled model, Troponin C binds free intracellular Ca^{2+} and

decreases the pool of free Ca^{2+} ions available in the cytoplasm ($[Ca]_i$) as shown in Figure 5.3C. During the early AP, the feedback via the $[Ca]_{Troponin}$ term (Equation 5.1) shown in Figures 5.2E and 5.3D in the bidirectionally coupled model, resulted in smaller peak $[Ca]_i$ than that in the unidirectionally coupled model. This smaller $[Ca]_i$ in the bidirectionally coupled model causes the sodium-calcium exchanger current (I_{NaCa}) in Figure 5.3E to be larger while functioning in its reverse mode (since it is a function of the Ca^{2+} gradient across the membrane), allowing more Ca^{2+} ions into the cell without dramatically increasing $[Ca]_i$ (since many of these Ca^{2+} ions then bind to Troponin C). As the AP progresses, the remaining Ca^{2+} ions in the cytoplasm are available to be extruded from the cell via I_{NaCa} during its forward mode or via the sarcolemmal calcium pump (I_{pCa}) shown in Figure 5.3F, or pumped into the sarcoplasmic reticulum (SR; Figure 5.3G) via the sarcoplasmic reticulum Ca^{2+}-ATPase (I_{up}; Figure 5.3H). However, since I_{NaCa} is a function of the Ca^{2+} gradient across the membrane and since $[Ca]_i$ is smaller due to buffering by Troponin C in the bidirectionally coupled model, less Ca^{2+} ions are extruded from the cell via I_{NaCa} thereby leaving more to be pumped into the SR via I_{up}. Larger $[Ca]_{SR}$ in simulations with the bidirectionally coupled model increases the opening rate and decreases the closing rate of the ryanodine receptor (RyR), resulting in larger Ca^{2+} release from the SR (I_{rel}; Figure 5.3I) and increased Ca^{2+} in the subspace ($[Ca]_{ss}$; Figure 5.3J). If $[Ca]_{ss}$ is sufficiently large (as it is for the bidirectionally but not unidirectionally coupled model), spontaneous calcium-induced calcium release (CICR) occurs. This further increases $[Ca]_{ss}$, which then via increased diffusion (I_{xfer}; Figure3K), dramatically increases $[Ca]_i$ during early repolarization resulting in increased I_{NaCa} in forward mode. If the inward current from I_{NaCa} in forward mode delays repolarization long enough (as it does with the

bidirectionally coupled model), I_{CaL}, as shown in Figure 5.3L, is able to recover from inactivation and increase enough to overcome the outward current through the rapid and slow delayed rectifier channels (I_{Kr} and I_{Ks}; Figures 5.3M-N), causing an EAD to form. This exemplifies how MEF can elicit EADs in bidirectionally coupled electrophysiology-force cell models under conditions of significant repolarization reserve, when EADs are not elicited in comparable simulations with the unidirectionally coupled model. Therefore, MEF diminishes the degree of repolarization reserve reduction necessary for EADs to emerge in simulations with the bidirectionally coupled model compared to those with the unidirectionally coupled model.

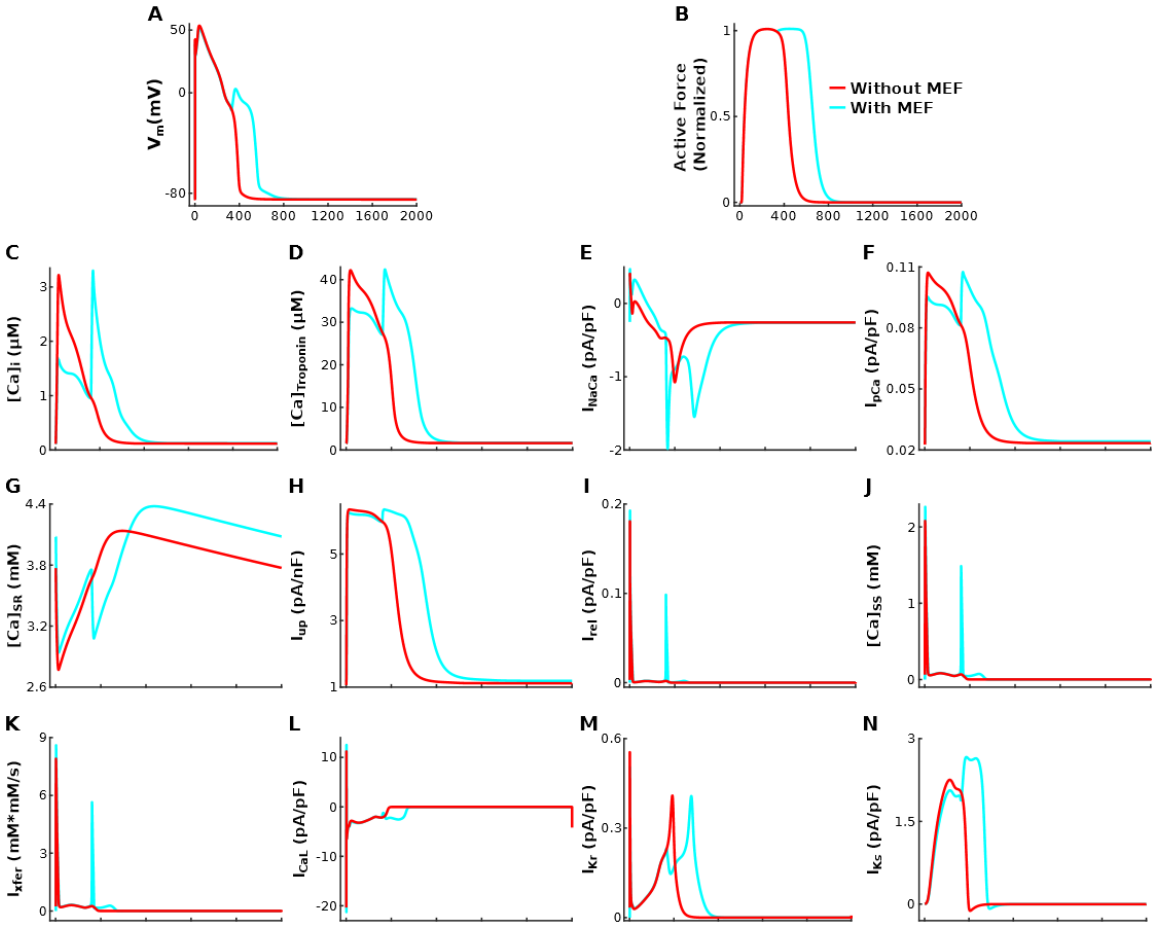

Figure 5.3 V_m (A), active force (B), $[Ca]_i$, (C), $[Ca]_{Troponin}$ (D), I_{NaCa} (E), I_{pCa} (F), $[Ca]_{SR}$ (G), I_{up} (H), I_{rel} (I), $[Ca]_{SS}$ (J), I_{xfer} (K), I_{CaL} (L), I_{Kr} (M), and I_{Ks} (N) are plotted over time for simulations incorporating HCM-induced ionic remodeling in the absence of myofilament remodeling for a pacing CL of 2000 ms, SL=1.90 μm, G_{Kr} 50% of baseline, and G_{CaL} 4.0 fold above baseline, highlighting the mechanism underlying the effects of MEF on EAD emergence and frequency by comparing the bidirectionally coupled model (with MEF; light blue) to the unidirectionally coupled model (without MEF; red).

When repolarization reserve is reduced further (G_{CaL} increased to 4.2 fold above baseline), both the bidirectionally and unidirectionally coupled models exhibit at least one AP with an EAD (Figure 5.2G) and one corresponding force trace that is of increased duration (Figure 5.2I). However, due to the difference in buffering of Ca^{2+} as a result of MEF (Figure 5.2H), the frequency of EAD occurrence is increased in the bidirectionally

coupled model relative to the unidirectionally coupled one (2 APs with an EAD vs 1). After an EAD occurs in beat one, there is an excess of Ca^{2+} ions in the cytoplasm, due to Ca^{2+} release from the SR and from reactivated I_{CaL}, for simulations with both the bidirectionally and unidirectionally coupled models. In the bidirectionally coupled model, some of those Ca^{2+} ions bind to Troponin C, reducing $[Ca]_i$ during the 2nd repolarization relative to that in the unidirectionally coupled model. The remaining free Ca^{2+} ions in the cytoplasm are then pumped into the SR by I_{up}, or extruded from the cell via I_{NaCa}, and I_{pCa}. However, the decreased $[Ca]_i$ reduces forward mode I_{NaCa} and enhances the amount of Ca^{2+} stored in the SR for bidirectionally vs unidirectionally coupled models. If sufficiently large (as it is in this example for the bidirectionally but not unidirectionally coupled simulations), this $[Ca]_{SR}$ load is enough to cause increased I_{rel} and elevated $[Ca]_{ss}$ in the second beat triggering spontaneous CICR and an EAD, thus increasing the frequency of EAD occurrence in bidirectionally vs unidirectionally coupled simulations due to MEF.

5.3.2 Faster Pacing Enhances Effects of MEF on EAD Emergence and Frequency

The stability diagrams of G_{Kr} and G_{CaL} in Figure 5.4A-C illustrate that EADs arise when HCM-induced repolarization reserve is sufficiently reduced (smaller G_{Kr} and larger G_{CaL}) in the absence of HCM-induced myofilament remodeling, most prominently at faster pacing rates; the light blue line divides simulations with the bidirectionally coupled model that elicited no EADs (on the left) from those that had at least one EAD (on the right) for CLs of 4000 ms (Figure 5.4A), 2000 ms (Figure 5.4B) and 1000 ms (Figure 5.4C), with

SL=1.90 µm. The red lines denote the same division for simulation results with the unidirectionally coupled model.

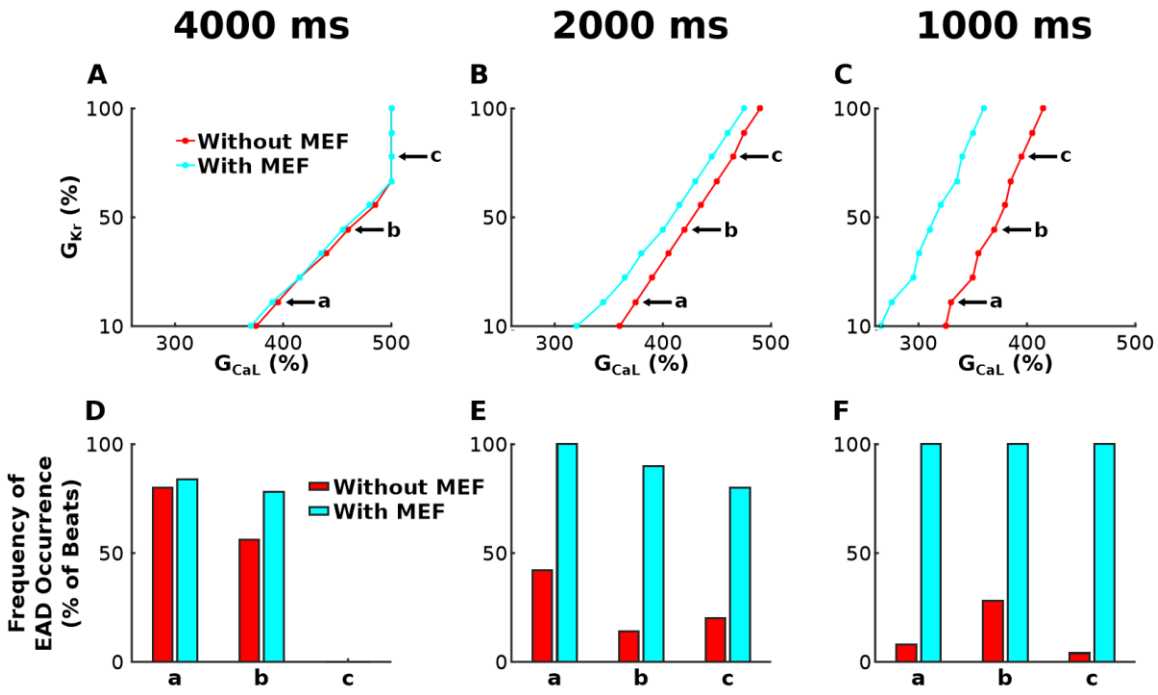

Figure 5.4 Stability diagrams of G_{Kr} and G_{CaL} for simulations with the bidirectionally (light blue) and unidirectionally (red) coupled model incorporating HCM-induced ionic remodeling in the absence of myofilament remodeling for SL=1.90 µm at pacing CL=4000 ms (A) 2000 ms (B) and 1000 ms (C). The light blue (and red) line divides results of simulations with the bidirectionally coupled (unidirectionally coupled) model that elicited no EADs (on the left) from those that had at least one EAD (on the right). Simulations represented by the points on the lines all contained at least one EAD, except for 3 simulations at CL=4000 ms, with G_{CaL}=5*baseline and G_{Kr} = 80, 90, 100% of baseline, respectively. Frequency of EAD occurrence is plotted in (D)-(F) for simulations at three representative points labeled a, b, and c in the corresponding stability diagrams in (A)-(C). Simulations at a, b, and c have G_{Kr}=20, 50 and 80% of baseline and the following G_{CaL} values: 3.95, 4.60 and 5.00 times larger than baseline at CL=4000 ms; 3.75, 4.20 and 4.65 times larger at CL=2000 ms; and 3.30, 3.70, 3.95 times larger at CL=1000 ms.

Faster pacing enhanced the effects of MEF on the emergence of EADs, which is evidenced by the progressive separation of the red and light blue lines in Figure 5.4A-C. For pacing at CL=4000 ms, the degree of repolarization reserve reduction necessary to elicit EADs was similar for the bidirectionally and unidirectionally coupled models as

shown in Figure 5.4A (minimal separation between lines); the minimum amount of repolarization reserve reduction necessary to elicit EADs was decreased on average by 1.0% for simulations with vs without MEF. At CL=2000 ms and CL=1000 ms, this effect was amplified; the minimum amount of repolarization reserve reduction necessary to elicit EADs was decreased on average by 4.6% at CL=2000 ms and 15.1% at CL=1000 ms for simulations with vs without MEF. This enhanced effect of MEF on the emergence of EADs with faster pacing was due to the progressively elevated $[Ca]_i$ during the early AP, which occurred due to a buildup of diastolic $[Ca]_i$ as a result of the progressively shorter time between beats needed for the I_{up}, I_{NaCa}, and I_{pCa} to restore $[Ca]_i$ to normal. In the bidirectionally coupled model, this elevation in $[Ca]_i$ was lower than it was in the unidirectionally coupled model because some of the excess Ca^{2+} ions were able to bind to Troponin C instead of remaining unbound in the cytosol. Since Troponin C did not become saturated with Ca^{2+} even at the fastest pacing rates, the difference between $[Ca]_i$ in simulations with the unidirectionally vs bidirectionally coupled models was progressively enhanced as pacing rates were increased (CLs decreased). This difference in $[Ca]_i$, as described in Results section 3.1 (via altered I_{NaCa} behavior, greater $[Ca]_{SR}$, enhanced I_{rel}, enlarged $[Ca]_{ss}$, and CICR), reduced the degree of repolarization reserve reduction necessary for EADs to emerge in simulations with the bidirectionally coupled model. Since the difference in $[Ca]_i$ between the unidirectionally and bidirectionally coupled models progressively increased with increased pacing rate, the difference in the degree of repolarization reserve reduction necessary for EADs to emerge also became progressively larger.

Faster pacing also heightened the effects of MEF on the frequency of EAD occurrence. In Figure 5.4D-F, the frequency of EAD occurrence (defined in Methods 2.4) was plotted at three representative points labeled a, b, and c in the corresponding stability diagrams in Figure 5.4A-C. At these points, MEF increased the frequency of EAD occurrence in bidirectionally vs unidirectionally coupled simulations on average by 8.7% for CL=4000 ms (Figure 5.4D), 64.7% for CL=2000 ms, and 86.7% at CL=1000 ms. This progressive increase in EAD frequency with faster pacing, is due to progressively elevated $[Ca]_i$ during the early AP resulting in increasingly elevated $[Ca]_{SR}$ in the bidirectionally vs unidirectionally coupled models, as described in the preceding paragraph. Via the mechanism described in Results section 3.1, this progressive elevation in $[Ca]_{SR}$ in the subsequent beat progressively increased the probability of spontaneous CICR and thus the frequency of EAD occurrence.

5.3.3 Longer Sarcomere Length Diminishes MEF Effects on EAD Emergence and Frequency

Stability diagrams of G_{Kr} and G_{CaL}, similar to those in Figure 5.4, illustrate how SL affects the degree of HCM-induced repolarization reserve reduction necessary for EAD emergence in simulations with the bidirectionally coupled electrophysiology-force myocyte model in the absence of HCM-induced myofilament remodeling for pacing at CL=2000 ms (Figure 5.5A) and CL=1000 ms (Figure 5.5B) for SL=1.70 µm (dark blue), 1.90 µm (light blue), and 2.40 µm (green). Since pacing at CL=4000 ms elicited little difference in the amount of repolarization reserve necessary for EAD formation or the frequency of EADs between the bidirectional and unidirectional models, we did not

evaluate the effects of SL for pacing at CL=4000 ms. Pacing at CL=2000 ms, contracted myocytes (SL=1.70 μm) compared to those at resting length (SL=1.90 μm) required on average 2.4% less reduction in repolarization reserve for EAD emergence (dark blue line left shifted relative to light blue line). Stretched myocytes (SL=2.40 μm) required on average 2.1% more repolarization reserve reduction for EAD emergence compared to those at resting length (green line right shifted relative to light blue line). These examples show that shorter SLs enhance EAD formation. By definition, increasingly shorter SLs have a progressively decreased fraction of single-overlap thin filament opposing the thick filament. Since this portion of the thin filament has a higher binding affinity to calcium, a progressively smaller fraction of it causes Ca^{2+} to dissociate increasingly faster from Troponin C during early repolarization in simulations with shorter vs longer SLs. This reduction of Ca^{2+} buffering by Troponin C enhances $[Ca]_i$ during early repolarization resulting in enhanced forward mode I_{NaCa}. Since forward mode I_{NaCa} produces an inward current, increasingly larger I_{NaCa} for shorter SLs resulted in longer delays in AP repolarization. These increased delays provided I_{CaL} with progressively longer times to recover from voltage-gated inactivation and to self-amplify sufficiently to become greater than the sum of outward currents (including I_{Kr}). Since I_{CaL} is a function of $G_{CaL,}$ cases with diminished G_{CaL} will require more time for self-amplification. Similarly, enhanced G_{Kr} will result in larger outward currents requiring that I_{CaL} be larger in order to overcome them, and thus requiring a longer period of delayed repolarization to allow greater self-amplification of I_{CaL}. Since shorter SLs at CL=2000 ms result in increased delays in AP repolarization, EADs are elicited in simulations with increasingly large repolarization reserve (progressively larger G_{Kr} and smaller G_{CaL}). However, SL does not affect the degree

of repolarization reserve reduction necessary for EAD emergence at CL=1000 ms (Figure 5.5B), since I_{CaL} had sufficient time to self-amplify in all cases due to the large $[Ca]_i$ at CL=1000ms.

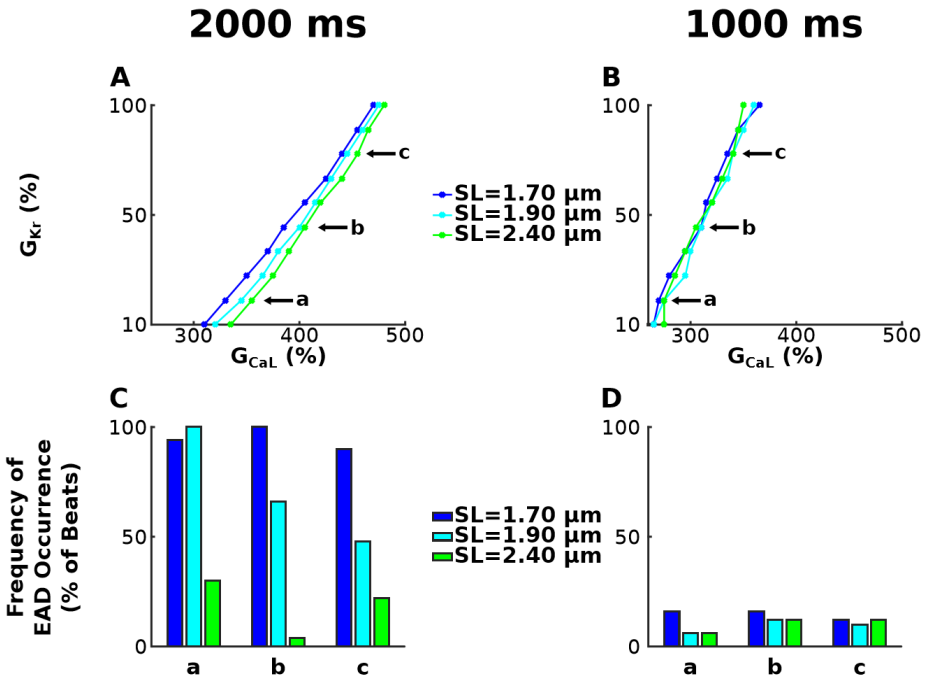

Figure 5.5 Stability diagrams of G_{Kr} and G_{CaL}, similar to those in Figure 5.4, for simulations with the bidirectionally coupled electrophysiology-force myocyte model without myofilament remodeling for pacing at CL=2000 ms (A) and CL=1000 ms (B) for SL=1.70 µm (dark blue), 1.90 µm (light blue), and 2.40 µm (green). Frequency of EAD occurrence is plotted in (C)-(D) for simulations at three representative points labeled a, b, and c in the corresponding stability diagrams in (A)-(B). Simulations at a, b, and c have G_{Kr}=20, 50 and 80% of baseline and the following G_{CaL} values: 3.55, 4.05 and 4.55 times larger than baseline at CL=2000 ms, and 2.75, 3.10 and 3.40 times larger at CL=1000 ms.

Longer SLs also diminished the effect of MEF on the frequency of EAD occurrence. In Figure 5.5C-D, the frequency of EAD occurrence was plotted for both models at three representative points labeled a, b, and c in the corresponding stability diagram in Figure 5.5A-B. The frequency of EAD occurrence at these points illustrates

longer SLs result in fewer EADs. At SL=2.40 μm there are 52.7% less EADs than at SL=1.90 μm and 76.0% less than at SL=1.70 μm for CL=2000 ms (Figure 5.5C). For CL=1000 ms (Figure 5.5D), SL=2.40 μm had 0.7% less EADs than SL=1.90 μm and 4.7% less than SL=1.70 μm. Similarly, SL=1.90 μm resulted in 23.3% less EADs than SL=1.70 μm at CL=2000 ms, and 5.3% less than SL=1.70 μm at CL=1000 ms. This decrease in the frequency of EAD occurrence for longer SLs is due to the enhanced binding affinity of Troponin C for Ca^{2+}. Via the mechanisms described in the preceding paragraph, this results in shorter delays in AP repolarization at longer SLs. When an equal degree of repolarization reserve reduction is incorporated in simulations, the cases with shorter delays in AP repolarization (due to diminished I_{NaCa} in forward mode) are less likely to have I_{CaL} recover from inactivation and are thus less likely to exhibit EADs. Therefore, longer SLs are associated with a diminished frequency of EAD occurrence.

5.3.4 Increased Severity of HCM-Induced Myofilament Remodeling Alters Effects of MEF on EAD Emergence and Frequency

Stability diagrams of G_{Kr} and G_{CaL}, similar to those in Figures 5.3 and 5.4, illustrate how the severity of HCM-induced myofilament remodeling affects the degree of HCM-induced repolarization reserve reduction necessary for EAD emergence in simulations with the bidirectionally coupled electrophysiology-force myocyte model. Figure 5.6 presents results regarding HCM-induced myofilament remodeling of parameters $perm_{50}$ (Figure 5.6A), k_{offH} (Figure 5.6B), and k_{on} (Figure 5.6C) for pacing at CL=2000 ms and SL=1.90 μm. Simulations for the bidirectionally coupled model with both HCM-induced ionic and myofilament remodeling with CL=4000 ms and 1000 ms, and for CL=2000 ms with SL=1.70 and 2.40 μm are not shown since the effects of myofilament remodeling severity

on MEF effects on EAD formation are similar to those shown in Figure 5.6. A 15% increase in $perm_{50}$, a 15% increase in k_{offH}, or a 15% decrease in k_{on}, decreases the degree of repolarization reserve reduction required for EAD emergence (left shifted lines in Figures 5.5A-C respectively) on average by 3.0%, 1.0%, and 1.4% respectively compared to no remodeling. The reverse is true for a 15% decrease in $perm_{50}$, a 15% decrease in k_{offH}, or a 15% increase in k_{on}; the degree of repolarization reserve reduction required for EAD emergence is increased on average by 1.2%, 1.2%, and 1.4% respectively compared to no remodeling. By definition, increasing $perm_{50}$ decreases nearest-neighbor cooperativity, resulting in decreased binding affinity of Troponin C on nearby RUs to Ca^{2+}, thus decreasing RU-based thin filament activation. By definition, increasing k_{offH} (and decreasing k_{on}) increases the unbinding rate (decreases the binding rate) of Ca to Troponin C, also resulting in decreased binding affinity of Troponin C to Ca^{2+}, thus decreasing Ca-based thin filament activation. These examples show that diminishing TroponinC-Ca^{2+} binding affinity via HCM-induced remodeling increases the likelihood for EAD formation and results in EADs in simulations under conditions of greater repolarization reserve, via the same mechanism described in Results section 3.3. Therefore, diminishing TroponinC-Ca^{2+} binding affinity via HCM-induced remodeling enhances the effects of MEF on EAD emergence.

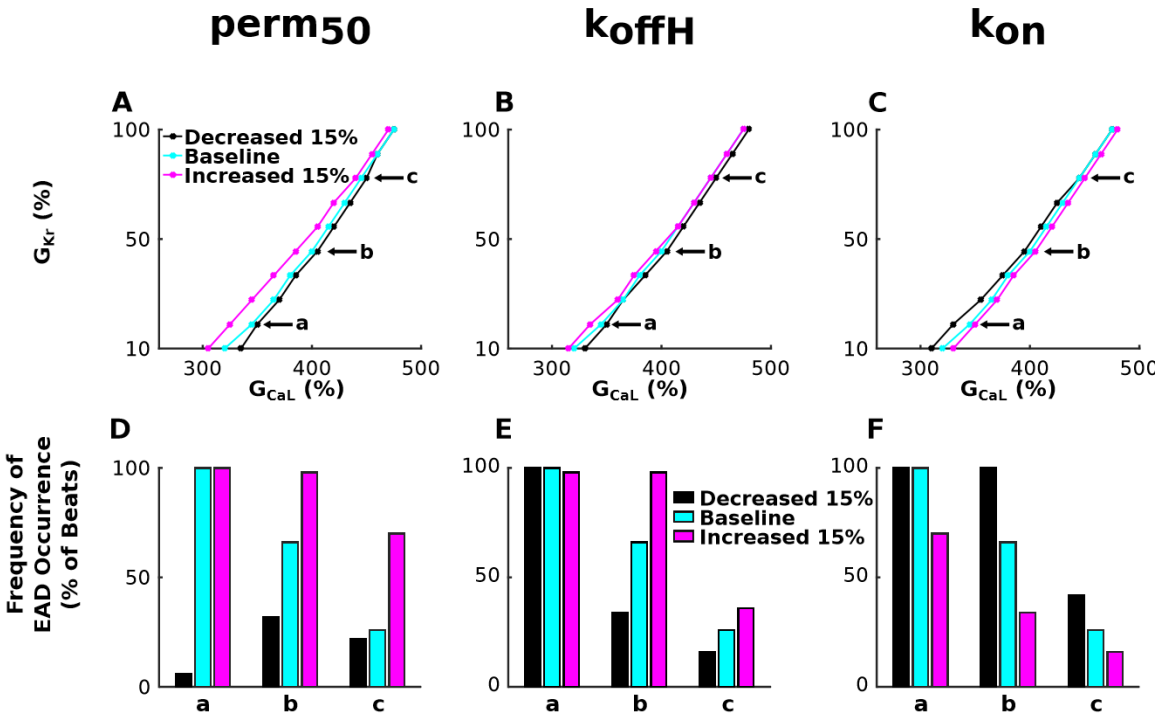

Figure 5.6 Stability diagrams of G_{Kr} and G_{CaL}, similar to those in Figures 5.3 and 5.4, for simulations with the bidirectionally coupled electrophysiology-force myocyte model with HCM myofilament remodeling in parameters $perm_{50}$ (A), k_{offH} (B), and k_{on} (C) for pacing at CL=2000 ms and SL=1.90 µm. Frequency of EAD occurrence is plotted in (D)-(F) for simulations at three representative points labeled a, b, and c in the corresponding stability diagrams in (A)-(C). Simulations at a, b, and c have G_{Kr}=20, 50 and 80% of baseline and G_{CaL} values 3.50, 4.05, and 4.50 times larger than baseline.

HCM-induced myofilament remodeling also affected the frequency of EAD occurrence. In Figure 5.6 D-F, the frequency of EAD occurrence was plotted for simulations with the bidirectionally coupled electrophysiology-force myocyte model at three representative points labeled a, b, and c in the corresponding stability diagram in Figure 5.6A-C. The graphs illustrate that HCM-induced myofilament remodeling that decrease the binding affinity of Troponin C to Ca^{2+} (increased $perm_{50}$, increased k_{offH}, decreased k_{on}) results in a larger number of EADs than in cases without remodeling.

Myofilament remodeling that increases TroponinC-Ca^{2+} binding affinity results in fewer EADs. Simulations with myofilament remodeling that decrease binding affinity (15% increase in $perm_{50}$, 15% increase in k_{offH}, and a 15% decrease in k_{on}) have an average of 25.3%, 13.3%, and 16.7% more EADs than respective simulations without myofilament remodeling at CL=2000 ms. Conversely, simulations with myofilament remodeling that increase binding affinity (15% decrease in $perm_{50}$, 15% decrease in k_{offH}, and a 15% increase in k_{on}) have an average of 44.0%, 14.0% and 24.0% less EADs than respective simulations without myofilament remodeling at the same pacing rate.

5.4 Discussion

The present study examines whether myofilament protein dynamics mechanisms in HCM affect the incidence of EAD formation, which have been implicated as the primary mechanism underlying many arrhythmias associated with HCM. The goal of our study was to utilize the capability of mechanistic computer simulations to investigate whether myofilament protein dynamics mechanisms modulate EAD formation for varying degrees of reduced repolarization reserve in HCM, and to uncover how these mechanisms are affected by pacing rate, sarcomere length, and the severity of HCM-induced myofilament remodeling. Using bidirectionally and unidirectionally coupled human electrophysiology-force ventricular myocyte models, we showed that MEF on calcium dynamics in the bidirectionally coupled model, via Troponin C buffering of cytoplasmic Ca^{2+}, was the myofilament protein dynamics mechanism underlying EADs. We showed that incorporating MEF diminished the degree of repolarization reserve reduction necessary for EADs to emerge and increased the frequency of EAD occurrence, especially at faster

pacing rates. We also found that longer sarcomere lengths and enhanced thin filament activation diminished the effects of MEF on EADs. Together these findings demonstrate that myofilament protein dynamics mechanisms plays an important role in EAD formation and suggest that targeting MEF may be an alternative treatment approach for prevention of arrhythmia and thus SCD in HCM patients.

5.4.1 Modulation of EAD Incidence Occurs via MEF

SCD and arrhythmias have been shown to occur in patients with HCM, an inherited sarcomeric mutation-based disease (Coppini et al., 2013; Coppini et al., 2014; Maron et al., 2000). In addition, HCM patients with more than one sarcomeric mutation have a higher risk of SCD and a worse phenotype, independent of other risk factors (Van Driest et al., 2004). An important mechanism underlying many lethal arrhythmias found in HCM patients is EADs (Weiss et al., 2010; Yan et al., 2001), which also occur in patients with HCM (Coppini et al., 2013). In this HCM EAD study, the sarcomeric proteins cardiac myosin binding protein C and myosin heavy chain were mutated and evidence of altered $[Ca]_i$ transient kinetics was found. Furthermore, additional sarcomere mutations such as Troponin I (Messer et al., 2007), T (Miller et al., 2001), and C (Olivotto et al., 2015) and tropomyosin (Olivotto et al., 2015) have been found in HCM, all of which are sarcomeric proteins integral to Ca^{2+}-Troponin C binding (Tardiff et al., 2015). Taken together, the results from these previous studies suggest that MEF, via altered Troponin C-Ca^{2+} buffering, is a likely mechanism by which sarcomeric mutations can modulate the incidence of EADs. Our results presented here provide proof that sarcomeric mutations, via altered Troponin C buffering of cytosolic Ca^{2+} (resulting from MEF), can indeed alter

the degree of repolarization reserve reduction necessary for EADs to emerge and the frequency of EAD occurrence.

5.4.2 Effects of Altered Ca^{2+} Sensitivity on EADs and Arrhythmia in HCM

Ca^{2+} sensitivity is defined as the amount of Ca^{2+} necessary to produce half maximal force. When Ca^{2+} sensitivity is increased, less Ca^{2+} is required to produce half maximal force. Several studies have shown that increased Ca^{2+} sensitivity is associated with increased arrhythmogenicity (Baudenbacher et al., 2008; Huke and Knollmann, 2010). One animal study showed that the myosin inhibitor blebbistatin (which decreases Ca^{2+} sensitivity) reduced arrhythmia propensity in mice who had been hypersensitized to Ca^{2+} due to troponin mutations or Ca^{2+} sensitizing agents (Baudenbacher et al., 2008). Another showed that transgenic mice with different troponin T and I mutations had an increased incidence of premature ventricular complexes when injected with isoproterenol and an increased occurrence of ventricular tachycardia (Baudenbacher et al., 2008). However, none of these studies were conducted on human tissue or models and none incorporated the ionic remodeling changes that have been shown to occur in human HCM (Coppini et al., 2013). Neither did they investigate the myofilament protein dynamics mechanisms linking increased Ca^{2+} sensitivity to EADs or arrhythmia.

Human studies of HCM have shown that Ca^{2+} sensitivity is increased and that ventricular arrhythmias and SCD occur in HCM patients (Tardiff et al., 2015). However, ventricular arrhythmias and SCD also occur in dilated cardiomyopathy (DCM), which is characterized by a decrease in Ca^{2+} sensitivity (Sen-Chowdhry and McKenna, 2012). Therefore, to understand how altered Ca^{2+} sensitivity may potentially promote arrhythmogenicity in these sarcomeric mutation-based cardiac diseases, studies

investigating the effects of Ca^{2+} sensitivity on the mechanisms underlying arrhythmia are needed.

This study investigated the effects of increased Ca^{2+} sensitivity on EADs in a bidirectionally coupled human HCM myocyte model. Our results show that sarcomeric mutations, which disrupt the regulation of the thin filament (decreased $perm_{50}$, decreased k_{offH}, increased k_{on}) in a way that has a downstream effect of increasing Ca^{2+} sensitivity, increase the degree of repolarization reserve reduction necessary for EADs to emerge and decreases the frequency of EAD occurrence. Combined with the observations from the previous studies, this suggests that the enhanced arrhythmogenicity seen in HCM is not due to altered Ca^{2+} sensitivity, but rather due to HCM-induced ionic remodeling as suggested by Coppini et al (Coppini et al., 2013) or from secondary effects of myofilament remodeling at the tissue level, such as hypertrophy and fibrosis (Chan et al., 2014; Nucifora et al., 2015).

5.4.3 Limitations

A limitation of this study is that we do not incorporate sympathetic and parasympathetic stimulation, which is present during the cardiac cycle and could influence calcium cycling. Additionally, the conclusions of this study are in the context of a single myocyte; full understanding of the effects of myofilament dynamics on triggered activity (the manifestation of EADs at the organ level) will require tissue and whole heart simulations.

5.5 Conclusions

MEF, via Troponin C buffering of cytoplasmic Ca^{2+}, was the myofilament protein dynamics mechanism modulating EAD formation in a bidirectionally coupled human electrophysiology-force myocyte model of HCM. Our results demonstrate that accounting for MEF on calcium dynamics diminished the degree of repolarization reserve reduction necessary for EADs to emerge and increased the frequency of EAD occurrence, especially at faster pacing rates. Longer sarcomere lengths and enhanced thin filament activation diminished the effects of MEF on EADs. These findings demonstrate that myofilament protein dynamics mechanisms play an important role in EAD formation.

Study 3:

Increased Thin Filament Activation Enhances Alternans in Human Chronic Atrial Fibrillation

6.1 Introduction

Atrial fibrillation (AF) is the most common type of human cardiac arrhythmia which, due to its association with increased morbidity and mortality and its rising prevalence, has become a global health care concern (Ball et al., 2013; Chugh et al., 2014; Lip et al., 2012). Unfortunately, current therapies do not directly target the underlying mechanisms of AF (Fabritz et al., 2016; Hanley et al., 2016), due in part to an incomplete understanding of atrial arrhythmogenesis. Therefore, to enhance prevention and treatment of AF, our understanding of its underlying disease mechanisms needs to be expanded.

Action potential duration (APD) alternans (APD-ALT) is defined as beat-to-beat oscillations in APD. In human chronic AF (cAF), APD-ALT has been found to occur at heart rates of 120-200 beats per minute (bpm) (Narayan et al., 2002). Consequently, APD-ALT has been proposed as an important clinical marker for AF risk since its onset is at slower rates in cAF patients than in healthy subjects and since it always precedes AF initiation (Narayan et al., 2002). In addition, an increased propensity for APD-ALT in cAF has been shown to increase arrhythmia complexity and persistence (Chang and Trayanova, 2016). These findings indicate that APD-ALT occurring at slower rates (120-200 bpm) may be an important therapeutic target in AF patients.

APD-ALT at these clinically-relevant slower rates has been found to be driven by calcium transient alternans (CA-ALT) (Chang et al., 2014). Specifically, altered ryanodine receptor (RyR) kinetics and down regulation of L-type calcium (Ca2+) current have been identified as the components of the cAF-associated ionic remodeling that drive APD-ALT formation at the clinically-relevant slow heart rates (Chang et al., 2014). While the ionic mechanisms of APD-ALT formation in human cAF have been elucidated, little is known

about the effects of myofilament protein dynamics on APD-ALT, particularly at the clinically-relevant slower rates. Understanding whether myofilament protein dynamics modulates APD-ALT is important because it has been previously shown to alter Ca2+-driven voltage alternans in failing human ventricular myocytes (Zile and Trayanova, 2016). Myofilament remodeling has been documented in myocytes from cAF patients, including alterations in sarcomeric protein expression and phosphorylation, active and passive tension, myofilament calcium sensitivity, and crossbridge (XB) cycling rates (Belus et al., 2010; Eiras et al., 2006; El-Armouche et al., 2006). Finally, mechanical stretch, common in cAF (Thanigaimani et al., 2017), has been shown to increase the susceptibility of atrial myocytes to APD-ALT and enhance their spatial discordance (Tsai et al., 2011). Therefore, our goal in this study was to utilize the capability of mechanistic computer simulations to investigate whether remodeling in myofilament protein dynamics in human cAF alters APD-ALT at the clinically-relevant slow heart rates, and how the established relationships are affected by sarcomere length (SL) and the degree of cAF-induced myofilament remodeling.

6.2 Methods

6.2.1 Human Atrial Electromechanical Myocyte Model

To achieve the goals of this study, a human atrial electromechanical myocyte model was developed that combined the human atrial ionic model by Chang et al (Chang et al., 2014), shown in Figure 6.1A, and the human myofilament dynamics model by Zile et al (Zile and Trayanova, 2016; Zile and Trayanova, 2017) shown in Figure 6.1B. This human atrial ionic model was chosen due to its ability to generate APD-ALT at slower clinically-relevant pacing rates (Chang et al., 2014; Chang and Trayanova, 2016), consistent with findings in human cAF (Narayan et al., 2011). We modeled both right atrial (RA) and left atrial (LA) myocytes as done in Chang et al (Chang et al., 2014).

The Zile et al myofilament dynamics model, an extension of the Rice et al model (Rice et al., 2008) to the human myocyte from the original rabbit model, describes the activation of the thin filament by intracellular calcium binding to the regulatory site on Troponin C as well as thin filament binding to thick filament crossbridges (XBs) using a 6-state Markov model. Since the Zile et al myofilament model was developed to match human ventricular myocyte force data, here we made additional adjustments to match human atrial force data as described below.

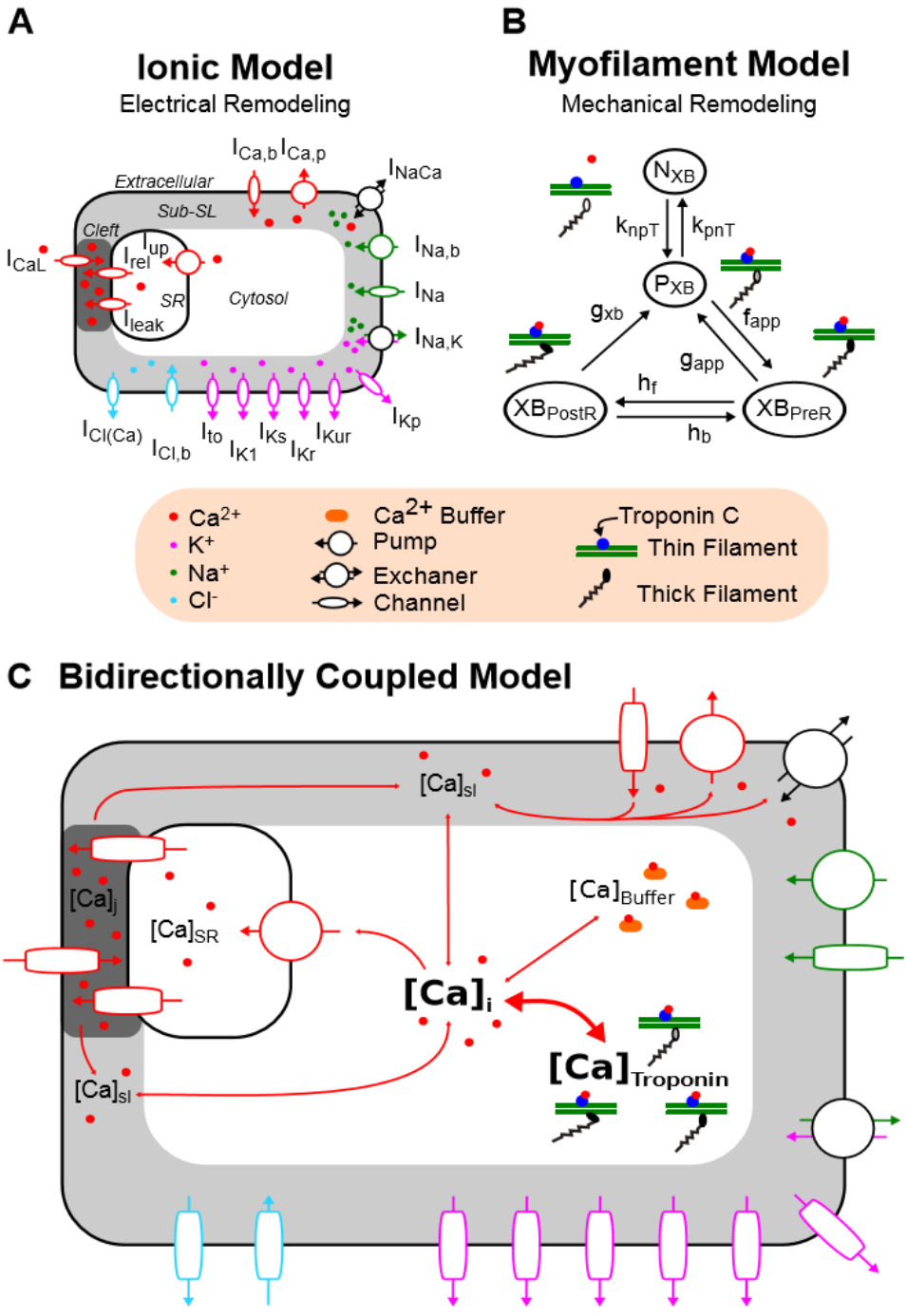

Figure 6.1 Bidirectionally Coupled Electromechanical Model of the Atrial Myocyte. The human atrial ionic model by Chang *et al* (A) and the human myofilament model by Zile *et al* modified to match human atrial force data (B) are coupled (C) by incorporating mechanoelectric feedback (thick red arrow linking $[Ca^{2+}]_i$ and $[Ca^{2+}]_{Troponin}$).

The ionic and myofilament models were bidirectionally coupled by having thin filament activation depend on the amount of free calcium in the cytosol ($[Ca^{2+}]_i$) and by incorporating mechanoelectric feedback (MEF) on calcium dynamics. Specifically, the $[Ca^{2+}]_i$ transient derived from the ionic model was used to drive thin filament activation in the myofilament model. Further, similarly to our previously developed approach (Zile and Trayanova, 2016; Zile and Trayanova, 2017), we incorporated MEF on calcium dynamics by replacing the existing state variable formulation for regulatory troponin C buffering of intracellular calcium ($[Ca^{2+}]_{Troponin}$) in the ionic model with the myofilament protein dynamics-dependent formulation from the myofilament model. Coupling the ionic and myofilament models bidirectionally with a myofilament protein dynamics-dependent representation of $[Ca^{2+}]_{Troponin}$ was necessary here because such coupling has been shown to be crucial for accurately reproducing contractile experimental data in myocyte simulations (Ji et al., 2015).

Using this bidirectionally coupled electromechanical model, we adjusted myofilament parameters to match normal human atrial force data. To do this, we solved a minimization problem similar to the approach by de Oliveira *et al* (de Oliveira et al., 2013), where the myofilament parameters (*par*) were adjusted to minimize the error between simulated and experimental values of total twitch time (TT), time to peak tension (TPT), and time to 50% relaxation of force ($T_{rel50\%}$), using the following equation:

$$Error(par) = \left|TT_{sim}(par) - TT_{exp}\right| + \left|TPT_{sim}(par) - TPT_{exp}\right| + \left|T_{rel50\%,\ sim}(par) - T_{rel50\%,\ exp}\right|$$

(Equation 6.1)

where TT_{exp}, TPT_{exp}, and $T_{rel50\%,\,exp}$ are the values (listed in Table 6.1, row 4) of each force characteristic averaged across three sets of experimental data (Bisping et al., 2007; Goetzenich et al., 2009; Maier et al., 2000). In these experiments, human RA myocytes (with SL of 2.4 μm and at temperature of 37 °F) were isometrically paced at 1Hz (1000 ms pacing cycle length) until steady state was reached. The variables $TT_{sim}(par)$, $TPT_{sim}(par)$, and $T_{rel50\%,\,sim}(par)$ were computed from our simulations with human RA myocytes, each run with a unique set of 11 adjusted myofilament parameters (*par*) as listed in the following notation:

$$par = [k_{np}, k_{pn}, g_{app}, f_{app}, h_f, h_b, g_{xb}, perm_{50}, k_{on}, k_{offH}, k_{offL}]$$

For each unique set of *par*, the myofilament parameters above were each assigned a value between 25% and 400% (in increments of 25%) of their control value from our earlier electromechanical model of the normal human ventricular myocytes (Zile and Trayanova, 2016). The set of adjusted myofilament parameters which resulted in the smallest error (0.2093) between simulation results and experimental data (the set to be referred to as par_{min}), as calculated from Equation 6.1, was used in this study. In par_{min}, the majority of myofilament parameters ended up not being altered, with the exception of k_{np} (25% of control), k_{pn} (150% of control), and g_{app} (200% of control). These adjusted myofilament parameter values are listed in Table 6.2. The force characteristic values ($TT_{sim}(par_{min})$, $TPT_{sim}(par_{min})$, and $T_{rel50\%,\,sim}(par_{min})$) from simulations with this normal human RA myocyte model are shown in row 6 of Table 6.1 for comparison with experimental values. Since no experimental human LA force data could be found, we also used par_{min} for our model of the myofilament dynamics of the healthy human LA myocyte.

		TT (ms)	TPT (ms)	$T_{rel50\%}$ (ms)
Experimental Values	Bisping *et al*	N/A	89 ± 10	N/A
	Goetzenich *et al*	N/A	95 ± 17	89 ± 14
	Maier *et al*	300 ± 24	91 ± 11	85 ± 7
	Average	*300*	*92*	*87*
	Range	*276 – 324*	*78-112*	*75-103*
	Simulation	**301**	**77**	**91**

Table 6.1 Force Characteristics of Human Right Atrial Myocytes
Force characteristics of human RA myocytes from experiments (Bisping et al., 2007; Goetzenich et al., 2009; Maier et al., 2000) and from simulations with our healthy human RA myocyte model using the myofilament parameter values par_{min} listed below in Table 6.2. Force characteristics in row 4 are averaged from the available experimental data (in rows 1-3) and appear in Equation 6.1 as TT_{exp}, TPT_{exp}, and $T_{rel50\%,exp,}$ respectively. TT = total twitch time, TPT = time to peak tension, $T_{rel50\%}$ = time to 50% relaxation of force.

6.2.2 Incorporating cAF-Induced Remodeling

Ionic remodeling in cAF resulting in the development of APD-ALT at clinically-relevant slow rates as well as arrhythmogenesis was incorporated in LA and RA myocytes as described previously (Chang et al., 2014; Chang and Trayanova, 2016). Specifically, Chang *et al* decreased g_{Na} by 10%, decreased g_{CaL} by 50%, increased $Ibar_{NCX}$ by 40%, increased ryanodine receptor Ca^{2+}-dependent activation rate (ko_{Ca}) 3-fold, decreased RyR Ca^{2+}-dependent inactivation rate (ki_{Ca}) by 50%, increased sarcoplasmic reticulum (SR) Ca^{2+} leak by 25%, and increased g_{Ks} and g_{K1} each 2-fold compared to normal in both the

LA and RA myocytes. Chang *et al* also added a late component to the sodium current (I_{NaL}) in the LA and RA myocytes. Finally, Chang *et al* decreased g_{Kur} by 45% and 55% and g_{to} by 45% and 80% compared to normal in LA and RA myocytes, respectively.

Myofilament remodeling representing abnormal force generation and myofilament Ca^{2+} sensitivity found in cAF was incorporated next. Active tension generation and relaxation rates have been shown to be slower and maximum active and passive force generation to be decreased in cAF myofibrils, suggesting that XB cycling rates are depressed (Belus et al., 2010; Eiras et al., 2006). In addition, myofilament Ca^{2+} sensitivity in human cAF myofibrils, as compared to normal, was found to be either significantly increased (Belus et al., 2010) or unchanged (Eiras et al., 2006). Furthermore, research has found alterations in sarcomeric protein expression and phosphorylation levels (Belus et al., 2010; Cazorla et al., 2006; Eiras et al., 2006; El-Armouche et al., 2006), suggesting that myofilament Ca^{2+} sensitivity is increased (Belus et al., 2010; Cazorla et al., 2006).

To incorporate decreased force generation rates and enhanced Ca^{2+} sensitivity in our atrial myofilament model, we increased thin filament activation and reduced XB cycling rates. We increased thin filament activation by increasing 2 parameters (k_{on}, k_{n_p}) and decreasing 4 parameters ($perm_{50}$, k_{offL}, k_{offH}, k_{p_n}). The parameters k_{npT} and k_{pnT} are nonlinear transition rates that are functions of these 6 parameters and represent calcium based activation of the thin filament, which is shown in Fig. 1 as the transition of the thin filament from the N_{XB} state (XB formation is inhibited) to the P_{XB} state (weakly bound XB formation is possible). The parameter $perm_{50}$ is the half activation constant for the shift of a thin filament regulatory unit (RU) from N_{XB} to P_{XB}, k_{offH} (k_{offL}) is the rate constant for Ca^{2+} unbinding from the high (low) affinity binding site of Troponin C, and k_{on} is the rate

constant for Ca^{2+} binding to Troponin C. The parameters k_{n_p} and k_{p_n} are constant scaling factors of the k_{npT} and k_{pnT} transition rates. We reduced XB cycling rates by increasing 2 parameters (g_{app}, h_b) and decreasing another three (f_{app}, h_f, g_{xb}). The rates f_{app} and g_{app} regulate the transition of the thin filament from the P_{XB} state to the strongly bound XB state, where the myosin head has not yet rotated and thus not induced strain in the neck region (XB_{PreR}). The parameters h_f and h_b are transition rates between the XB_{PreR} and XB_{PostR} states (thin filament is strongly bound to a XB, which has a rotated myosin head and has induced distortion). The parameter g_{xb} represents the ATP consuming transition rate from XB_{PostR} to P_{XB}. Since cAF-induced changes in mechanical properties (described in the preceding paragraph) do not directly translate to changes in myofilament model parameters, and due to the progressive nature of remodeling in cAF (Narayan et al., 2011), we explored cAF–induced remodeling of these myofilament model parameters within the range of 100% to 300% of their control values (increments of 25%) for k_{on}, k_{n_p}, g_{app}, and h_b, and within the range of 100% to 20% of their control values (increments of 10%) for $perm_{50}$, k_{offL}, k_{offH}, k_{p_n}, f_{app}, h_f, and g_{xb} (Table 6.2).

Myofilament Parameter	Normal (N)	Chronic AF (cAF)
k_{on}	47.5 1/μMs	**H*100% to H*300%** (25% Increments)
k_{n_p}	**152.5 s^{-1}**	
g_{app}	**186 s^{-1}**	
h_b	34 s^{-1}	
$perm_{50}$	0.5 (unitless)	**H*100% to H*20%** (10% Increments)
k_{offL}	250 s^{-1}	
k_{offH}	25 s^{-1}	
k_{p_n}	**24 s^{-1}**	
f_{app}	4800 s^{-1}	
h_f	10 s^{-1}	
g_{xb}	30 s^{-1}	

Table 6.2 Healthy and cAF Values for Myofilament Model Parameters.
Normal (N) and chronic atrial fibrillation (cAF) values of myofilament model parameters in the human LA and RA myocyte models. Myofilament parameters in par_{min} are bolded in column 2.

6.2.3 Alternans Protocol

To induce APD-ALT in our RA and LA cAF atrial myocyte models, we used a pacing protocol similar to that used in a clinical study by Narayan *et al* (Narayan et al., 2011) and in alternans computational studies (Chang et al., 2014; Chang and Trayanova, 2016). We first isometrically paced the myocyte model at a CL of 750 ms (80 bpm) until steady state was reached. Then, we paced it for 74 beats at each successive CL starting at 500 ms and descending, in 50 ms increments, to 300 ms. The analysis of simulation results focused particularly on assessing alternans levels from beats paced at a CL of 400 ms (150 bpm), since Narayan *et al* (Narayan et al., 2011) observed that that was the average alternans onset CL in cAF patients.

To determine how the severity of cAF-induced myofilament remodeling alters APD-ALT, we incorporated different amounts of cAF-induced myofilament remodeling in our simulations. One of the 11 myofilament parameters ($perm_{50}$, k_{offL}, k_{offH}, k_{p_n}, f_{app}, h_f, g_{xb}, k_{on}, k_{n_p}, g_{app}, and h_b) was assigned a non-control value (as described in the previous section) for a given simulation. To determine how SL modifies the effects of MEF on APD-ALT formation, we ran each of these simulations for a SL value between 1.7 and 2.3 μm (in increments of 0.1 μm). These SLs were chosen because they represent the SL range that occurs during a normal cardiac cycle (Trayanova and Rice, 2011a).

.

6.2.4 Analysis of Alternans

APD was defined as the time from maximal upstroke velocity to 90% repolarization of transmembrane voltage (V_m) from peak amplitude (Hayashi et al., 2003; Kim et al., 1997). APD alternans normalized magnitude (APD-ANM) was calculated (Chang et al., 2014; Chang and Trayanova, 2016; Narayan et al., 2011) as the mean magnitude of change in APD over the last 10 pairs of beats (11 total beats) at a given pacing CL divided by the mean APD over the final 10 beats, using the equation below:

$$APD - ANM = \frac{\sum_{i=beat\ \#63}^{beat\ \#73}(\,|APD_i - APD_{i+1}|\,)/10}{average\ APD\ for\ beats\ 64{-}74}$$

(Equation 6.3)

$[Ca^{2+}]_i$ and $[Ca^{2+}]_{Troponin}$ (CA-ALT and CaT-ALT respectively) were quantified in the same manner as APD-ALT with the change in each variable defined as the difference in

amplitude between beats. Alternans normalized magnitude (ANM) > 5% was the threshold for ANM to be considered significant.

6.3 Results

6.3.1 The Effect of Bidirectionally Coupling a Myofilament Model to the Ionic Model: MEF Alters Normal Membrane Kinetics

Coupling our model of the normal myocyte bidirectionally (i.e. representing the effect of MEF on the ionic component of the model) altered the membrane kinetics in the ionic component of our electrotechnical model compared to the uncoupled ionic model of the normal myocyte. This is shown in Figure 6.2 for the action potential, $[Ca^{2+}]_i$, and $[Ca^{2+}]_{Troponin}$. APD_{90} and $[Ca^{2+}]_i$ transient behavior are slightly different in our electromechanical RA model compared to the RA ionic model (APD_{90} 300 vs 284 ms; $[Ca^{2+}]_{i,diastolic}$ 0.1997 vs 0.2066 μM; $[Ca^{2+}]_i$ transient amplitude 0.3631 vs 0.2570 μM). Importantly, the APD_{90}, $[Ca^{2+}]_{i,diastolic}$, and $[Ca^{2+}]_i$ transient amplitude derived from our electromechanical model are in better agreement with currently available experimental human RA data (range 255-344 ms; 0.1197 μM; 0.3449 μM) (Christ et al., 2008; Voigt et al., 2009) than the uncoupled ionic model.

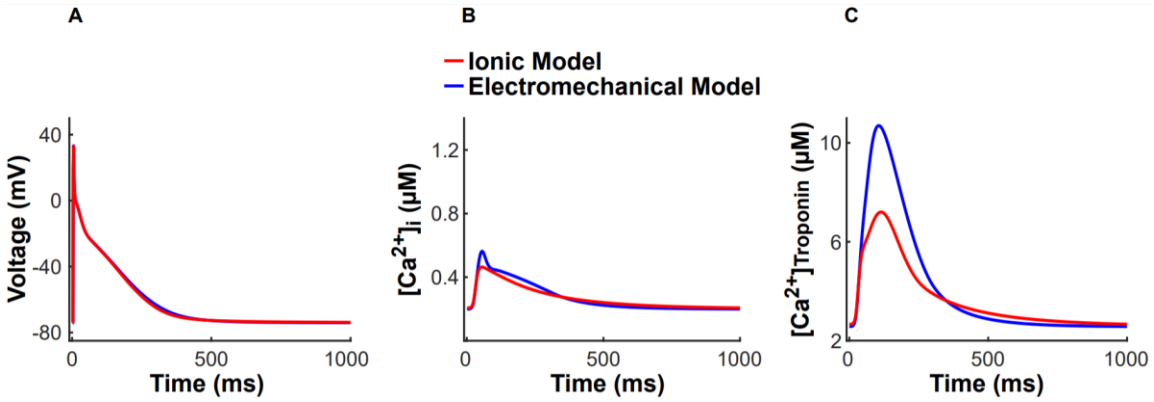

Figure 6.2 V_m (A), $[Ca^{2+}]_i$ (B), and $[Ca^{2+}]_{Troponin}$ (C) plotted over time for our electromechanical model (blue) and the uncoupled ionic model of the normal RA myocyte (Chang et al., 2014; Chang and Trayanova, 2016).

6.3.2 The Effect of Coupling a Myofilament Model to the cAF Ionic Model: Presence of MEF Diminishes APD-ANM

Since MEF changed the $[Ca]_i$ transient in our bidirectionally coupled electromechanical models compared to the uncoupled ionic models of the normal RA and LA myocytes (Chang et al., 2014; Chang and Trayanova, 2016), we investigated whether MEF could also modulate alternans in our cAF RA and LA electromechanical myocyte models. Incorporating only cAF-induced ionic remodeling (without myofilament remodeling, i.e. the myofilament model was that of a normal RA or LA myocyte) in our RA and LA electromechanical myocyte models resulted in sub-threshold alternans (ANM <5%) in APD, $[Ca^{2+}]_i$, and $[Ca^{2+}]_{Troponin}$ for the last 62 beats of the 74 beat train. An example is shown by the blue traces in Figure 6.3A-C, where V_m, $[Ca^{2+}]_i$, and $[Ca^{2+}]_{Troponin}$ are plotted for the RA myocyte as functions of time for the final two beats. APD-ANM, CA-ALT normalized magnitude (CA-ANM), and CaT-ALT normalized magnitude (CaT-ANM) values are 0.03%, 0.02%, and 0.04% respectively. Although ANM was below

threshold for the final 62 beats, there were significant, though progressively diminishing, alternans for the first 12 beats of the 74 beat train (not shown). This is in contrast to results from our uncoupled ionic model, which demonstrated that ANM were maintained above threshold for the duration of the 74 beats. An example is shown by the red traces in Figure 6.3A-C for V_m, $[Ca^{2+}]_i$, and $[Ca^{2+}]_{Troponin}$ (ANM 16%, 75%, 99%, respectively). The dampening effect of MEF on alternans is owed to the difference in how the models represent Troponin C buffering of free cytosolic Ca^{2+}. The uncoupled ionic model uses an equation that does not incorporate cooperativity (Michaelis-Menton formulation) unlike our electromechanical model, which uses a formulation that does incorporate key cooperativity mechanisms. The cooperativity mechanisms include the ability of strongly bound XBs to increase the binding affinity of Ca^{2+} to Troponin C on nearby RUs. Therefore, Ca^{2+}-Troponin C affinity is enhanced when the amplitude of the $[Ca]_i$ transient is greater, resulting in more cytosolic Ca^{2+} ions binding to Troponin C during a long compared to a short beat. Since Ca^{2+} ions are removed from the cytosol when they bind to Troponin C, as the beat number progresses within the train of 74 beats, there is a progressive dampening of CA-ANM, and thus APD-ALM.

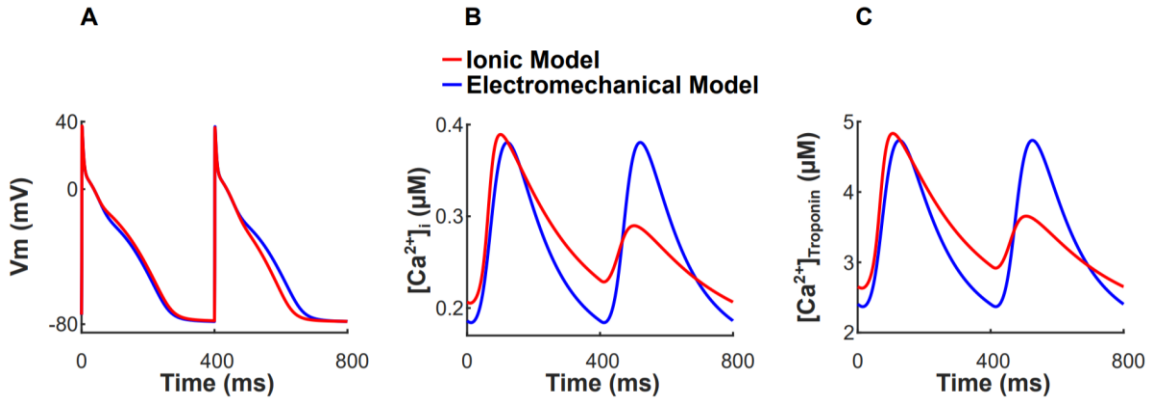

Figure 6.3 V_m (A), $[Ca^{2+}]_i$ (B), and $[Ca^{2+}]_{Troponin}$ (C) plotted over time for simulations with our electromechanical RA myocyte model with only cAF-induced *ionic* remodeling incorporated (blue traces) and the uncoupled cAF RA ionic model (red traces). The final two beats (of the 74 total beats) isometrically paced at a CL of 400 ms and a SL of 1.9 μm are shown for each model.

6.3.3 Increased cAF-Induced Myofilament Remodeling Predominantly Increases APD-ANM

Incorporating both cAF-induced ionic and myofilament remodeling in our human RA and LA electromechanical myocyte models resulted, predominantly, in APD-ANM increases (Figure 6.4). Specifically, bifurcations in APD as functions of myofilament parameters occurred as the level of thin filament remodeling increased following changes in kon, koffH, and perm50 in RA and LA myocyte models (Figure 6.4, top). The increase in thin filament activation caused a transition from stable APD to beat-to-beat APD oscillations. In RA and LA models, significant APD-ANM (Figure 6.4, bottom) occurred for cAF-induced remodeling of kon>200% (RA) or kon>250% (LA); koffH< 40% (RA) or koffH< 30% (LA); and 30%<perm50< 60% (both LA and RA) of control values. cAF-induced remodeling of other myofilament parameters that increased thin filament

activation (knp, kpn, koffL) or those which led to a reduced rate of XB cycling (gapp, hb, fapp, hf, and gxb) did not alter APD-ANM (not shown).

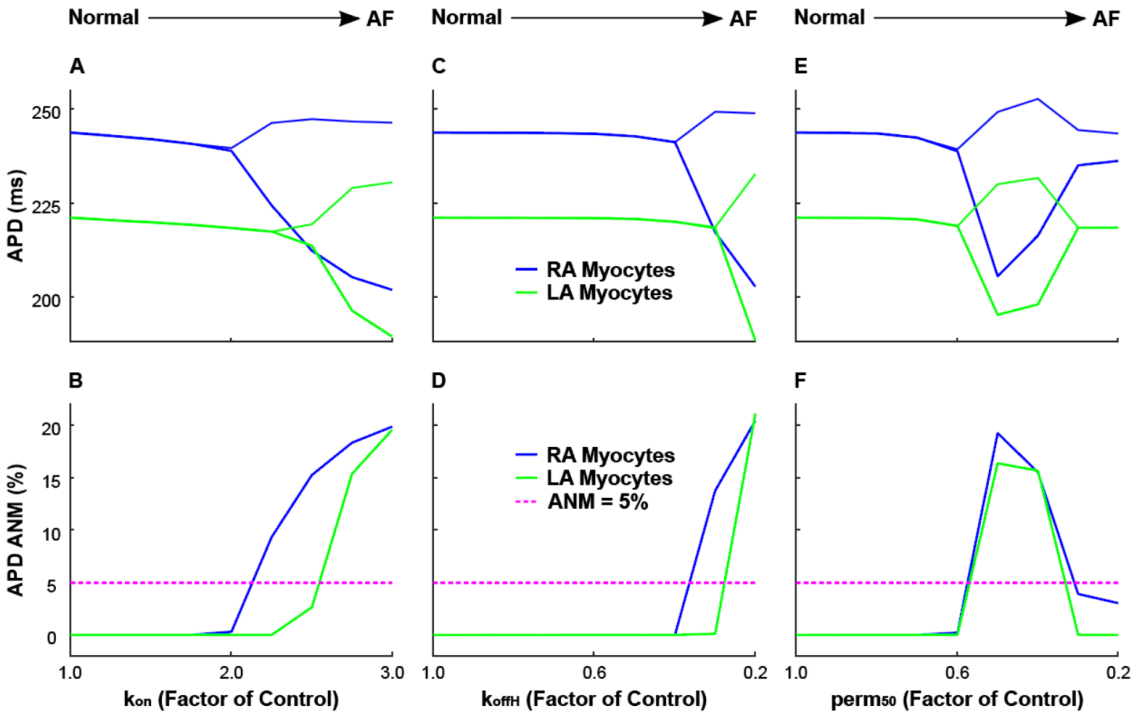

Figure 6.4 Bifurcation diagrams for APD (row 1) and sensitivity of APD-ANM (row 2) as functions of cAF-induced myofilament remodeling in simulations with our RA (blue) and LA (green) electromechanical models with cAF-induced ionic remodeling and a SL of 1.9 µm. To incorporate cAF-induced increased thin filament activation, each unique simulation has a cAF-remodeled value of k_{on} (column 1), k_{offH} (column 2), or $perm_{50}$ (column 3) ranging from normal (100% of control) to diseased (300% of control for k_{on}; 20% of control for k_{offH} and $perm_{50}$). The pink dashed line in row 2 indicates the division between sub-threshold ANM and significant ANM (> 5%).

An increase in thin filament activation enhanced the binding affinity of Troponin C for Ca^{2+}, thus increasing the fraction of Troponin C with bound Ca^{2+} during both long and short beats. However, as more Ca^{2+} binds to Troponin C, the fraction of Troponin C with bound Ca^{2+} reached saturation (i.e., a value of one) during the long beat. As a result, the fraction of Troponin C bound to Ca^{2+} during the short beat increased relative to that during

the long, causing a concomitant relative increase in the fraction of strongly bound XBs. Due to the cooperativity between strongly bound XBs and Ca^{2+}-Troponin C binding affinity on nearby RUs, this caused a further increase in Ca^{2+}-Troponin C affinity. As a result, $[Ca]_{Troponin}$ increased, and the peak magnitude of $[Ca]_i$ decreased during the short beat relative to the long, increasing CA-ANM. Therefore, as cAF-induced thin filament activation increased, APD-ANM also became larger. An example of this is shown in Figure 6.5, where we compare V_m, $[Ca]_i$, the fraction of strongly bound XBs, and $[Ca]_{Troponin}$ for simulations with different amounts of cAF-induced remodeling of thin filament activation. When cAF-induced remodeling of thin filament activation is increased from 150% to 225% of control, increases are found in APD-ANM (to 9.4% from 0.03%), CA-ANM (to 43% from 0.02%), CaT-ANM (to 74% from 0.03%), and the maximum percent of XBs in a strongly bound state (to 25% from1.8% during the first beat; to 11% from 1.8% during the second beat).

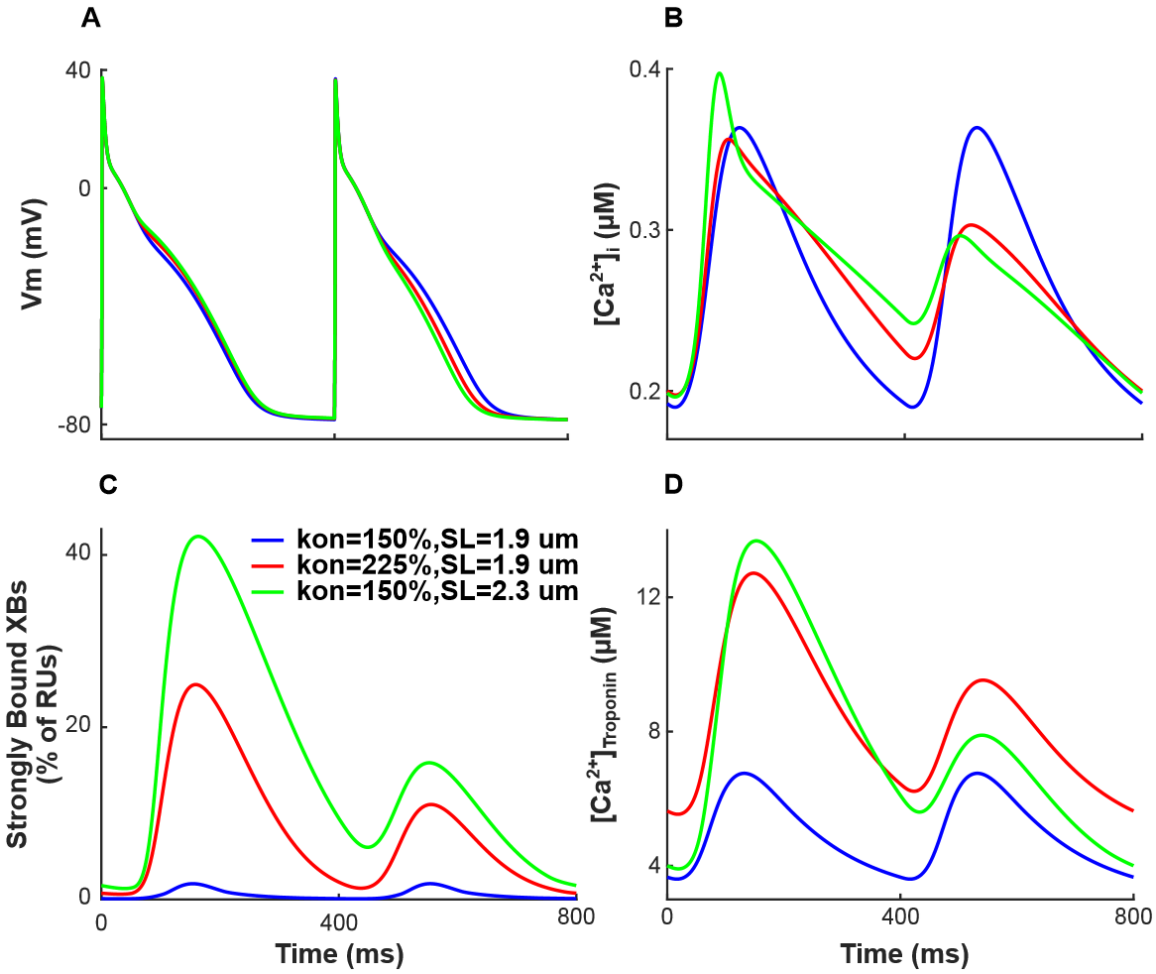

Figure 6.5 V_m (A), $[Ca^{2+}]_i$ (B), the percentage of regulatory units with strongly bound XBs (C), and $[Ca^{2+}]_{Troponin}$ (D), plotted over time for our RA electromechanical myocyte models with cAF-induced ionic remodeling. The final two beats (of the 74 total beats) isometrically paced at a SL of 1.9 μm with cAF-induced myofilament remodeling with a value of k_{on} = 150% (blue lines), at a SL of 1.9 μm with k_{on} = 225% (red lines), or at a SL of 2.3 μm with k_{on} = 150% (green line) are shown. The percentage of regulatory units with strongly bound XBs is calculated as the sum of RUs in the XB_{PreR} and XB_{PostR} states divided by the total number of RUs.

Sub-threshold APD-ANM (Figure 6.4, bottom) occurred for RA and LA models with values of $perm_{50}$<=30%. In these cases, the fraction of Troponin C with bound Ca^{2+} became close to saturation during both short and long beats. Therefore, the binding affinity of Troponin C to Ca^{2+} was reduced in the short beat relative to that in the long one, causing the difference in the amount of Ca^{2+} buffered by Troponin C between successive beats to

progressively diminish. Since Ca^{2+} ions are removed from the cytosol when they bind to Troponin C, this leads to progressive dampening of CA-ALT, and thus of APD-ALT.

6.3.4 Longer SLs Predominantly Increase APD-ANM

Finally, we investigated the effect of SL on APD-ANM, since stretch is common in cAF (Thanigaimani et al., 2017) and has been shown to increase the susceptibility of atrial myocytes to APD-ALT (Tsai et al., 2011). The results of the simulations revealed that longer SLs predominantly increase APD-ANM for both RA and LA electromechanical myocyte models, as seen in Figure 6.6 for simulations with cAF-induced myofilament remodeling represented by k_{on} (column 1), k_{offH} (column 2), and $perm_{50}$ (column 3). An increase in SL increases the thin filament single overlap region, resulting in greater thin filament activation and enhanced binding affinity of Troponin C to Ca^{2+}. As described in Section 6.3.3, when binding affinity is heightened, the fraction of Troponin C with bound Ca^{2+} reaches saturation during only the long beats, resulting in larger APD-ANM. An example of this is shown in Figure 6.5 for simulations at two different SLs. When SL is increased from 1.9 μm to 2.3 μm, increases are found in APD-ANM (to 15% from 0.03%), CA-ANM (to 94% from 0.02%), CaT-ANM (to 124% from 0.03%), and the maximum percent of XBs in a strongly bound state (to 42% from 1.8% during the first beat; to 16% from 1.8% during the second beat). For simulations with SLs above 2.1 μm and with the greatest cAF-induced myofilament remodeling (k_{on} >275% for RA only, k_{offH}<30% and $perm_{50}$< 50% for both RA and LA), the binding affinity of Troponin C to Ca^{2+} was largest. When the binding affinity is greatest, the fraction of Troponin C with bound Ca^{2+} reaches saturation during both the long and short beats, resulting in smaller APD-ANM.

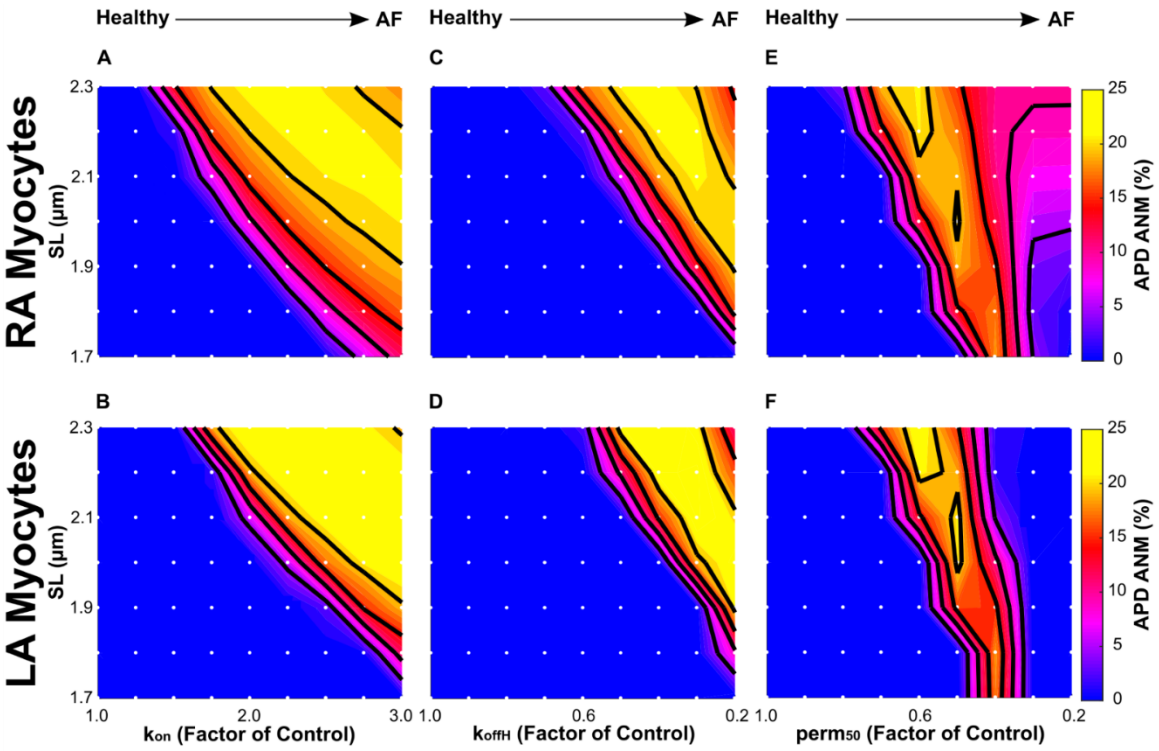

Figure 6.6 Sensitivity of APD-ANM to SL in simulations with our RA (row 1) and LA (row 2) electromechanical myocyte models with cAF-induced ionic remodeling and varying degrees of cAF-induced myofilament remodeling. cAF-induced myofilament remodeling was incorporated as in Figure 6.4. Each white dot represents a unique simulation in which the model was isometrically paced at a specific SL ranging from 1.7 to 2.3 μm in increments of 0.1 μm. Colors represent APD-ANM. Contour lines were drawn at APD-ANM of 5, 10, 15, and 20%.

6.4 Discussion

An increased propensity for APD-ALT has been shown to render the human atria vulnerable to ectopy-induced arrhythmia and to increase arrhythmia complexity and its persistence in computational models of human cAF (Chang and Trayanova, 2016). These simulation results are consistent with studies demonstrating that atrial alternans is linked to disease progression in AF patients (Narayan et al., 2011), and is associated with enhanced AF susceptibility following myocardial infarction in clinical studies (Kettlewell et al., 2013; Miyauchi et al., 2003) and atrial tachycardia in animal models (Jousset et al.,

2012; Monigatti-Tenkorang et al., 2014). Recent studies have also examined the cellular mechanism underling the occurrence of APD-ALT at clinically-relevant slow pacing rates, 120-200 bpm (Chang et al., 2014; Chang and Trayanova, 2016). Although researchers have examined the ionic mechanisms underlying APD-ALT, the effects of myofilament protein dynamics on APD-ALT had not been elucidated. Here, we investigated whether myofilament protein dynamics mechanisms modulate APD-ALT formation in cAF at clinically-relevant pacing rates. By comparing our human electromechanical atrial myocyte model to the human ionic atrial model, we showed that MEF has a dampening effect on APD-ANM. These results are consistent with our previous simulation study, where we showed that MEF diminished calcium and voltage alternans, driven by heart failure-induced downregulation of the SR Ca^{2+} uptake current, in simulations of failing human ventricular myocytes (Zile and Trayanova, 2016). Since APD-ALT has been advocated as a clinical marker for AF risk and has been suggested as a new therapeutic target in cAF patients (Chang et al., 2014; Chang and Trayanova, 2016; Narayan et al., 2002), our results propose that targeting myofilament protein dynamics may offer an alternative approach for prevention of arrhythmia in cAF patients.

We also examined how APD-ALT is affected by cAF-induced myofilament remodeling. Previous studies have suggested that myofilament Ca^{2+} sensitivity, the amount of Ca^{2+} necessary to produce half maximal force, is increased in AF (Belus et al., 2010; Eiras et al., 2006), although the degree to which it is increased and whether it promotes arrhythmogenicity in AF has not been elucidated. Therefore, in this study we investigated how varying degrees of increased thin filament activation, which enhances Ca^{2+} sensitivity, altered the formation of APD-ALT. Our results show that increasing thin filament

activation and thus Ca^{2+} sensitivity, via MEF, predominantly enhanced APD-ANM. Since APD-ALT has been identified as a dynamic arrhythmogenic substrate underlying human AF and since APD-ANM is larger in cAF patients than in paroxysmal AF ones (Narayan et al., 2002), our observations suggest that myofilament remodeling may occur in cAF patients but not in paroxysmal ones. This is supported by Belus *et al* (Belus et al., 2010) who found that myofilament Ca^{2+} sensitivity was increased in human cAF (long-standing persistent AF), while Eiras *et al* (Eiras et al., 2006) found that there was no significant difference in myocytes from healthy and persistent AF patients. Therefore, enhanced Ca^{2+} sensitivity may be responsible for the enhanced arrhythmogenicity found in cAF patients compared to persistent AF patients. However, organ-scale simulations will be necessary to verify this hypothesis. Furthermore, our results suggest that therapies decreasing the disease-enhanced thin filament activation could reduce APD-ANM, thus potentially reducing the propensity for arrhythmia in AF patients.

Acute and chronic stretch are known to cause abnormal atrial remodeling and to increase vulnerability to AF (Thanigaimani et al., 2017). Acute atrial stretch causes transient electrophysiological changes such as conduction slowing and altered atrial refractoriness in animal (Ravelli and Allessie, 1997; Sideris et al., 1994; Solti et al., 1989) and human (Elvan et al., 2013; Ravelli et al., 2011) studies. Chronic atrial stretch has been implicated in structural atrial remodeling and persistent conduction slowing in both animal (Takeuchi et al., 2006) and human (Morton et al., 2003) studies. Although investigators have examined some of the proposed mechanisms by which atrial stretch can lead to AF (Franz and Bode, 2003), such as stretch-activated ion channels (Kim, 1992; Tavi et al., 1996), few studies have examined the effects of atrial stretch on APD-ALT. One study by

Tsai *et al* (Tsai et al., 2011) found that mechanical stretch in an HL-1 atrial myocyte monolayer led to increased susceptibility to CA-ALT and APD-ALT, due to slower calcium reuptake kinetics via decreased expression of SR adenosine triphosphatase 2. However, only rapid field pacing could induce APD-ALT in this study. This is in contrast to the clinical observations (Narayan et al., 2011) showing that APD-ALT occurs in cAF patients at slower rates, thus these finding may be more relevant to paroxysmal AF patients (Kalifa and Yamazaki, 2011). Therefore, we investigated how stretched sarcomeres affected the formation of APD-ALT at clinically-relevant pacing rates in human cAF. Our findings at slower clinically-relevant rates of 150 bpm (400 ms CL), similar to those from Tsai *et al* (Tsai et al., 2011) at faster pacing rates of 240-360 bpm (250 ms – 167 ms CL), showed that simulated myocytes with longer SLs resulted in enhanced APD-ANM due to larger CA-ANM, suggesting that atrial stretch is an important modulator of APD-ALT. Therefore, therapies designed to reduce the mechanical stretch commonly found in cAF may reduce the propensity for arrhythmia in these patients.

6.5 Conclusions

Our results demonstrate that enhanced thin filament activation was the key feature of cAF-induced myofilament remodeling that predominantly enhanced CA-ANM and thus APD-ANM in simulated human cAF myocytes. Furthermore, longer SLs chiefly heightened APD-ANM at slower clinically-relevant rates of 400 ms (150 bpm). Together our findings demonstrate that myofilament dynamics mechanisms play an important role in altering APD-ALT in human cAF.

Chapter 6 Future Directions

In this thesis, we have demonstrated that cardiac disease induced-remodeling of myofilament parameters and sarcomere length, due to the presence of MEF, altered the formation of alternans in human HF and cAF, and EADs in human HCM. Furthermore, we showed that CA-ALT, induced by decreased I_{up}, was the link between APV-ALT and FORCE-ALT in human HF. Unfortunately, we were only able to simulate human atrial and ventricular myocytes; we did not have the opportunity to explore the effects of MEF, deranged myofilament dynamics, or stretch on the initiation of arrhythmia in myocardial tissue. However, computational modeling is uniquely placed to address this gap of knowledge. To explore the exciting future directions listed below, the first step would be to build bidirectionally coupled multiscale models of the human tissue and ventricles incorporating HF-induced and HCM-induced ionic and myofilament remodeling, and a bidirectionally coupled multiscale model of the human tissue and atria incorporating cAF-induced ionic and myofilament remodeling. Building these models would allow one to investigate the following:

Future Directions from Study 1:

- *At the Tissue Level:* Investigate if spatially discordant force alternans arises at fast pacing rates in human HF. If it does arise, characterize discordant force alternans sensitivity to pacing rate and heterogeneity of electrical and mechanical properties.
- *At the Organ Scale:* Investigate whether the summation of force alternans in the ventricles results in clinically observed pressure alternans. Characterize if and how pressure alternans enhance prediction of arrhythmia propensity.

Future Directions from Study 2:

- *At the Tissue and Organ Levels:* Investigate the effects of myofilament dynamics on triggered activity (the manifestation of EADs at the tissue/organ level) and arrhythmogenesis. Determine how heterogeneity of myofilament remodeling across the tissue/organ effects arrhythmogenesis.

Future Directions from Study 3:

- *At the Tissue Level:* Investigate if spatially discordant APD alternans arises in human cAF and how it is modulated by MEF.
- *At the Organ Scale:* Investigate how myofilament dynamics affects the vulnerability, complexity, and persistence of arrhythmia in human cAF.

Bibliography

Ambardekar, A.V., Walker, J.S., Walker, L.A., Cleveland, J.C., Jr., Lowes, B.D. and Buttrick, P.M., 2011. Incomplete recovery of myocyte contractile function despite improvement of myocardial architecture with left ventricular assist device support, Circ Heart Fail. 4, 425-32.

Bardy, G.H., Lee, K.L., Mark, D.B., Poole, J.E., Packer, D.L., Boineau, R., Domanski, M., Troutman, C., Anderson, J., Johnson, G., McNulty, S.E., Clapp-Channing, N., Davidson-Ray, L.D., Fraulo, E.S., Fishbein, D.P., Luceri, R.M. and Ip, J.H., 2005. Amiodarone or an implantable cardioverter-defibrillator for congestive heart failure, N Engl J Med. 352, 225-37.

Baudenbacher, F., Schober, T., Pinto, J.R., Sidorov, V.Y., Hilliard, F., Solaro, R.J., Potter, J.D. and Knollmann, B.C., 2008. Myofilament Ca2+ sensitization causes susceptibility to cardiac arrhythmia in mice, J Clin Invest. 118, 3893-903.

Bayer, J.D., Narayan, S.M., Lalani, G.G. and Trayanova, N.A., 2010. Rate-dependent action potential alternans in human heart failure implicates abnormal intracellular calcium handling, Heart Rhythm. 7, 1093-101.

Belin, R.J., Sumandea, M.P., Allen, E.J., Schoenfelt, K., Wang, H., Solaro, R.J. and de Tombe, P.P., 2007. Augmented protein kinase C-alpha-induced myofilament protein phosphorylation contributes to myofilament dysfunction in experimental congestive heart failure, Circ Res. 101, 195-204.

Belin, R.J., Sumandea, M.P., Kobayashi, T., Walker, L.A., Rundell, V.L., Urboniene, D., Yuzhakova, M., Ruch, S.H., Geenen, D.L., Solaro, R.J. and de Tombe, P.P., 2006. Left ventricular myofilament dysfunction in rat experimental hypertrophy and congestive heart failure, Am J Physiol Heart Circ Physiol. 291, H2344-53.

Belus, A., Piroddi, N., Ferrantini, C., Tesi, C., Cazorla, O., Toniolo, L., Drost, M., Mearini, G., Carrier, L., Rossi, A., Mugelli, A., Cerbai, E., van der Velden, J. and Poggesi, C., 2010. Effects of chronic atrial fibrillation on active and passive force generation in human atrial myofibrils, Circ Res. 107, 144-52.

Berger, R.D., Kasper, E.K., Baughman, K.L., Marban, E., Calkins, H. and Tomaselli, G.F., 1997. Beat-to-beat QT interval variability: novel evidence for repolarization lability in ischemic and nonischemic dilated cardiomyopathy, Circulation. 96, 1557-65.

Bers, D.M., 2002. Cardiac excitation-contraction coupling, Nature. 415, 198-205.

Bezzina, C.R., Lahrouchi, N. and Priori, S.G., 2015. Genetics of sudden cardiac death, Circ Res. 116, 1919-36.

Bisping, E., Tenderich, G., Barckhausen, P., Stumme, B., Bruns, S., von Lewinski, D. and Pieske, B., 2007. Atrial myocardium is the predominant inotropic target of adrenomedullin in the human heart, Am J Physiol Heart Circ Physiol. 293, H3001-7.

Bloomfield, D.M., Bigger, J.T., Steinman, R.C., Namerow, P.B., Parides, M.K., Curtis, A.B., Kaufman, E.S., Davidenko, J.M., Shinn, T.S. and Fontaine, J.M., 2006. Microvolt T-wave alternans and the risk of death or sustained ventricular

arrhythmias in patients with left ventricular dysfunction, J Am Coll Cardiol. 47, 456-63.
Bos, J.M., Towbin, J.A. and Ackerman, M.J., 2009. Diagnostic, prognostic, and therapeutic implications of genetic testing for hypertrophic cardiomyopathy, J Am Coll Cardiol. 54, 201-11.
Brooks, W.W., Bing, O.H., Litwin, S.E., Conrad, C.H. and Morgan, J.P., 1994. Effects of treppe and calcium on intracellular calcium and function in the failing heart from the spontaneously hypertensive rat, Hypertension. 24, 347-56.
Carrier, L., Mearini, G., Stathopoulou, K. and Cuello, F., 2015. Cardiac myosin-binding protein C (MYBPC3) in cardiac pathophysiology, Gene. 573, 188-97.
Cazorla, O., Szilagyi, S., Vignier, N., Salazar, G., Kramer, E., Vassort, G., Carrier, L. and Lacampagne, A., 2006. Length and protein kinase A modulations of myocytes in cardiac myosin binding protein C-deficient mice, Cardiovasc Res. 69, 370-80.
Chan, R.H., Maron, B.J., Olivotto, I., Pencina, M.J., Assenza, G.E., Haas, T., Lesser, J.R., Gruner, C., Crean, A.M., Rakowski, H., Udelson, J.E., Rowin, E., Lombardi, M., Cecchi, F., Tomberli, B., Spirito, P., Formisano, F., Biagini, E., Rapezzi, C., De Cecco, C.N., Autore, C., Cook, E.F., Hong, S.N., Gibson, C.M., Manning, W.J., Appelbaum, E. and Maron, M.S., 2014. Prognostic value of quantitative contrast-enhanced cardiovascular magnetic resonance for the evaluation of sudden death risk in patients with hypertrophic cardiomyopathy, Circulation. 130, 484-95.
Chang, K.C., Bayer, J.D. and Trayanova, N.A., 2014. Disrupted calcium release as a mechanism for atrial alternans associated with human atrial fibrillation, PLoS Comput Biol. 10, e1004011.
Chang, K.C. and Trayanova, N.A., 2016. Mechanisms of arrhythmogenesis related to calcium-driven alternans in a model of human atrial fibrillation, Sci Rep. 6, 36395.
Charron, P., Arad, M., Arbustini, E., Basso, C., Bilinska, Z., Elliott, P., Helio, T., Keren, A., McKenna, W.J., Monserrat, L., Pankuweit, S., Perrot, A., Rapezzi, C., Ristic, A., Seggewiss, H., van Langen, I. and Tavazzi, L., 2010. Genetic counselling and testing in cardiomyopathies: a position statement of the European Society of Cardiology Working Group on Myocardial and Pericardial Diseases, Eur Heart J. 31, 2715-26.
Chen, X., Hu, Y., Fetics, B.J., Berger, R.D. and Trayanova, N.A., 2011. Unstable QT interval dynamics precedes ventricular tachycardia onset in patients with acute myocardial infarction: a novel approach to detect instability in QT interval dynamics from clinical ECG, Circ Arrhythm Electrophysiol. 4, 858-66.
Chen, X., Tereshchenko, L.G., Berger, R.D. and Trayanova, N.A., 2013. Arrhythmia risk stratification based on QT interval instability: an intracardiac electrocardiogram study, Heart Rhythm. 10, 875-80.
Chen, X. and Trayanova, N.A., 2012. A novel methodology for assessing the bounded-input bounded-output instability in QT interval dynamics: application to clinical ECG with ventricular tachycardia, IEEE Trans Biomed Eng. 59, 2111-7.
Christ, T., Wettwer, E., Voigt, N., Hala, O., Radicke, S., Matschke, K., Varro, A., Dobrev, D. and Ravens, U., 2008. Pathology-specific effects of the IKur/Ito/IK,ACh blocker AVE0118 on ion channels in human chronic atrial fibrillation, Br J Pharmacol. 154, 1619-30.

Coppini, R., Ferrantini, C., Yao, L., Fan, P., Del Lungo, M., Stillitano, F., Sartiani, L., Tosi, B., Suffredini, S., Tesi, C., Yacoub, M., Olivotto, I., Belardinelli, L., Poggesi, C., Cerbai, E. and Mugelli, A., 2013. Late sodium current inhibition reverses electromechanical dysfunction in human hypertrophic cardiomyopathy, Circulation. 127, 575-84.

Coppini, R., Ho, C.Y., Ashley, E., Day, S., Ferrantini, C., Girolami, F., Tomberli, B., Bardi, S., Torricelli, F., Cecchi, F., Mugelli, A., Poggesi, C., Tardiff, J. and Olivotto, I., 2014. Clinical phenotype and outcome of hypertrophic cardiomyopathy associated with thin-filament gene mutations, J Am Coll Cardiol. 64, 2589-600.

Couderc, J.P., Zareba, W., McNitt, S., Maison-Blanche, P. and Moss, A.J., 2007. Repolarization variability in the risk stratification of MADIT II patients, Europace. 9, 717-23.

Coulton, A.T. and Stelzer, J.E., 2012. Cardiac myosin binding protein C and its phosphorylation regulate multiple steps in the cross-bridge cycle of muscle contraction, Biochemistry. 51, 3292-301.

Cutler, M.J. and Rosenbaum, D.S., 2009. Risk stratification for sudden cardiac death: is there a clinical role for T wave alternans?, Heart Rhythm. 6, S56-61.

Das, M.K., Khan, B., Jacob, S., Kumar, A. and Mahenthiran, J., 2006. Significance of a fragmented QRS complex versus a Q wave in patients with coronary artery disease, Circulation. 113, 2495-501.

de Oliveira, B.L., Rocha, B.M., Barra, L.P., Toledo, E.M., Sundnes, J. and Weber dos Santos, R., 2013. Effects of deformation on transmural dispersion of repolarization using in silico models of human left ventricular wedge, Int J Numer Method Biomed Eng. 29, 1323-37.

de Waard, M.C., van der Velden, J., Bito, V., Ozdemir, S., Biesmans, L., Boontje, N.M., Dekkers, D.H., Schoonderwoerd, K., Schuurbiers, H.C., de Crom, R., Stienen, G.J., Sipido, K.R., Lamers, J.M. and Duncker, D.J., 2007. Early exercise training normalizes myofilament function and attenuates left ventricular pump dysfunction in mice with a large myocardial infarction, Circ Res. 100, 1079-88.

Eiras, S., Narolska, N.A., van Loon, R.B., Boontje, N.M., Zaremba, R., Jimenez, C.R., Visser, F.C., Stooker, W., van der Velden, J. and Stienen, G.J., 2006. Alterations in contractile protein composition and function in human atrial dilatation and atrial fibrillation, J Mol Cell Cardiol. 41, 467-77.

El-Armouche, A., Boknik, P., Eschenhagen, T., Carrier, L., Knaut, M., Ravens, U. and Dobrev, D., 2006. Molecular determinants of altered Ca2+ handling in human chronic atrial fibrillation, Circulation. 114, 670-80.

El-Armouche, A., Pohlmann, L., Schlossarek, S., Starbatty, J., Yeh, Y.H., Nattel, S., Dobrev, D., Eschenhagen, T. and Carrier, L., 2007. Decreased phosphorylation levels of cardiac myosin-binding protein-C in human and experimental heart failure, J Mol Cell Cardiol. 43, 223-9.

Elliott, P.M., Anastasakis, A., Borger, M.A., Borggrefe, M., Cecchi, F., Charron, P., Hagege, A.A., Lafont, A., Limongelli, G., Mahrholdt, H., McKenna, W.J., Mogensen, J., Nihoyannopoulos, P., Nistri, S., Pieper, P.G., Pieske, B., Rapezzi, C., Rutten, F.H., Tillmanns, C. and Watkins, H., 2014. 2014 ESC Guidelines on diagnosis and management of hypertrophic cardiomyopathy: the Task Force for the

Diagnosis and Management of Hypertrophic Cardiomyopathy of the European Society of Cardiology (ESC), Eur Heart J. 35, 2733-79.

Elvan, A., Adiyaman, A., Beukema, R.J., Sie, H.T. and Allessie, M.A., 2013. Electrophysiological effects of acute atrial stretch on persistent atrial fibrillation in patients undergoing open heart surgery, Heart Rhythm. 10, 322-30.

Flashman, E., Redwood, C., Moolman-Smook, J. and Watkins, H., 2004. Cardiac myosin binding protein C: its role in physiology and disease, Circ Res. 94, 1279-89.

Franz, M.R. and Bode, F., 2003. Mechano-electrical feedback underlying arrhythmias: the atrial fibrillation case, Prog Biophys Mol Biol. 82, 163-74.

Gersh, B.J., Maron, B.J., Bonow, R.O., Dearani, J.A., Fifer, M.A., Link, M.S., Naidu, S.S., Nishimura, R.A., Ommen, S.R., Rakowski, H., Seidman, C.E., Towbin, J.A., Udelson, J.E. and Yancy, C.W., 2011. 2011 ACCF/AHA Guideline for the Diagnosis and Treatment of Hypertrophic Cardiomyopathy: a report of the American College of Cardiology Foundation/American Heart Association Task Force on Practice Guidelines. Developed in collaboration with the American Association for Thoracic Surgery, American Society of Echocardiography, American Society of Nuclear Cardiology, Heart Failure Society of America, Heart Rhythm Society, Society for Cardiovascular Angiography and Interventions, and Society of Thoracic Surgeons, J Am Coll Cardiol. 58, e212-60.

Goetzenich, A., Schroth, S.C., Emmig, U., Autschbach, R., Pieske, B., Rossaint, R. and Christiansen, S., 2009. Hypothermia exerts negative inotropy in human atrial preparations: in vitro-comparison to rabbit myocardium, J Cardiovasc Surg (Torino). 50, 239-45.

Goldberger, J.J., Buxton, A.E., Cain, M., Costantini, O., Exner, D.V., Knight, B.P., Lloyd-Jones, D., Kadish, A.H., Lee, B., Moss, A., Myerburg, R., Olgin, J., Passman, R., Rosenbaum, D., Stevenson, W., Zareba, W. and Zipes, D.P., 2011. Risk stratification for arrhythmic sudden cardiac death: identifying the roadblocks, Circulation. 123, 2423-30.

Gopalan, S.M., Flaim, C., Bhatia, S.N., Hoshijima, M., Knoell, R., Chien, K.R., Omens, J.H. and McCulloch, A.D., 2003. Anisotropic stretch-induced hypertrophy in neonatal ventricular myocytes micropatterned on deformable elastomers, Biotechnol Bioeng. 81, 578-87.

Gordon, A.M., Huxley, A.F. and Julian, F.J., 1966. The variation in isometric tension with sarcomere length in vertebrate muscle fibres, J Physiol. 184, 170-92.

Gray, B., Ingles, J. and Semsarian, C., 2011. Natural history of genotype positive-phenotype negative patients with hypertrophic cardiomyopathy, Int J Cardiol. 152, 258-9.

Hasenfuss, G., Reinecke, H., Studer, R., Meyer, M., Pieske, B., Holtz, J., Holubarsch, C., Posival, H., Just, H. and Drexler, H., 1994. Relation between myocardial function and expression of sarcoplasmic reticulum Ca(2+)-ATPase in failing and nonfailing human myocardium, Circ Res. 75, 434-42.

Hayashi, H., Miyauchi, Y., Chou, C.C., Karagueuzian, H.S., Chen, P.S. and Lin, S.F., 2003. Effects of cytochalasin D on electrical restitution and the dynamics of ventricular fibrillation in isolated rabbit heart, J Cardiovasc Electrophysiol. 14, 1077-84.

Hirashiki, A., Izawa, H., Cheng, X.W., Unno, K., Ohshima, S. and Murohara, T., 2010. Dobutamine-induced mechanical alternans is a marker of poor prognosis in idiopathic dilated cardiomyopathy, Clin Exp Pharmacol Physiol. 37, 1004-9.

Hirashiki, A., Izawa, H., Somura, F., Obata, K., Kato, T., Nishizawa, T., Yamada, A., Asano, H., Ohshima, S., Noda, A., Iino, S., Nagata, K., Okumura, K., Murohara, T. and Yokota, M., 2006. Prognostic value of pacing-induced mechanical alternans in patients with mild-to-moderate idiopathic dilated cardiomyopathy in sinus rhythm, J Am Coll Cardiol. 47, 1382-9.

Hodgkin, A.L. and Huxley, A.F., 1952. A quantitative description of membrane current and its application to conduction and excitation in nerve, J Physiol. 117, 500-44.

Hohnloser, S.H., Ikeda, T. and Cohen, R.J., 2009. Evidence regarding clinical use of microvolt T-wave alternans, Heart Rhythm. 6, S36-44.

Huke, S. and Knollmann, B.C., 2010. Increased myofilament Ca2+-sensitivity and arrhythmia susceptibility, J Mol Cell Cardiol. 48, 824-33.

Huxley, A.F., 1957. Muscle structure and theories of contraction, Prog Biophys Biophys Chem. 7, 255-318.

Ingles, J., Sarina, T., Yeates, L., Hunt, L., Macciocca, I., McCormack, L., Winship, I., McGaughran, J., Atherton, J. and Semsarian, C., 2013. Clinical predictors of genetic testing outcomes in hypertrophic cardiomyopathy, Genet Med. 15, 972-7.

Ito, M., Kodama, M., Kashimura, T., Obata, H., Mitsuma, W., Hirono, S., Tomita, M., Ohno, Y., Tanabe, N. and Aizawa, Y., 2012. Comparison of patients with pulmonary arterial hypertension with versus without right-sided mechanical alternans, Am J Cardiol. 109, 428-31.

Ji, Y.C., Gray, R.A. and Fenton, F.H., 2015. Implementation of Contraction to Electrophysiological Ventricular Myocyte Models, and Their Quantitative Characterization via Post-Extrasystolic Potentiation, PLoS One. 10, e0135699.

Jousset, F., Tenkorang, J., Vesin, J.M., Pascale, P., Ruchat, P., Rollin, A.G., Fromer, M., Narayan, S.M. and Pruvot, E., 2012. Kinetics of atrial repolarization alternans in a free-behaving ovine model, J Cardiovasc Electrophysiol. 23, 1003-12.

Kalifa, J. and Yamazaki, M., 2011. Repolarization alternans in dilated pulsing atria: a preventable "prelude" to atrial fibrillation?, J Am Coll Cardiol. 58, 2116-7.

Kampourakis, T., Yan, Z., Gautel, M., Sun, Y.B. and Irving, M., 2014. Myosin binding protein-C activates thin filaments and inhibits thick filaments in heart muscle cells, Proc Natl Acad Sci U S A. 111, 18763-8.

Kashimura, T., Kodama, M., Tanaka, K., Sonoda, K., Watanabe, S., Ohno, Y., Tomita, M., Obata, H., Mitsuma, W., Ito, M., Hirono, S., Hanawa, H. and Aizawa, Y., 2013. Mechanical alternans in human idiopathic dilated cardiomyopathy is caused with impaired force-frequency relationship and enhanced poststimulation potentiation, Heart Vessels. 28, 336-44.

Kashimura, T., Kodama, M., Watanabe, T., Tanaka, K., Hayashi, Y., Ohno, Y., Obata, H., Ito, M., Hirono, S., Hanawa, H. and Minamino, T., 2014. Relative refractoriness of left ventricular contraction underlies human tachycardia-induced mechanical and electrical alternans, Pacing Clin Electrophysiol. 37, 197-206.

Kettlewell, S., Burton, F.L., Smith, G.L. and Workman, A.J., 2013. Chronic myocardial infarction promotes atrial action potential alternans, afterdepolarizations, and fibrillation, Cardiovasc Res. 99, 215-24.

Kihara, Y. and Morgan, J.P., 1991. Abnormal Cai2+ handling is the primary cause of mechanical alternans: study in ferret ventricular muscles, Am J Physiol. 261, H1746-55.

Kim, D., 1992. A mechanosensitive K+ channel in heart cells. Activation by arachidonic acid, J Gen Physiol. 100, 1021-40.

Kim, R., Cingolani, O., Wittstein, I., McLean, R., Han, L., Cheng, K., Robinson, E., Brinker, J., Schulman, S.S., Berger, R.D., Henrikson, C.A. and Tereshchenko, L.G., 2014. Mechanical alternans is associated with mortality in acute hospitalized heart failure: prospective mechanical alternans study (MAS), Circ Arrhythm Electrophysiol. 7, 259-66.

Kim, Y.H., Garfinkel, A., Ikeda, T., Wu, T.J., Athill, C.A., Weiss, J.N., Karagueuzian, H.S. and Chen, P.S., 1997. Spatiotemporal complexity of ventricular fibrillation revealed by tissue mass reduction in isolated swine right ventricle. Further evidence for the quasiperiodic route to chaos hypothesis, J Clin Invest. 100, 2486-500.

Kockskamper, J. and Blatter, L.A., 2002. Subcellular Ca2+ alternans represents a novel mechanism for the generation of arrhythmogenic Ca2+ waves in cat atrial myocytes, J Physiol. 545, 65-79.

Kodama, M., Kato, K., Hirono, S., Okura, Y., Hanawa, H., Ito, M., Fuse, K., Shiono, T., Watanabe, K. and Aizawa, Y., 2001. Mechanical alternans in patients with chronic heart failure, J Card Fail. 7, 138-45.

Kotsanas, G., Holroyd, S.M., Young, R. and Gibbs, C.L., 1996. Mechanisms contributing to pulsus alternans in pressure-overload cardiac hypertrophy, Am J Physiol. 271, H2490-500.

Kuchar, D.L., Thorburn, C.W. and Sammel, N.L., 1987. Prediction of serious arrhythmic events after myocardial infarction: signal-averaged electrocardiogram, Holter monitoring and radionuclide ventriculography, J Am Coll Cardiol. 9, 531-8.

Lab, M.J. and Lee, J.A., 1990. Changes in intracellular calcium during mechanical alternans in isolated ferret ventricular muscle, Circ Res. 66, 585-95.

Lamberts, R.R., Hamdani, N., Soekhoe, T.W., Boontje, N.M., Zaremba, R., Walker, L.A., de Tombe, P.P., van der Velden, J. and Stienen, G.J., 2007. Frequency-dependent myofilament Ca2+ desensitization in failing rat myocardium, J Physiol. 582, 695-709.

Lee, H.C., Mohabir, R., Smith, N., Franz, M.R. and Clusin, W.T., 1988. Effect of ischemia on calcium-dependent fluorescence transients in rabbit hearts containing indo 1. Correlation with monophasic action potentials and contraction, Circulation. 78, 1047-59.

Levine, R.J., Kensler, R.W., Yang, Z., Stull, J.T. and Sweeney, H.L., 1996. Myosin light chain phosphorylation affects the structure of rabbit skeletal muscle thick filaments, Biophys J. 71, 898-907.

Lloyd-Jones, D., Adams, R., Carnethon, M., De Simone, G., Ferguson, T.B., Flegal, K., Ford, E., Furie, K., Go, A., Greenlund, K., Haase, N., Hailpern, S., Ho, M., Howard, V., Kissela, B., Kittner, S., Lackland, D., Lisabeth, L., Marelli, A., McDermott, M., Meigs, J., Mozaffarian, D., Nichol, G., O'Donnell, C., Roger, V., Rosamond, W., Sacco, R., Sorlie, P., Stafford, R., Steinberger, J., Thom, T., Wasserthiel-Smoller, S., Wong, N., Wylie-Rosett, J. and Hong, Y., 2009. Heart disease and stroke

statistics--2009 update: a report from the American Heart Association Statistics Committee and Stroke Statistics Subcommittee, Circulation. 119, 480-6.
Maier, L.S., Barckhausen, P., Weisser, J., Aleksic, I., Baryalei, M. and Pieske, B., 2000. Ca(2+) handling in isolated human atrial myocardium, Am J Physiol Heart Circ Physiol. 279, H952-8.
Maron, B.J., 2002. Hypertrophic cardiomyopathy: a systematic review, Jama. 287, 1308-20.
Maron, B.J., 2010. Contemporary insights and strategies for risk stratification and prevention of sudden death in hypertrophic cardiomyopathy, Circulation. 121, 445-56.
Maron, B.J., Gardin, J.M., Flack, J.M., Gidding, S.S., Kurosaki, T.T. and Bild, D.E., 1995. Prevalence of hypertrophic cardiomyopathy in a general population of young adults. Echocardiographic analysis of 4111 subjects in the CARDIA Study. Coronary Artery Risk Development in (Young) Adults, Circulation. 92, 785-9.
Maron, B.J., Kogan, J., Proschan, M.A., Hecht, G.M. and Roberts, W.C., 1994. Circadian variability in the occurrence of sudden cardiac death in patients with hypertrophic cardiomyopathy, J Am Coll Cardiol. 23, 1405-9.
Maron, B.J. and Maron, M.S., 2013. Hypertrophic cardiomyopathy, Lancet. 381, 242-55.
Maron, B.J., Maron, M.S. and Semsarian, C., 2012. Genetics of hypertrophic cardiomyopathy after 20 years: clinical perspectives, J Am Coll Cardiol. 60, 705-15.
Maron, B.J., McKenna, W.J., Danielson, G.K., Kappenberger, L.J., Kuhn, H.J., Seidman, C.E., Shah, P.M., Spencer, W.H., 3rd, Spirito, P., Ten Cate, F.J. and Wigle, E.D., 2003. American College of Cardiology/European Society of Cardiology clinical expert consensus document on hypertrophic cardiomyopathy. A report of the American College of Cardiology Foundation Task Force on Clinical Expert Consensus Documents and the European Society of Cardiology Committee for Practice Guidelines, J Am Coll Cardiol. 42, 1687-713.
Maron, B.J., Ommen, S.R., Semsarian, C., Spirito, P., Olivotto, I. and Maron, M.S., 2014. Hypertrophic cardiomyopathy: present and future, with translation into contemporary cardiovascular medicine, J Am Coll Cardiol. 64, 83-99.
Maron, B.J. and Semsarian, C., 2010. Emergence of gene mutation carriers and the expanding disease spectrum of hypertrophic cardiomyopathy, Eur Heart J. 31, 1551-3.
Maron, B.J., Semsarian, C., Shen, W.K., Link, M.S., Epstein, A.E., Estes, N.A., 3rd, Almquist, A., Giudici, M.C., Haas, T.S., Hodges, J.S. and Spirito, P., 2009. Circadian patterns in the occurrence of malignant ventricular tachyarrhythmias triggering defibrillator interventions in patients with hypertrophic cardiomyopathy, Heart Rhythm. 6, 599-602.
Maron, B.J., Shen, W.K., Link, M.S., Epstein, A.E., Almquist, A.K., Daubert, J.P., Bardy, G.H., Favale, S., Rea, R.F., Boriani, G., Estes, N.A., 3rd and Spirito, P., 2000. Efficacy of implantable cardioverter-defibrillators for the prevention of sudden death in patients with hypertrophic cardiomyopathy, N Engl J Med. 342, 365-73.
Maron, B.J., Spirito, P., Ackerman, M.J., Casey, S.A., Semsarian, C., Estes, N.A., 3rd, Shannon, K.M., Ashley, E.A., Day, S.M., Pacileo, G., Formisano, F., Devoto, E., Anastasakis, A., Bos, J.M., Woo, A., Autore, C., Pass, R.H., Boriani, G., Garberich,

R.F., Almquist, A.K., Russell, M.W., Boni, L., Berger, S., Maron, M.S. and Link, M.S., 2013. Prevention of sudden cardiac death with implantable cardioverter-defibrillators in children and adolescents with hypertrophic cardiomyopathy, J Am Coll Cardiol. 61, 1527-35.

Maron, B.J., Spirito, P., Shen, W.K., Haas, T.S., Formisano, F., Link, M.S., Epstein, A.E., Almquist, A.K., Daubert, J.P., Lawrenz, T., Boriani, G., Estes, N.A., 3rd, Favale, S., Piccininno, M., Winters, S.L., Santini, M., Betocchi, S., Arribas, F., Sherrid, M.V., Buja, G., Semsarian, C. and Bruzzi, P., 2007. Implantable cardioverter-defibrillators and prevention of sudden cardiac death in hypertrophic cardiomyopathy, Jama. 298, 405-12.

Maron, B.J., Yeates, L. and Semsarian, C., 2011. Clinical challenges of genotype positive (+)-phenotype negative (-) family members in hypertrophic cardiomyopathy, Am J Cardiol. 107, 604-8.

Messer, A.E., Jacques, A.M. and Marston, S.B., 2007. Troponin phosphorylation and regulatory function in human heart muscle: dephosphorylation of Ser23/24 on troponin I could account for the contractile defect in end-stage heart failure, J Mol Cell Cardiol. 42, 247-59.

Miller, T., Szczesna, D., Housmans, P.R., Zhao, J., de Freitas, F., Gomes, A.V., Culbreath, L., McCue, J., Wang, Y., Xu, Y., Kerrick, W.G. and Potter, J.D., 2001. Abnormal contractile function in transgenic mice expressing a familial hypertrophic cardiomyopathy-linked troponin T (I79N) mutation, J Biol Chem. 276, 3743-55.

Miyauchi, Y., Zhou, S., Okuyama, Y., Miyauchi, M., Hayashi, H., Hamabe, A., Fishbein, M.C., Mandel, W.J., Chen, L.S., Chen, P.S. and Karagueuzian, H.S., 2003. Altered atrial electrical restitution and heterogeneous sympathetic hyperinnervation in hearts with chronic left ventricular myocardial infarction: implications for atrial fibrillation, Circulation. 108, 360-6.

Monigatti-Tenkorang, J., Jousset, F., Pascale, P., Vesin, J.M., Ruchat, P., Fromer, M., Narayan, S.M. and Pruvot, E., 2014. Intermittent atrial tachycardia promotes repolarization alternans and conduction slowing during rapid rates, and increases susceptibility to atrial fibrillation in a free-behaving sheep model, J Cardiovasc Electrophysiol. 25, 418-27.

Morton, J.B., Sanders, P., Vohra, J.K., Sparks, P.B., Morgan, J.G., Spence, S.J., Grigg, L.E. and Kalman, J.M., 2003. Effect of chronic right atrial stretch on atrial electrical remodeling in patients with an atrial septal defect, Circulation. 107, 1775-82.

Moss, R.L. and Fitzsimons, D.P., 2006. Myosin light chain 2 into the mainstream of cardiac development and contractility, Circ Res. 99, 225-7.

Mulieri, L.A., Hasenfuss, G., Leavitt, B., Allen, P.D. and Alpert, N.R., 1992. Altered myocardial force-frequency relation in human heart failure, Circulation. 85, 1743-50.

Mun, J.Y., Previs, M.J., Yu, H.Y., Gulick, J., Tobacman, L.S., Beck Previs, S., Robbins, J., Warshaw, D.M. and Craig, R., 2014. Myosin-binding protein C displaces tropomyosin to activate cardiac thin filaments and governs their speed by an independent mechanism, Proc Natl Acad Sci U S A. 111, 2170-5.

Narayan, S.M., 2006. T-wave alternans and the susceptibility to ventricular arrhythmias, J Am Coll Cardiol. 47, 269-81.

Narayan, S.M., Bayer, J.D., Lalani, G. and Trayanova, N.A., 2008. Action potential dynamics explain arrhythmic vulnerability in human heart failure: a clinical and modeling study implicating abnormal calcium handling, J Am Coll Cardiol. 52, 1782-92.

Narayan, S.M., Bode, F., Karasik, P.L. and Franz, M.R., 2002. Alternans of atrial action potentials during atrial flutter as a precursor to atrial fibrillation, Circulation. 106, 1968-73.

Narayan, S.M., Franz, M.R., Clopton, P., Pruvot, E.J. and Krummen, D.E., 2011. Repolarization alternans reveals vulnerability to human atrial fibrillation, Circulation. 123, 2922-30.

Narayan, S.M., Franz, M.R., Lalani, G., Kim, J. and Sastry, A., 2007. T-wave alternans, restitution of human action potential duration, and outcome, J Am Coll Cardiol. 50, 2385-92.

Niimura, H., Bachinski, L.L., Sangwatanaroj, S., Watkins, H., Chudley, A.E., McKenna, W., Kristinsson, A., Roberts, R., Sole, M., Maron, B.J., Seidman, J.G. and Seidman, C.E., 1998. Mutations in the gene for cardiac myosin-binding protein C and late-onset familial hypertrophic cardiomyopathy, N Engl J Med. 338, 1248-57.

Noble, D., 1962. A modification of the Hodgkin—Huxley equations applicable to Purkinje fibre action and pacemaker potentials, J Physiol. 160, 317-52.

Nucifora, G., Muser, D., Gianfagna, P., Morocutti, G. and Proclemer, A., 2015. Systolic and diastolic myocardial mechanics in hypertrophic cardiomyopathy and their link to the extent of hypertrophy, replacement fibrosis and interstitial fibrosis, Int J Cardiovasc Imaging. 31, 1603-10.

Olivotto, I., d'Amati, G., Basso, C., Van Rossum, A., Patten, M., Emdin, M., Pinto, Y., Tomberli, B., Camici, P.G. and Michels, M., 2015. Defining phenotypes and disease progression in sarcomeric cardiomyopathies: contemporary role of clinical investigations, Cardiovasc Res. 105, 409-23.

Olsson, M.C., Patel, J.R., Fitzsimons, D.P., Walker, J.W. and Moss, R.L., 2004. Basal myosin light chain phosphorylation is a determinant of Ca2+ sensitivity of force and activation dependence of the kinetics of myocardial force development, Am J Physiol Heart Circ Physiol. 287, H2712-8.

Orchard, C.H., McCall, E., Kirby, M.S. and Boyett, M.R., 1991. Mechanical alternans during acidosis in ferret heart muscle, Circ Res. 68, 69-76.

Pastore, J.M., Girouard, S.D., Laurita, K.R., Akar, F.G. and Rosenbaum, D.S., 1999. Mechanism linking T-wave alternans to the genesis of cardiac fibrillation, Circulation. 99, 1385-94.

Pate, E. and Cooke, R., 1986. A model for the interaction of muscle cross-bridges with ligands which compete with ATP, J Theor Biol. 118, 215-30.

Patel, J.R., Diffee, G.M., Huang, X.P. and Moss, R.L., 1998. Phosphorylation of myosin regulatory light chain eliminates force-dependent changes in relaxation rates in skeletal muscle, Biophys J. 74, 360-8.

Pfeiffer, E.R., Tangney, J.R., Omens, J.H. and McCulloch, A.D., 2014. Biomechanics of cardiac electromechanical coupling and mechanoelectric feedback, J Biomech Eng. 136, 021007.

Pieske, B., Sutterlin, M., Schmidt-Schweda, S., Minami, K., Meyer, M., Olschewski, M., Holubarsch, C., Just, H. and Hasenfuss, G., 1996. Diminished post-rest potentiation

of contractile force in human dilated cardiomyopathy. Functional evidence for alterations in intracellular Ca2+ handling, J Clin Invest. 98, 764-76.
Previs, M.J., Prosser, B.L., Mun, J.Y., Previs, S.B., Gulick, J., Lee, K., Robbins, J., Craig, R., Lederer, W.J. and Warshaw, D.M., 2015. Myosin-binding protein C corrects an intrinsic inhomogeneity in cardiac excitation-contraction coupling, Sci Adv. 1.
Qu, Z., Xie, Y., Garfinkel, A. and Weiss, J.N., 2010. T-wave alternans and arrhythmogenesis in cardiac diseases, Front Physiol. 1, 154.
Quinn, T.A., 2014. The importance of non-uniformities in mechano-electric coupling for ventricular arrhythmias, J Interv Card Electrophysiol. 39, 25-35.
Ravelli, F. and Allessie, M., 1997. Effects of atrial dilatation on refractory period and vulnerability to atrial fibrillation in the isolated Langendorff-perfused rabbit heart, Circulation. 96, 1686-95.
Ravelli, F., Mase, M., del Greco, M., Marini, M. and Disertori, M., 2011. Acute atrial dilatation slows conduction and increases AF vulnerability in the human atrium, J Cardiovasc Electrophysiol. 22, 394-401.
Rice, J.J., Wang, F., Bers, D.M. and de Tombe, P.P., 2008. Approximate model of cooperative activation and crossbridge cycling in cardiac muscle using ordinary differential equations, Biophys J. 95, 2368-90.
Robinson, P., Griffiths, P.J., Watkins, H. and Redwood, C.S., 2007. Dilated and hypertrophic cardiomyopathy mutations in troponin and alpha-tropomyosin have opposing effects on the calcium affinity of cardiac thin filaments, Circ Res. 101, 1266-73.
Rosenbaum, D.S., Jackson, L.E., Smith, J.M., Garan, H., Ruskin, J.N. and Cohen, R.J., 1994. Electrical alternans and vulnerability to ventricular arrhythmias, N Engl J Med. 330, 235-41.
Schinkel, A.F., Vriesendorp, P.A., Sijbrands, E.J., Jordaens, L.J., ten Cate, F.J. and Michels, M., 2012. Outcome and complications after implantable cardioverter defibrillator therapy in hypertrophic cardiomyopathy: systematic review and meta-analysis, Circ Heart Fail. 5, 552-9.
Schmidt, U., Hajjar, R.J., Kim, C.S., Lebeche, D., Doye, A.A. and Gwathmey, J.K., 1999. Human heart failure: cAMP stimulation of SR Ca(2+)-ATPase activity and phosphorylation level of phospholamban, Am J Physiol. 277, H474-80.
Seidman, C.E. and Seidman, J.G., 2011. Identifying sarcomere gene mutations in hypertrophic cardiomyopathy: a personal history, Circ Res. 108, 743-50.
Selvaraj, R.J., Suszko, A., Subramanian, A., Mak, S., Wainstein, R. and Chauhan, V.S., 2011. Microscopic systolic pressure alternans in human cardiomyopathy: noninvasive evaluation of a novel risk marker and correlation with microvolt T-wave alternans, Heart Rhythm. 8, 236-43.
Semsarian, C., French, J., Trent, R.J., Richmond, D.R. and Jeremy, R.W., 1997. The natural history of left ventricular wall thickening in hypertrophic cardiomyopathy, Aust N Z J Med. 27, 51-8.
Sen-Chowdhry, S. and McKenna, W.J., 2012. Sudden death from genetic and acquired cardiomyopathies, Circulation. 125, 1563-76.
Sequeira, V., Najafi, A., Wijnker, P.J., Dos Remedios, C.G., Michels, M., Kuster, D.W. and van der Velden, J., 2015. ADP-stimulated contraction: A predictor of thin-filament activation in cardiac disease, Proc Natl Acad Sci U S A. 112, E7003-12.

Shkryl, V.M., Maxwell, J.T., Domeier, T.L. and Blatter, L.A., 2012. Refractoriness of sarcoplasmic reticulum Ca2+ release determines Ca2+ alternans in atrial myocytes, Am J Physiol Heart Circ Physiol. 302, H2310-20.

Sideris, D.A., Toumanidis, S.T., Thodorakis, M., Kostopoulos, K., Tselepatiotis, E., Langoura, C., Stringli, T. and Moulopoulos, S.D., 1994. Some observations on the mechanism of pressure related atrial fibrillation, Eur Heart J. 15, 1585-9.

Solti, F., Vecsey, T., Kekesi, V. and Juhasz-Nagy, A., 1989. The effect of atrial dilatation on the genesis of atrial arrhythmias, Cardiovasc Res. 23, 882-6.

Spirito, P., Autore, C., Formisano, F., Assenza, G.E., Biagini, E., Haas, T.S., Bongioanni, S., Semsarian, C., Devoto, E., Musumeci, B., Lai, F., Yeates, L., Conte, M.R., Rapezzi, C., Boni, L. and Maron, B.J., 2014. Risk of sudden death and outcome in patients with hypertrophic cardiomyopathy with benign presentation and without risk factors, Am J Cardiol. 113, 1550-5.

Spirito, P., Autore, C., Rapezzi, C., Bernabo, P., Badagliacca, R., Maron, M.S., Bongioanni, S., Coccolo, F., Estes, N.A., Barilla, C.S., Biagini, E., Quarta, G., Conte, M.R., Bruzzi, P. and Maron, B.J., 2009. Syncope and risk of sudden death in hypertrophic cardiomyopathy, Circulation. 119, 1703-10.

Spirito, P., Bellone, P., Harris, K.M., Bernabo, P., Bruzzi, P. and Maron, B.J., 2000. Magnitude of left ventricular hypertrophy and risk of sudden death in hypertrophic cardiomyopathy, N Engl J Med. 342, 1778-85.

Spoladore, R., Maron, M.S., D'Amato, R., Camici, P.G. and Olivotto, I., 2012. Pharmacological treatment options for hypertrophic cardiomyopathy: high time for evidence, Eur Heart J. 33, 1724-33.

Taggart, P. and Sutton, P.M., 1999. Cardiac mechano-electric feedback in man: clinical relevance, Prog Biophys Mol Biol. 71, 139-54.

Takeuchi, S., Akita, T., Takagishi, Y., Watanabe, E., Sasano, C., Honjo, H. and Kodama, I., 2006. Disorganization of gap junction distribution in dilated atria of patients with chronic atrial fibrillation, Circ J. 70, 575-82.

Tardiff, J.C., Carrier, L., Bers, D.M., Poggesi, C., Ferrantini, C., Coppini, R., Maier, L.S., Ashrafian, H., Huke, S. and van der Velden, J., 2015. Targets for therapy in sarcomeric cardiomyopathies, Cardiovasc Res. 105, 457-70.

Tavi, P., Laine, M. and Weckstrom, M., 1996. Effect of gadolinium on stretch-induced changes in contraction and intracellularly recorded action- and afterpotentials of rat isolated atrium, Br J Pharmacol. 118, 407-13.

ten Tusscher, K.H., Noble, D., Noble, P.J. and Panfilov, A.V., 2004. A model for human ventricular tissue, Am J Physiol Heart Circ Physiol. 286, H1573-89.

ten Tusscher, K.H. and Panfilov, A.V., 2006. Alternans and spiral breakup in a human ventricular tissue model, Am J Physiol Heart Circ Physiol. 291, H1088-100.

Thanigaimani, S., McLennan, E., Linz, D., Mahajan, R., Agbaedeng, T.A., Lee, G., Kalman, J.M., Sanders, P. and Lau, D.H., 2017. Progression and reversibility of stretch induced atrial remodeling: Characterization and clinical implications, Prog Biophys Mol Biol.

Trayanova, N.A. and Rice, J.J., 2011a. Cardiac electromechanical models: from cell to organ, Front Physiol. 2, 43.

Trayanova, N.A. and Rice, J.J., 2011b. Cardiac Electromechanical Models: From Cell to Organ, Front Physiol. 2.

Tsai, C.T., Chiang, F.T., Tseng, C.D., Yu, C.C., Wang, Y.C., Lai, L.P., Hwang, J.J. and Lin, J.L., 2011. Mechanical stretch of atrial myocyte monolayer decreases sarcoplasmic reticulum calcium adenosine triphosphatase expression and increases susceptibility to repolarization alternans, J Am Coll Cardiol. 58, 2106-15.

van der Velden, J., de Jong, J.W., Owen, V.J., Burton, P.B. and Stienen, G.J., 2000. Effect of protein kinase A on calcium sensitivity of force and its sarcomere length dependence in human cardiomyocytes, Cardiovasc Res. 46, 487-95.

van Der Velden, J., Klein, L.J., Zaremba, R., Boontje, N.M., Huybregts, M.A., Stooker, W., Eijsman, L., de Jong, J.W., Visser, C.A., Visser, F.C. and Stienen, G.J., 2001. Effects of calcium, inorganic phosphate, and pH on isometric force in single skinned cardiomyocytes from donor and failing human hearts, Circulation. 104, 1140-6.

van der Velden, J., Narolska, N.A., Lamberts, R.R., Boontje, N.M., Borbely, A., Zaremba, R., Bronzwaer, J.G., Papp, Z., Jaquet, K., Paulus, W.J. and Stienen, G.J., 2006. Functional effects of protein kinase C-mediated myofilament phosphorylation in human myocardium, Cardiovasc Res. 69, 876-87.

van der Velden, J., Papp, Z., Boontje, N.M., Zaremba, R., de Jong, J.W., Janssen, P.M., Hasenfuss, G. and Stienen, G.J., 2003a. The effect of myosin light chain 2 dephosphorylation on Ca2+ -sensitivity of force is enhanced in failing human hearts, Cardiovasc Res. 57, 505-14.

van der Velden, J., Papp, Z., Zaremba, R., Boontje, N.M., de Jong, J.W., Owen, V.J., Burton, P.B., Goldmann, P., Jaquet, K. and Stienen, G.J., 2003b. Increased Ca2+-sensitivity of the contractile apparatus in end-stage human heart failure results from altered phosphorylation of contractile proteins, Cardiovasc Res. 57, 37-47.

Van Driest, S.L., Vasile, V.C., Ommen, S.R., Will, M.L., Tajik, A.J., Gersh, B.J. and Ackerman, M.J., 2004. Myosin binding protein C mutations and compound heterozygosity in hypertrophic cardiomyopathy, J Am Coll Cardiol. 44, 1903-10.

Vandersickel, N., Kazbanov, I.V., Nuitermans, A., Weise, L.D., Pandit, R. and Panfilov, A.V., 2014. A study of early afterdepolarizations in a model for human ventricular tissue, PLoS One. 9, e84595.

Voigt, N., Trafford, A.W., Ravens, U. and Dobrev, D., 2009. Abstract 2630: Cellular and Molecular Determinants of Altered Atrial Ca²⁺ Signaling in Patients With Chronic Atrial Fibrillation, Circulation. 120, S667-S668.

Vriesendorp, P.A., Schinkel, A.F., Van Cleemput, J., Willems, R., Jordaens, L.J., Theuns, D.A., van Slegtenhorst, M.A., de Ravel, T.J., ten Cate, F.J. and Michels, M., 2013. Implantable cardioverter-defibrillators in hypertrophic cardiomyopathy: patient outcomes, rate of appropriate and inappropriate interventions, and complications, Am Heart J. 166, 496-502.

Warren, C.M., Karam, C.N., Wolska, B.M., Kobayashi, T., de Tombe, P.P., Arteaga, G.M., Bos, J.M., Ackerman, M.J. and Solaro, R.J., 2015. Green Tea Catechin Normalizes the Enhanced Ca2+ Sensitivity of Myofilaments Regulated by a Hypertrophic Cardiomyopathy-Associated Mutation in Human Cardiac Troponin I (K206I), Circ Cardiovasc Genet. 8, 765-73.

Weiss, J.N., Garfinkel, A., Karagueuzian, H.S., Chen, P.S. and Qu, Z., 2010. Early afterdepolarizations and cardiac arrhythmias, Heart Rhythm. 7, 1891-9.

Weiss, J.N., Karma, A., Shiferaw, Y., Chen, P.S., Garfinkel, A. and Qu, Z., 2006. From pulsus to pulseless: the saga of cardiac alternans, Circ Res. 98, 1244-53.

Witayavanitkul, N., Ait Mou, Y., Kuster, D.W., Khairallah, R.J., Sarkey, J., Govindan, S., Chen, X., Ge, Y., Rajan, S., Wieczorek, D.F., Irving, T., Westfall, M.V., de Tombe, P.P. and Sadayappan, S., 2014. Myocardial infarction-induced N-terminal fragment of cardiac myosin-binding protein C (cMyBP-C) impairs myofilament function in human myocardium, J Biol Chem. 289, 8818-27.

Wolff, M.R., Buck, S.H., Stoker, S.W., Greaser, M.L. and Mentzer, R.M., 1996. Myofibrillar calcium sensitivity of isometric tension is increased in human dilated cardiomyopathies: role of altered beta-adrenergically mediated protein phosphorylation, J Clin Invest. 98, 167-76.

Wolff, M.R., Whitesell, L.F. and Moss, R.L., 1995. Calcium sensitivity of isometric tension is increased in canine experimental heart failure, Circ Res. 76, 781-9.

Xie, W., Santulli, G., Guo, X., Gao, M., Chen, B.X. and Marks, A.R., 2013. Imaging atrial arrhythmic intracellular calcium in intact heart, J Mol Cell Cardiol. 64, 120-3.

Yan, G.X., Wu, Y., Liu, T., Wang, J., Marinchak, R.A. and Kowey, P.R., 2001. Phase 2 early afterdepolarization as a trigger of polymorphic ventricular tachycardia in acquired long-QT syndrome : direct evidence from intracellular recordings in the intact left ventricular wall, Circulation. 103, 2851-6.

Zaremba, R., Merkus, D., Hamdani, N., Lamers, J.M., Paulus, W.J., Dos Remedios, C., Duncker, D.J., Stienen, G.J. and van der Velden, J., 2007. Quantitative analysis of myofilament protein phosphorylation in small cardiac biopsies, Proteomics Clin Appl. 1, 1285-90.

Zhuang, J., Yamada, K.A., Saffitz, J.E. and Kleber, A.G., 2000. Pulsatile stretch remodels cell-to-cell communication in cultured myocytes, Circ Res. 87, 316-22.

Zile, M.A. and Trayanova, N.A., 2016. Rate-dependent force, intracellular calcium, and action potential voltage alternans are modulated by sarcomere length and heart failure induced-remodeling of thin filament regulation in human heart failure: A myocyte modeling study, Prog Biophys Mol Biol. 120, 270-80.

Zile, M.A. and Trayanova, N.A., 2017. Myofilament protein dynamics modulate EAD formation in human hypertrophic cardiomyopathy, Prog Biophys Mol Biol.

Zimik, S., Vandersickel, N., Nayak, A.R., Panfilov, A.V. and Pandit, R., 2015. A Comparative Study of Early Afterdepolarization-Mediated Fibrillation in Two Mathematical Models for Human Ventricular Cells, PLoS One. 10, e0130632.

Vita

Melanie Anne Zile was born in Providence, RI on January 30th, 1989 and grew up in North Kingstown, RI. She graduated with *Magna Cum Laude* honors in May 2011 from Boston University, where she received her B.S. in Biomedical Engineering. As an undergraduate, she received a Boston University Engineering Merit Scholarship for three years and in her senior year was awarded the prestigious Harold C. Case Merit Scholarship. In August 2011, she enrolled in the Biomedical Engineering Ph.D. program at Johns Hopkins University. While at Johns Hopkins she received a National Science Foundation Graduate Research Honorable Mention in 2013, received the David C. Gakenheimer Fellowship from 2015-2016, and won a prestigious Poster Competition at the Cardiac Mechano-Electric Coupling Workshop in Freiburg, Germany in September 2016. Her research focuses on computational modeling of cardiac myocytes and the mechanisms underlying the cellular drivers of arrhythmogenesis. Melanie also worked for Boston Scientific as an intern in the summer of 2017 and her work resulted in a US patent being filed.

After graduation, Melanie plans to visit her family, go on many exciting backpacking adventures, and job hunt.